University of Leoben

Dissertation

Uniaxial Straining of Brittle Film/Compliant Substrate Systems

Aidan Taylor

Leoben, November 2011

Erich Schmid Institute of Materials Science
Austrian Academy of Sciences
Jahnstrasse 12
A–8700 Leoben

This thesis was typeset by the use of KOMA-Script and LaTeX 2_ε.

Dedicated to all my friends

Affidavit

I declare in lieu of oath, that I wrote this thesis and performed the associated research myself, using only literature cited in this volume.

Leoben, November 2011

Acknowledgements

My first thanks go to Prof. Dr. Gerhard Dehm, my advisor, for giving me the opportunity to live and work in Leoben for the past 4 years. It has been an enjoyable experience and I will miss Leoben's many charms. Thanks also go to Prof. Rishi Raj of The University of Colorado at Boulder for the time I spent working in his laboratory and the many ideas he has given me. I would also like to extend my deepest gratitude to Dr. Megan Jo Cordill. Megan and I arrived in Leoben at the same time and our similar subject areas and complementary specialities has led to a productive working relationship. Regarding research, I would finally like to thank the people who produced the thin films with which I have worked; Vicki Edlmayr, Kalvis Terauds and Stephan Grasser, without whose hard work this thesis would not be possible.

The Erich Schmid Schmid Institute has been an incredible place to come to work every day. Gabi Moser and Herwig Felber have always been ready to assist me in producing TEM samples and Jörg Thomas has helped me on many occasions when I couldn't get either of the microscopes to work. I have learned much about the practical use of TEMs from Jörg; everything from the best ways to find a sample dropped on the floor to dealing with dark spots on a LaB_6 cathode. Franz Hubner and Christian Scheiner have been very helpful in producing samples and experimental apparatus, and this despite my broken German and poor technical drawing! Doris Schrutt has helped me with the complicated bureaucracy of the University and Academy on more occasions than I am able to remember, let alone the invaluable assistance she gave me in finding a flat and settling in to another country. I would like to thank all the people I have worked with in ESI over the years for the many stimulating conversations, whether about science, skiing, hiking or beer. Particular gratitude is extended to Bernd Gludovatz, Toni Hohenwarter and Daniel Kiener for the excellent company and assistance. Thanks should also go to Georg Rathmayr and Bo Yang for letting me play whatever music I wanted to in our office all this time.

It is also important that I thank all the other people who have made my time in Leoben so enjoyable. Autumn for the many heated arguments, Mimoza for the teaching me Steirisch and Shqip, Marco for the relaxed company and Micha for the long evenings playing Doppelkopf and equally long days playing sport together. I

would like to thank Martin and Dnyan for always having a place for me to stay in London and new computer games to play while there. Lastly I would like to thank IBC Leoben, LUFT and my family.

Abstract

The characterisation of thin films and the film/substrate interface is technologically very important. It is through characterisation that the properties of thin films are understood and this understanding leads to methods for optimising coatings for a wide range of applications. Fragmentation testing is one such characterisation technique applicable to the quantitative comparison of the mechanical properties of brittle film/compliant substrate systems. Several aspects of fragmentation testing are discussed in this thesis; the macro - and microstructural characterisation of film/substrate systems with transmission electron microscopy (TEM), the theoretical framework and experimental application of a model to account for variation in the coating thickness and fragmentation testing at elevated temperature.

A novel route for preparing TEM specimens from brittle film/compliant substrate systems is demonstrated. This technique is purely mechanical and gives a means of assessing both the film microstructure and an upper limit to the film thickness. The application of the method allowed for the TEM assessment of Cr films on polyethylene teraphthalate (PET) and amorphous-Al_xO_y films on Cu. Conventional sample preparation of TEM samples is not possible for the Cr/PET system and it is shown that conventional preparation leads to artefacts in the Al_xO_y/Cu system.

The most practical application of fragmentation testing is in the comparison of films produced with different compositions, deposition parameters or substrate surface conditions. To ensure a fair and truly quantitative comparison it is important to ensure only the experimental variable changes between samples. An analytical analysis of film thickness variation in a fragmentation testing experiment shows that variation should be separated into two length scales, variation over a horizontal range shorter, **roughness**, or longer, **unevenness**, than the maximum crack spacing. Roughness is important as it leads to a systematic error in the interfacial shear stress if not assessed and accounted for. The application of **neighbour ratios** to compensate for the effects of unevenness is shown to bring Al_xO_y/Cu and TiN/Cu systems into compliance with the prediction that the largest spacing between cracks is twice as large as the smallest. This prediction has never previously been observed. The failure of the neighbour ratio approach for Cr films on PET and polyimide (PI) is an indicator that quantitative calculation of interfacial shear stress is not valid

for brittle film/polymer systems. The presence of out-of-plane film bending during straining of the Cr/PET and Cr/PI systems confirms this.

As many coated systems are processed or operated at elevated temperatures, the application of fragmentation testing characterisation to elevated temperatures is of technological interest. Testing a model Al_xO_y/Cu system at room temperature and at 650°C at high, $3.5 \cdot 10^{-2}\ s^{-1}$, and low, $1.7 \cdot 10^{-5}\ s^{-1}$, strain rates showed that diffusional interfacial sliding as seen by Jobin et al. (Acta Mater., 1992) did not take place. It was additionally shown that testing at higher strain rates than found in the literature led to a broadening of the crack spacing distribution. This effect is attributed to the effective fracture toughness of the film/substrate interface being dependent on the strain rate. Elevated temperature testing of a Ti/PI adhesion layer system for flexible electronics showed a stark change in cracking behaviour and film adhesion energy with temperature. The behaviour of adhesion layers with temperature is important to understand as changes in properties like those observed could lead to unexpected failure of flexible circuitry. The reasons for the change in behaviour of the Ti coating are discussed.

Contents

1

Motivation and aim of the present work

Thin films and coated products are used in all areas of technological development. This includes everything from the metallisations in microelectronic devices to gas barrier coatings on food packaging to help keep products fresh. The common factor in all coated systems is that failure of the coating or failure at the film/substrate interface constitutes failure of the components, despite the film comprising 1% or less of the product volume/mass. Much effort is therefore devoted to improving coatings and optimising the performance of the interface. In order to characterise and quantify the difference between coatings and interfaces it has been necessary to develop a range of characterisation techniques. The most significant of these techniques are instrumented indentation [1–4], tribological methods [5–7], micromechanical testing [8–10] and fragmentation testing [11–14]. This thesis focusses on the refinement of the fragmentation testing methodology and its application to film/substrate systems at elevated temperature.

The principle advantage of fragmentation testing (also known as periodic cracking) over other characterisation methods is the simplicity of the experimentation. Instrumented indentation requires highly specialised equipment and experienced users, micromechanical testing requires either focussed ion beam (FIB) manufacture of samples [8,9] or specialised photolithography methods [10] and it is very difficult to extract fundamental material properties from tribological testing. At its most basic, fragmentation testing requires only the production of coated tensile samples and a means of controlled tensile testing [13]. In practice the technique benefits from *in situ* observation (optical microscopy, x-ray strain measurement, scanning electron microscopy) during testing and rigorous film/substrate characterisation techniques (transmission electron microscopy, atomic force microscopy, FIB, x-ray diffraction), but this can also be said of the other techniques mentioned above.

While the experimental aspect of fragmentation testing is very straightforward,

the interpretation of the resultant data can be carried out according to a number of different models [13–16]. These models make different assumptions about the stress distribution at the film/substrate interface [13, 16], whether the film fracture stress is single-valued or has a statistical distribution [13, 15] and if the interface is fully yielded or predominantly elastic [13, 14]. The principal aim of this thesis is to explore the theoretical side of fragmentation testing and to use experimental methods to investigate how applicable the models are in the interpretation of data. In doing so, this work investigates amorphous-Al_xO_y and TiN coatings on Cu substrates, Cr and Ti coatings on polyimide (PI) substrates and Cr coatings on polyethylene teraphthalate (PET) substrates.

The secondary aim of this thesis is the application of fragmentation testing to film/substrate systems at elevated temperature. The work of Jobin et al. [17] and Peterson et al. [18] indicated interfacial sliding in ceramic/metal systems at temperatures as low as $0.4T_m$, T_m being the melting point of the metal. In the present work the elevated temperature fragmentation experiment of Jobin et al [17] is repeated for a model Al_xO_y/Cu system to investigate the effect of higher strain rates.

The characterisation of film/substrate systems at elevated temperature can be important technologically. Leterrier et at. [15] and Yanaka et al. [19] showed that the crack density of SiO_2 films on PET **decreased** as the test temperature **increased**, an important finding for the processing and recycling of SiO_2-coated PET for food packaging [20]. A growing interest in flexible electronic devices [21–23] has led to a resurgence of interest in fragmentation testing for films on polymer substrates [24–28]. The production, processing and use of flexible electronic devices all lead to heating of the system to varying degrees, understanding the effect of temperature on coated polymer systems is therefore essential in optimising the lifetime and performance of the devices. Cordill et al. [28] showed that a Cu/Ti/PI system had a significantly lower measured adhesion at the Ti/PI interface after annealing. To further investigate this phenomenon, a simplified Ti/PI system is investigated at 350°C as well as in the as-deposited and annealed states.

2
Fragmentation Testing

2.1 Shear Lag

The concept of **shear lag** was first introduced by Cox [29] to describe the loading of fibres in a matrix. The concept essentially describes how load is transferred from the matrix to the fibres when the fibres themselves are not directly connected to the applied load, this is shown schematically in figure 2.1a. This theory is readily extended to thin, cracked films on a substrate [14, 25], figure 2.1b, as the film is also disconnected from the direct load in this scenario. By using the mathematical framework devised by Cox [29] it is therefore possible to accurately describe the stress state in the film fragments in the **elastic** regime. Frank et al. [25] demonstrated this by x-ray diffraction measurement of the average stresses in a Ta coating on PI during straining, close correlation of the measured and predicted stresses were found up to 1.5% applied strain. More recently, Ahmed et al. [14] used Raman measurements to demonstrate that the stress profile in an individual film fragment can be well described with shear lag methodology, this work was also limited to the sub-1.5% regime. In order to describe film fragmentation and the observed phenomenon of a saturation in cracking in the high strain regime (>10%) it is necessary to introduce certain assumptions about the plastic behaviour of the interface, this leads to the interfacial yield model.

2.2 Interfacial Yield

First proposed by Kelly and Tyson [11] for ceramic fibres in a metal matrix, the **interfacial yield model** was developed to explain the observed phenomenon that brittle fibres in a composite would continue to fragment with increasing strain until

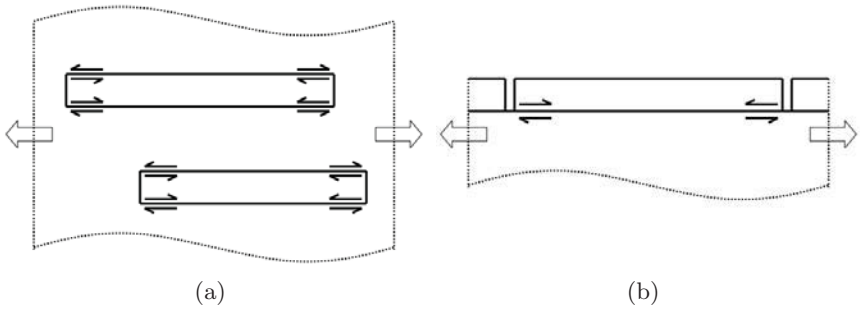

Figure 2.1 Schematic illustration of the elastic loading of a) fibres in a matrix and b) a cracked film on a substrate. In both cases, all loading in the fibres/film is transferred via shear at the fibre/matrix, film/substrate interface.

a point was reached where no further fragmentation was observed. The same phenomenon was subsequently observed for brittle films on compliant substrates [13]. For clarity, only films, not fibres, will be discussed from this point onwards. To explain the crack saturation problem, the interfacial yield model assumes that the film/substrate interface has a specific strength, the **interfacial yield strength**, and once this strength is reached the interface is assumed to yield at this location. If the shear stress at the interface is highest at the fragment edges, as predicted by shear lag and shown by Ahmed et al., then the interfacial yield zone will begin at the fragment edges and move inwards as the substrate is strained further, this is shown schematically in figures 2.2a and 2.2b. After sufficient straining it can be expected that the entire interface has yielded, at this point the loading of the film fragment is at its maximum and further straining is not expected to increase the tensile stress in the film fragment, figure 2.2c. Once all film fragments have reached this fully yielded interface condition it is expected that further fragmentation is halted.

A key prediction of the interfacial yield model [11,13] is that in the crack saturation regime the longest spacing between cracks is twice as large as the smallest. This can be understood as follows; the transfer of tensile stress to the film via shear at the interface requires a finite interfacial length, the length of interface required to load a film to its fracture stress is often referred to as the shear transfer length, λ_s, figure 2.3a. A film fragment exactly twice the shear transfer length can only fracture further at its exact midpoint, producing two fragments of length λ_s, these fragments are unable to fracture further. Conversely, for a film fragment whose length is infinitesimally smaller than twice the shear transfer length, i.e. it has a length of approximately $2\lambda_s$, the fracture stress for the film is not reached and further fracture is not possible, figure 2.3. These limits provide the factor of two difference.

The interfacial yield approach gives a means of quantifying the interfacial shear strength through measurement of the minimum crack spacing in the saturation regime, λ_s [13, 16]:

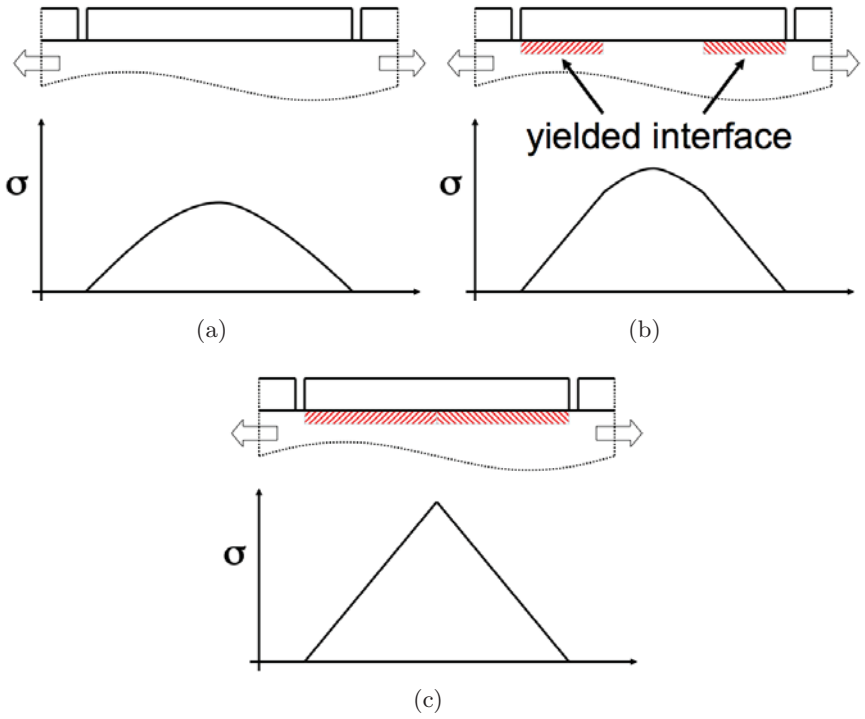

Figure 2.2 Illustration of the progression of interfacial yield from film fragment edges. In a) the interface is purely elastic. Following further substrate straining, yielding begins at the fragment edges, b), and continues until the entire interface has yielded, c). No further tensile stress can develop in the film fragment once the entire interface has yielded.

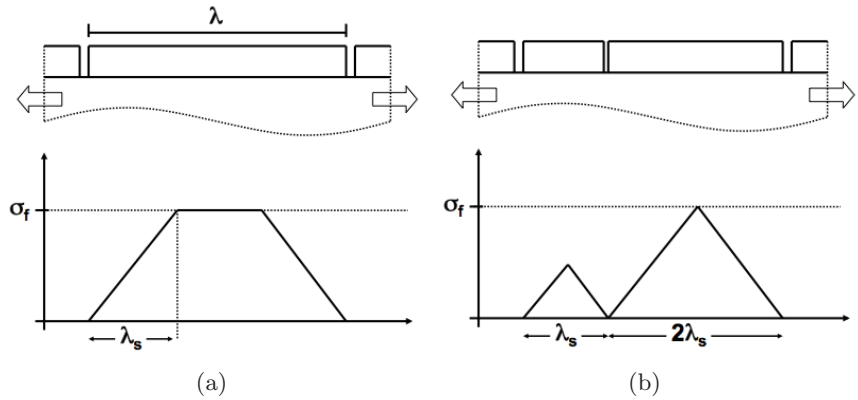

Figure 2.3 Schematic indicating the origin of the factor two difference in crack spacing prediction. In a) the stress in the film has reached the failure stress, if the film cracks immediately where the fracture stress is reached a fragment of width λ_s is produced, b). If the larger fragment has a width of slightly less than $2\lambda_s$ then no further cracking is possible.

$$\tau_{IFSS} = K\frac{(\epsilon_f + \epsilon_r)E_f\delta}{\lambda_s} \tag{2.1}$$

where E_f is the Young's modulus, δ is the thickness, ϵ_f is the fracture strain and ϵ_r is the residual strain, all relating to the film. K is a numerical constant dependent upon exactly how the distribution of shear stress at the interface is modelled. Following the work of Agrawal and Raj [13] this constant is: $K_{A+R} = \pi/2$. If the work of Chen et al. [16] is followed then this constant becomes: $K_{Chen} = 4/(\pi + 4)$. Quantification of the interfacial shear stress through a simple tensile test is the real strength of fragmentation testing. Through this quantification the effect of surface pre-treatments on the coating process [30–32], substrate roughness [33, 34] and the influence of coating bond/reaction layers [35, 36] can be investigated. From an industrial perspective this approach has great potential for the assessment of different pre-treatments and coatings for specific applications. Wherever accurate sample comparison is to be considered it is of the utmost importance that changes between samples other than the investigated variable are quantified and compensated for.

2.3 Statistical/Weibull Approach

The predicted bound of two in the crack spacings is never observed experimentally, neither for fibre/matrix or film/substrate systems. One reason for this is that the fracture stress of the film is not really single-valued. Several authors [37–40] have demonstrated that the distribution of fibre/film fragment lengths can be well described by a **Weibull distribution** [41], indicative of a statistical distribution of film strength. Analysis of such distributions delivers the parameters α and β, the Weibull shape and scale parameters, respectively [15, 39]. The Weibull shape parameter is also known as the Weibull modulus. Figure 2.4 illustrates the concept of a statistical distribution of strength in the coating. Initial coating cracks appear where the failure stress of the film is lowest, figure 2.4a. Further coating cracks appear as the far-field loading of the substrate is increased and the local failure stresses in other areas of the coating are reached, figures 2.4b and 2.4c. Cracking finally ceases when the shear transfer lengths of the breaks interact along the length of the coating, preventing further transfer of tensile load, figure 2.4d.

These simple diagrams illustrate why a crack bounding ratio greater than two can be expected if the film does not possess a single-valued fracture stress. Three film fragments are shown in figure 2.4d, the shortest, left-most, fragment is clearly more than three times shorter than the longest, right-most, fragment. This is possible when a coating does not have a single-valued fracture stress as the shortest fragment was defined by a lower fracture stress, at location *1*, and hence lower shear transfer length than the longest, defined by fracture at location *3*. In this analysis, the interfacial shear stress and film thickness remain constant while variation in the film fracture stress, σ_f, causes variation in the shear transfer length, i.e. $\lambda_s = f(\sigma_f)$.

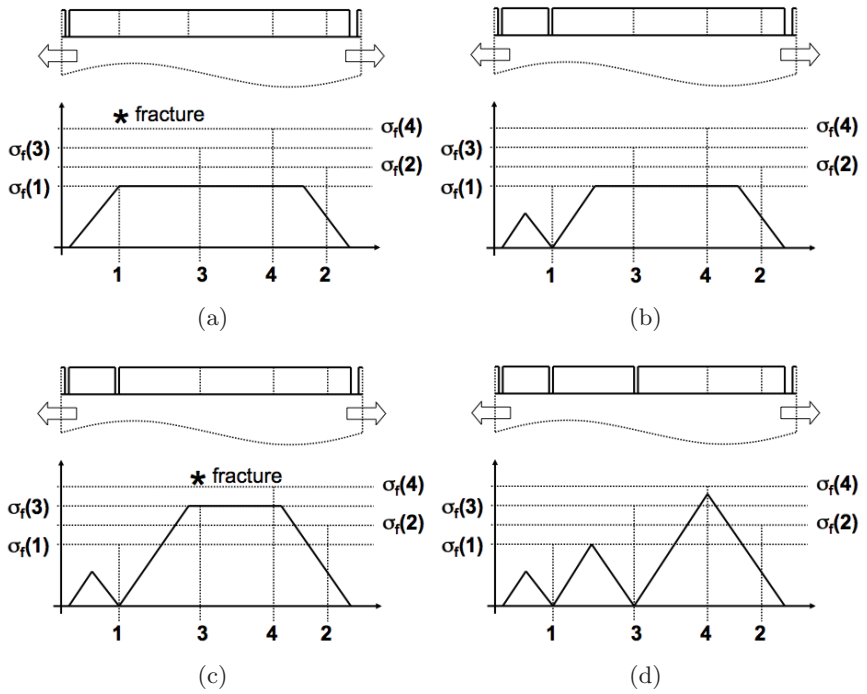

Figure 2.4 The effect of a statistical distribution of strength in the film; failure occurs at locations i when the film failure stress at that location, $\sigma(i)$, is reached. In a) cracks begin to appear at the weakest points in the film. Cracking continues, b) and c), until the stress drops associated with cracking all overlap and further cracking becomes impossible, d).

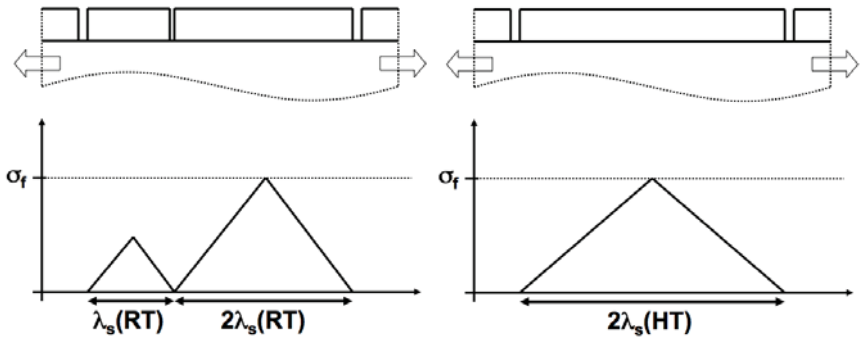

(a) (b)

Figure 2.5 Illustration of the effect of temperature of the crack spacing. The higher yield stress of the substrate at room temperature in a) results in a shorter average crack spacing. The elevated temperature in b) leads to a lower interfacial shear stress and hence longer average crack spacing.

Two predictions follow on from this work; firstly, it is expected that the shortest measured crack spacings will be formed in the earliest stages of straining when the effective shear transfer length is at its lowest. Secondly, the film fragments defined by cracks formed in the final strain increment prior to saturation should follow the predictions of a coating possessing a single-valued fracture stress. The concept of considering the film fragments produced during successive strain increments is dealt with mathematically by Curtin [37].

2.4 The Influence of Temperature

Several studies have looked at the influence of temperature on the fragmentation testing of thin films [15, 17, 19, 36]. In all cases an **increase in the saturation crack spacing** was observed with **increasing temperature**. Leterrier et al. [15] observed a strong correlation between the change in the average crack spacing at saturation and the elastic load in the substrate. This makes sense if the interfacial shear stress is limited by the yield stress of the substrate, i.e. the measured shear stress at which the interface yields actually corresponds to the yield of the substrate material next to the interface. The result of this is that the temperature dependence of the **substrate yield stress** leads to the observed dependence of the average crack spacing on test temperature. This phenomenon is illustrated schematically in figure 2.5.

In addition to observing temperature dependence in the average crack spacings, Jobin et al. [17] found that at elevated temperatures the average crack spacing became dependent on the strain rate of the test. This behaviour was attributed to **diffusional sliding** at the film/substrate interface. In this case, stress-driven

diffusional sliding at the interface reduces the effective interfacial shear stress when the strain rate is sufficiently low. In a different experimental set-up, Peterson et al. [18] also observed interfacial sliding for a Si/Al system at temperatures as low as 0.4 T_m, showing in the process that the sliding rate depends on the magnitude of the interfacial shear stress and the interface roughness.

3
Summary of the Results

In this chapter a summary of the most important results from the papers incorporated in this thesis is presented. Regarding the motivation and experimental set-up of the research the reader is referred to the individual manuscripts found in the appendix as this section is intended to keep the focus on the critical data and conclusions.

3.1 A novel TEM sample Preparation Technique for Brittle Films on Compliant Substrates

3.1.1 Background

Preparing electron transparent samples of material for TEM characterisation can often be difficult. This is particularly true for thin films where the region of interest is very small. The majority of the literature concerning fragmentation testing of thin films presents no information about film microstructure and only gives nominal film thicknesses, i.e. the thickness predicted from the deposition parameters. This is a risky approach in the analysis of thin films where changes in film thickness and microstructure can significantly affect the mechanical properties [42]. From equation 2.1 it can also be seen that any error in film thickness estimation transfers directly to error in interfacial shear stress calculation. Both of these points become doubly significant if two systems are to be compared as errors will compound, making meaningful analysis difficult.

Conventional TEM sample preparation techniques (FIB lift-out [43] or dimple grinding and ion milling [44]) were either not possible or introduced major image artefacts for several of the materials systems studied in this thesis. One case is examined in this chapter, Cr films on PET (polyethylene teraphthalate). PET is

unstable in the electron beam due to its electrical insulation and relatively low melting point, leading to very rapid heating, distortion and vaporisation of the material. Due to these problems, conventional TEM sample preparation routes, where at least some of the substrate remains with the film, lead to serious difficulties during imaging. It is therefore very difficult to get an accurate description of the microstructure and crystallinity of such a film.

To avoid these effects a means of removing film fragments from a cracked coating was devised, a description of the technique and some results are given in the following chapter but the technique was generally used throughout this thesis for TEM assessment of coatings.

3.1.2 The Method

The first stage of the preparation of the TEM samples is to uniaxially strain the samples to 15-30% (engineering strain) in order to induce cracking and delamination of the films at the interface (figure 3.1). Film fragments were then carefully transferred from the substrate onto a carbon-coated Cu TEM grid using a ceramic blade. The grid was then loaded into a plasma cleaner (Fischione Model 1020) using a 80% Ar and 20% O_2 plasma gas mix and cleaned for 10 min. This helped to remove any remnants of PET that may have been transferred with the film.

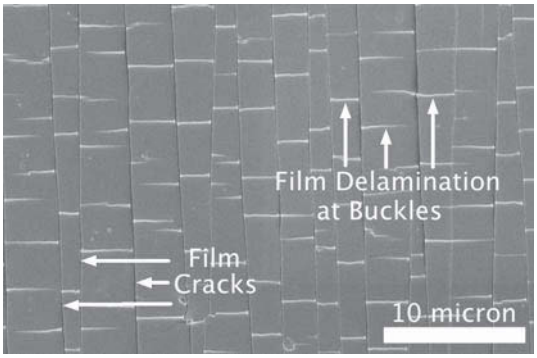

Figure 3.1 SEM image a 15 nm thick Cr film on PET following 18% straining, note the fragmentation of the film through cracking and buckling.

The technique produces an agglomeration of film fragments as shown in figure 3.2. Due to the wide variation in orientation angles of the film fragments it is important to use a double tilt holder in analysing films made by this technique in order to ensure the film plane is perpendicular to the beam. A useful side effect of this technique is that an upper bound estimate of the film thickness can be made. This procedure is carried out through the following method. A film fragment lying reasonably parallel to the electron beam is identified at zero tilt. The goniometer tilt function is then used to tilt this fragment to an angle where it provides a minimum cross section to the electron beam. The minimum sample cross section should then be found using the secondary tilt of the holder by the same procedure. These two steps are iterated

several times to ensure that the minimum cross section of fragment with respect to the beam is achieved. This image can then be used to measure an upper bound to the film thickness. For better accuracy, the use of a TEM calibration standard and the smallest possible film fragments is recommended.

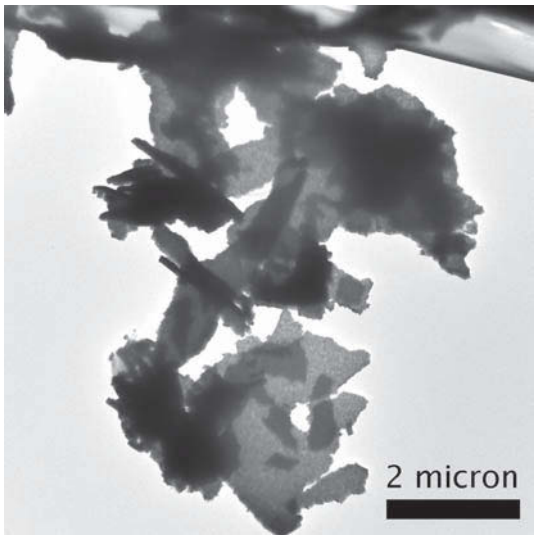

Figure 3.2 Low magnification TEM image of fragments from a 70 nm thick Cr film, the Cu grid supporting the fragments is at the top of the image.

3.1.3 Results for the 15 nm Thick Cr Film

Shown in figure 3.3 are conventional bright field TEM, selected area diffraction and high resolution TEM images of the 15 nm thick Cr film. It is possible to see from figure 3.3 that the film is crystalline, non-porous and of body centred cubic (bcc) crystal structure. The last point is of particular interest as the crystal structure of thin metal films can deviate from equilibrium structures [45] and it had not previously been possible to confirm this by laboratory x-ray diffraction measurements due to the film being so thin. The films were produced to a nominal 10 nm thickness, by imaging film fragments side-on a more accurate estimate of 15 nm thickness was made, figure 3.3a. This 50% difference highlights the importance of accurate film thickness characterisation. Due to the presence of moiré fringes, as observed in figure 3.3d, it can be deduced that even at this very low thickness the film is not purely composed of columnar grains. In fact the microstructure of this film seems to be quite complex, some grains appear to be significantly larger than the film thickness, as evident from the dark diffracting regions in figure 3.3c, these grains are surrounded, both to the sides as well as above and/or below, by far smaller grains, as seen in Figure 3.3d.

For further discussion of results obtained by this preparation method along with some limitations of the technique see appendix A.3.

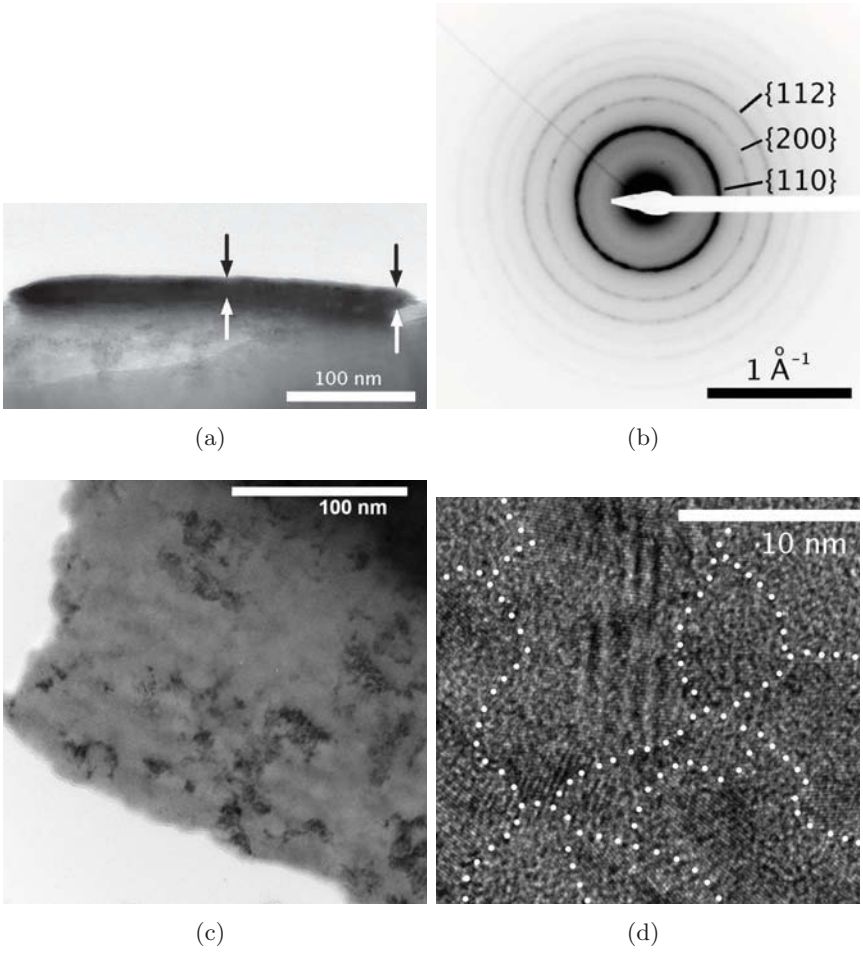

Figure 3.3 a) Film thickness estimation, b) selected area diffraction, c) conventional TEM and d) high resolution TEM of the 15 nm thick Cr film. Measurements indicate, a), that the nominal Cr film thickness of 10 nm is actually 15 nm. The ring pattern in b) is consistent with a bcc structure, indexed, while the fringes in the centre of c) are moiré fringes, indicative of the electron beam passing through two grains at that point. In d) some grain boundaries have been highlighted to aid interpretation.

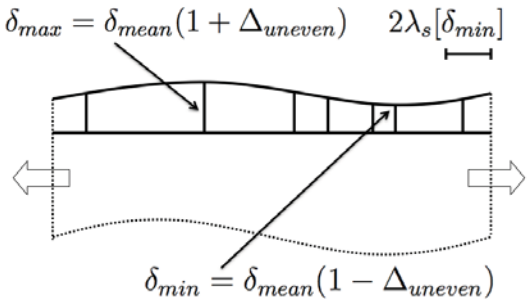

Figure 3.4 A schematic of film thickness variation with a wavelength greater than $2\lambda_s$, i.e. unevenness, and its effect on the crack bounding ratio. Crack spacings in the thicker regions of the film are greater than those in the thinner region. The locations of the maximum, δ_{max}, and minimum, δ_{min}, film thicknesses are indicated.

3.2 Film Thickness Variation and Neighbour Ratios

3.2.1 Theoretical Framework

As highlighted in section 2.3, the bound of two between the longest and shortest crack spacings has never been observed in practice. Variation in the film thickness over the surface of the sample is a possible cause of this behaviour. In order to analytically consider film thickness variation it is useful to define a very simple relation for the film thickness:

$$\delta = \delta_{mean} \pm \Delta\delta_{mean} = \delta_{mean}(1 \pm \Delta) \tag{3.1}$$

where δ is the film thickness and Δ is the fractional variation in thickness. It can be demonstrated that a systematic broadening of the crack spacing distribution is expected when film thickness variation is present. Some thickness variation is expected in all real systems. Firstly, a crack bounding ratio, M, is defined:

$$M = \frac{\lambda_{max}}{\lambda_{min}}. \tag{3.2}$$

This ratio is calculated from the experimentally observed largest, λ_{max}, and smallest, λ_{min}, crack spacings. For a system controlled by interfacial yield and possessing a single-valued fracture stress, M is predicted to be equal to 2. When considering film thickness variation the horizontal length scale of the variation is also important (appendix B.4), specifically whether the variation occurs over a length greater than or less than the maximum crack spacing, $2\lambda_s$. Variations over a length scale shorter than $2\lambda_s$ are termed **roughness** and are not expected to cause a broadening of the crack bounding ratio (appendix B.4.1). Variations over a horizontal scale greater than $2\lambda_s$ are termed **unevenness**, this is depicted in figure 3.4.

If the film thickness varies by an amount Δ_{uneven} over a horizontal length greater than $2\lambda_s$ then the crack bounding ratio is expected to increase with Δ_{uneven} as

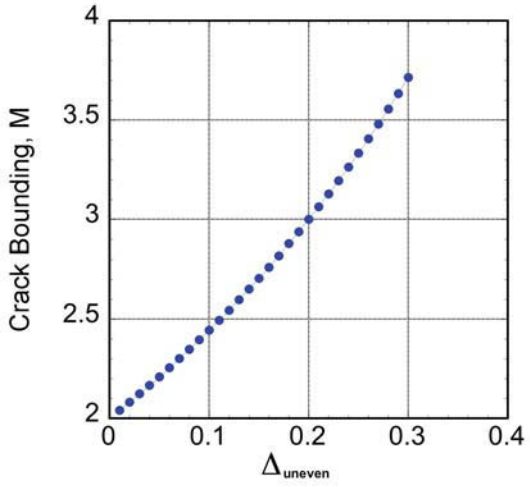

Figure 3.5 Chart depicting the dependence of the crack bounding ratio, M, on the film thickness variation on the unevenness length scale, Δ_{uneven}.

follows:

$$M_{uneven} = \frac{\lambda_{max}[\delta_{mean}(1+\Delta_{uneven})]}{\lambda_{min}[\delta_{mean}(1-\Delta_{uneven})]} = \frac{2(1+\Delta_{uneven})}{1-\Delta_{uneven}}. \tag{3.3}$$

Equation 3.3 infers that a film thickness variation of 20% in the unevenness range would lead to an observed crack bounding ratio of three rather than two. Equation 3.3 is plotted in figure 3.5.

In order to investigate whether unevenness is the cause of the observed broadening in the crack spacing distribution to values of M >2 the concept of a **neighbour ratio** must be introduced. Neighbour ratios are determined by comparing the length of each crack spacing with only the two adjacent spacings, the larger spacing always being divided by the smaller. This analysis removes the effects of longer length-scale variations in the film thickness. Neighbour ratio values ranging from one to two are predicted if a statistical variation in the fracture strength is actually due to film thickness variation. Conversely, if neighbour ratios of greater than 3 are measured, or if more than 10% of the neighbour ratios for an experiment are greater than 2 then validity of the interfacial yield model in analysing such a system's spacings is inaccurate.

3.2.2 Application to Ceramic/Cu Systems

The neighbour ratio approach is first applied to ceramic films on metal substrates, namely Al_xO_y/Cu and TiN/Cu. The samples have nominal thicknesses of 350 and 500 nm, respectively, but the TEM sample preparation technique described in section 3.1.2 revealed thicknesses of 250 and 490 nm. SEM images of the two systems are

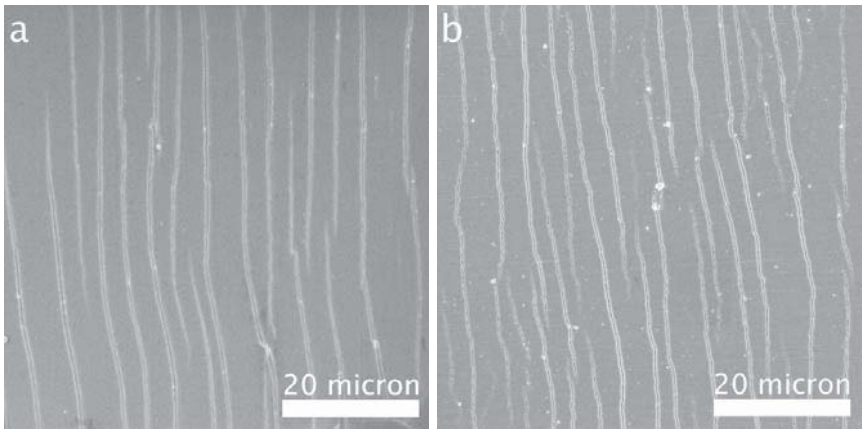

Figure 3.6 SEM micrographs of a) the Al_xO_y/Cu system and b) the TiN/Cu system. Both samples are strained to 6% engineering strain, the onset of crack saturation for both systems. The strain direction is along the horizontal.

presented in figure 3.6, the films crack in a very similar manner.

Crack spacing distributions and neighbour ratios for the two systems are shown in figure 3.7. The crack spacing distributions show relatively broad distributions of crack spacings, crack bounding ratios of $M_{AlxOy} = 4.8$ and $M_{TiN} = 3.9$ were calculated. The neighbour ratios have a much tighter distribution however. Only 4% of the ratios for the Al_xO_y/Cu system and 3% for TiN/Cu are greater than 2. The highest measured ratios for the two systems are only 2.6 for Al_xO_y/Cu and 2.4 for TiN/Cu. More than 250 crack spacings were measured for each sample to ensure good statistics. This indicates that the interfacial yield model is valid for these two ceramic film/metal substrate systems. Additionally, the success of the neighbour ratio approach infers that the statistical distribution of strength in the coating is due to the long range sample variations for which neighbour ratios can compensate, notably unevenness in the film thickness.

The properties measured for the Al_xO_y/Cu and TiN/Cu systems are summarised in table 3.1. The interfacial shear strength for the two systems calculated according to Agrawal and Raj [13] is also presented. At 1400 versus 690 MPa the TiN/Cu sample has double the interfacial shear strength of the Al_xO_y/Cu sample.

3.2.3 Application to Cr/polymer Systems

The same fragmentation testing and neighbour ratio analysis was carried out on different thickness Cr films on 50 μm thick polyethylene teraphthalate (PET) and polyimide (PI) substrates. Chromium is used as a model brittle film for this work although it is also technologically relevant as an adhesion layer for Au and Cu conducting lines in flexible circuitry [47, 48]. Figure 3.8 presents the crack spacing distributions, figures 3.8a and 3.8c, and neighbour ratios, figures 3.8b and 3.8d, for

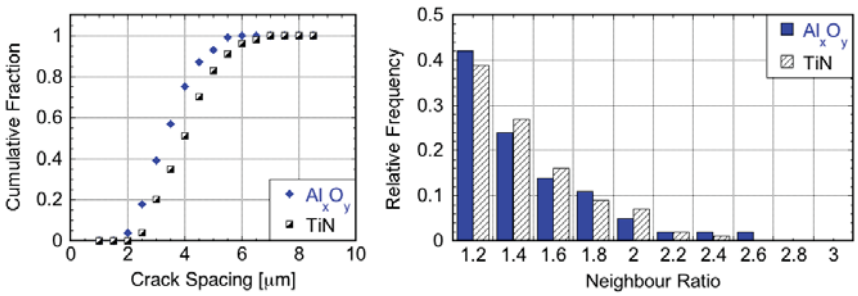

(a) (b)

Figure 3.7 Crack spacing distributions, a), and neighbour ratios, b), for Al_xO_y/Cu and TiN/Cu samples. The TiN has slightly larger crack spacings and a narrower distribution of neighbour ratios. For both systems fewer than 5% of the neighbour ratios exceed the predicted limit of two.

Table 3.1 A comparison of the Al_xO_y/Cu and TiN/Cu systems investigated. δ is the film thickness, ϵ_f the fracture strain, λ_{min} the minimum crack spacing, τ_{IFSS} the interfacial shear strength, M is the crack bounding ratio and R >2 represents the fraction of measured neighbour ratios greater than two. The τ_{IFSS} calculation is made according to the Agrawal and Raj model [13] using a Young's modulus of 160 GPa for Al_xO_y [46] and 450GPa for TiN [51].

	δ/nm	ϵ_f/%	$\lambda_{min}/\mu m$	τ_{IFSS}/MPa	M	R >2/%
Al_xO_y	250	2.2	2.0 ± 0.2	690	4.8	3.9
TiN	490	0.96	2.2 ± 0.1	1400	3.9	2.8

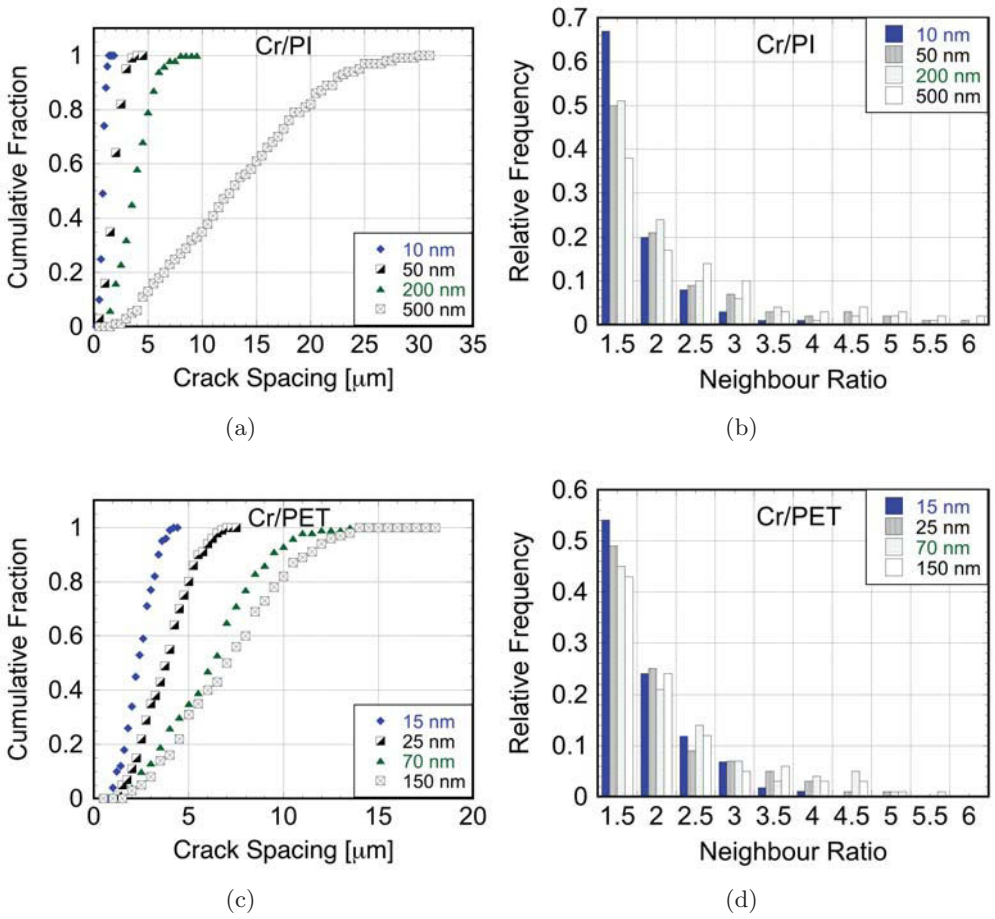

Figure 3.8 Crack spacing distribution, a), and neighbour ratios, b), for the Cr/PI, and Cr/PET, c) & d), systems. Note that the neighbour ratio distributions for all systems considerably exceed the predicted bound of two.

these systems. The crack spacing distributions show an increase in the crack spacings with increasing film thickness, as predicted by equation 2.1. The neighbour ratios for all the Cr/polymer samples are higher than the limits set in section 3.2.1. A summary of the mechanical properties of these systems is presented in table 3.2, the minimum measured crack spacing, λ_{min}, crack bounding ratio, M, maximum measured neighbour ratio, R_{max}, and percentage of neighbour ratios greater than two, R >2, are presented.

The results for the Cr/PET and Cr/PI systems suggest that film thickness plays a significant role in the cracking. In both systems the highest recorded R_{max} was for the thickest film and the lowest for the thinnest film, table 3.2. In addition, the lowest percentage of neighbour ratios greater than two was found for the thinnest films.

Neighbour ratios higher than 11 were observed on several occasions in the Cr/PI

Table 3.2 Comparison of experimentally determined parameters for the various Cr thicknesses on PI and PET investigated in this study. λ_{min} is the minimum measured crack spacing, M is the crack bounding ratio, R_{max} is the maximum measured neighbour ratio and R >2/% represents the percentage of measured neighbour ratios found to exceed two.

Substrate	Film Thickness, δ/nm	$\lambda_{min}/\mu m$	M	R_{max}	R >2/%
PET	15	0.63	6.8	4.1	22
PET	25	1.0	6.8	4.6	19
PET	70	1.5	10.7	4.9	34
PET	150	1.5	11.4	8.3	33
PI	10	0.31	5.7	3.8	12
PI	50	0.35	11.8	11.7	29
PI	200	0.78	11.2	5.4	25
PI	500	1.9	16.6	11.5	45

and Cr/Pet systems with up to 45% of the ratios being greater than the predicted value of two. These systems are fairly typical of those investigated elsewhere in the literature regarding both the substrate material and thickness and the coating thickness [24,25,49,50]. Closer investigation of what might be causing this deviation is therefore of some importance.

The theory and analysis relating to interfacial yield and the saturation of cracking in brittle films on compliant substrates makes several assumptions, the violation of which could lead to deviations from the mechanical predictions. It is inherent in the models that both the film fracture stress and interfacial strength are single-valued and that the interface remains parallel with the loading direction. In any real system some variation is to be expected in both the interfacial strength and the film fracture stress. However, an advantage of the neighbour ratio analysis is that it accounts for all long-range variations, not just variations in film thickness. It is therefore very unlikely that variation in these properties could lead to the large deviations observed. The extent to which the interface remains coplanar with the load axis during testing has never been assessed. In the following the parallel interface problem will be discussed as a possible cause of the anomalous behaviour of these brittle films on polymer substrates.

In order to understand why the film/substrate interface may not remain coplanar with the straining axis during testing it is useful to consider a simplified picture of the film and substrate during loading. In addition to this, only elastic strains are analysed in the following. In figure 3.9a the classical model of a brittle film/compliant substrate system is shown. In the model the interface is coplanar with the load axis and load can only be transferred to the film via shear at the interface. In figure 3.9b the film is shown alone with the shear along the interface simplified to a force, T, acting at the lower edges of the film. From this diagram it is easy to understand that the film would bend, as illustrated, in response to being loaded along one edge. In figure 3.9c the film is shown, once again attached to the substrate, but now with a curled interface. Some curling at the film/substrate interface is in fact

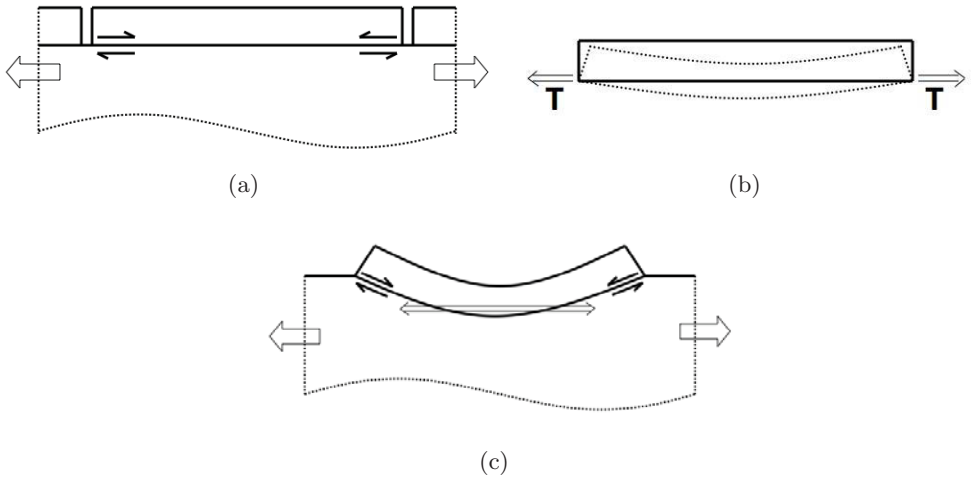

Figure 3.9 Schematic of a), the classical brittle film/compliant substrate model, b), a free body diagram of the film being loaded along one edge and c), a system with a curled film/substrate interface. Note in c) how the transfer of tensile load into the film is no longer purely through shear at the interface.

an inevitability of the tensile stress in the film loaded via the interface, the extent of this curling will depend on the difference in stiffness between the film and substrate. Lower stiffness substrates are expected to allow the interface to curl more as the force exerted by a given film fragment will be the same but the substrate deflection due to this force will be greater. This could explain why the model Al_xO_y/Cu and TiN/C systems previously analysed (E_{AlxOy} = 160 GPa, E_{TiN} = 450 GPa [51], E_{Cu} = 115 GPa) in section 3.2.2 complied well with the predictions while the polymer substrate systems (E_{Cr} = 290 GPa, $E_{PET} \approx E_{PI}$ = 3-4 GPa) do not. Figure 3.9c also illustrates schematically how significant curling of the film/substrate interface can complicate the mechanics of the system, leading to bending stresses in the coating and direct transferral of tensile stress from the substrate into the film.

To learn if the films investigated were curling in the manner described in figure 3.9 a small screw-driven tensile frame was designed such that the samples could be strained and held at load under an AFM. Figure 3.10 shows an AFM height image of a film fragment from a 150 nm Cr/PET sample strained to ∼10%, figure 3.10a, while figures 3.10b and 3.10c present a 3D view and a line scan across the same fragment. Figure 3.10d presents a film fragment line scan from a 50 nm Cr/PI sample, the scatter in the scan is due to the roughness of the film. This AFM data clearly shows vertical deflection of the films at the edges, the deflection is not as simple as that shown schematically in figure 3.9 because the substrates are in the plastic behaviour regime, complicating the forces involved. The magnitude of the deflections, around one third of the film thickness for both samples, is likely to be sufficient to cause major complications in the loading of the coating. Vertical deflections like

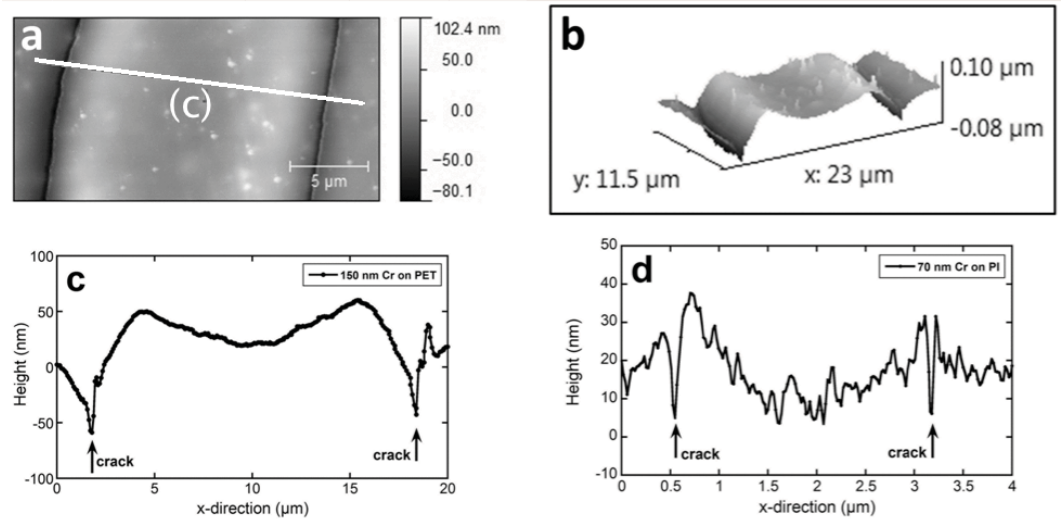

Figure 3.10 An AFM height image of the 150 nm Cr/PET system at ∼10% strain, a), shows the extent of the out-of-plane deflection in the film. This is made clearer with a 3D image, b), of the same area, c) presents a line scan across the film fragment marked in a). A similar line scan from a 50 nm Cr/PI sample is shown in d) to illustrate that this effect is general.

those shown in figure 3.10 were observed for every sample imaged under load, these deflections are not observed for unloaded samples. A recent paper by Douville et al. [52] found similar curling of the film/substrate interface both experimentally and through finite element analysis. The conclusion of these experiments is that the bending of the film causes the deviation from the predictions of the interfacial yield model. Further investigation is required to fully understand and quantify this effect.

3.3 Fragmentation Testing at Elevated Temperature

3.3.1 The Influence of Temperature on the Crack Spacing

Temperature is predicted to increase crack spacings as a result of reduced load in the substrate and hence reduced interfacial shear stresses, as explained in section 2.4. The two systems studied at elevated temperature in this thesis, Al_xO_y/Cu and Ti/PI, both show this effect. Post mortem SEM images of Al_xO_y/Cu samples strained at room temperature and at 650°C are shown along with crack spacing distributions in figure 3.11. The average crack spacing increases by 26% as the temperature of the test is increased to 650°C. This change is consistent with a 25% predicted drop in the yield stress for the Cu substrate [53]. This is consistent with the observations of Leterrier et al. [15] and Yanaka et al. [19] who observed an increase in the average saturation crack spacing of SiO_x films on PET with temperature. Leterrier et al. [15] noted that the observed increase in crack spacing correlated well with the measured decrease in elastic modulus of the PET.

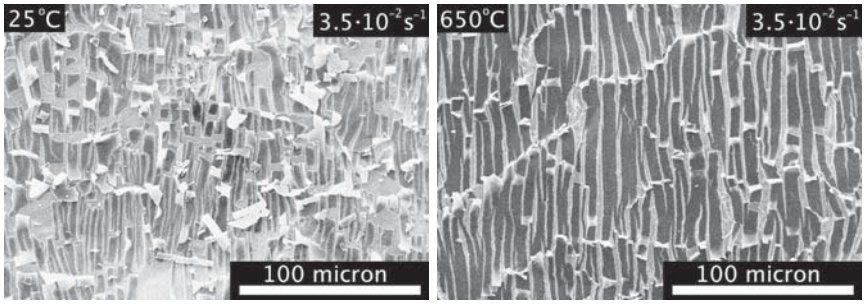

(a) (b)

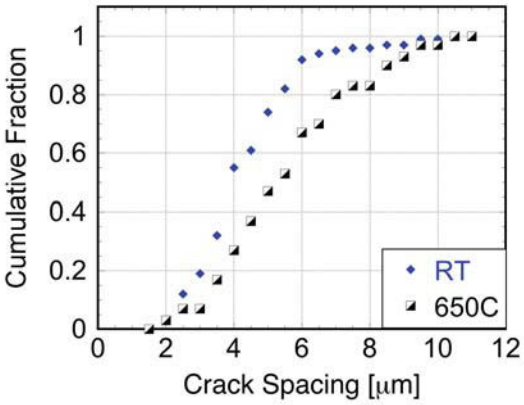

(c)

Figure 3.11 SEM micrographs of the Al_xO_y/Cu system strained to saturation at, a), room temperature and, b), 650°C. The crack spacing distributions of the two samples are plotted in c). The 26% increase in crack spacing seen for the 650°C test correlates well with the predicted drop in yield stress of the Cu substrate [53].

A Ti/PI system was investigated as a more technologically relevant application. Ti layers on polymer substrates are used as adhesion layers for conducting Au or Cu material in flexible circuitry [47, 48]. For the Ti/PI samples a comparison is made between a sample annealed at 350°C and subsequently strained at room temperature and a sample strained at 350°C, both samples are strained to the saturation regime (>20%). An annealed sample is used in place of as-deposited material as it is found, appendix E.3.1, that the Ti films undergo a transition in mechanical properties following heat treatment. Investigation of the effect of temperature on the crack spacing is therefore best made with samples having a similar thermal history. Figure 3.12 presents SEM micrographs of the annealed and 350°C tested Ti/PI samples along with crack spacing distributions.

From figure 3.12c it can be seen that the average crack spacing in the Ti films increases by more than a factor of two when straining at 350°C. This observation also fits well with the conclusions of Leterrier et al. [15]. The present experimental set-up for the elevated temperature tests does not allow for the measurement of sample load during testing so it is not possible to compare the observed increase in crack spacing with the decrease in substrate load. A factor two drop in the sample load at saturation does not however seem unreasonable for a polymer like PI.

3.3.2 The Influence of Temperature on Film Adhesion

Previous work by Cordill et al. [28] demonstrated that the adhesion of a Cu/Ti multilayer to a PI substrate reduced following thermal treatment. To investigate this effect further the adhesion of the Ti/PI system discussed in section 3.3.1 was assessed by a simple tape test. In addition, the film delamination due to buckling perpendicular to the film cracks was analysed to quantify film/substrate adhesion using a model developed by Fischer [54]. Optical micrographs of as-deposited and 350°C tested samples following a qualitative tape test are shown in figure 3.13. The increased removal of Ti film in the 350°C tested sample clearly shows that the adhesion of the thermally treated sample is lower.

The interfacial adhesion energy is quantitatively measured with the buckles that form between the cracks, figure 3.12. The model developed by Fischer et al [54] takes the strain energy between buckles, the debonding energy and the strain energy of the buckled material into account. This model was developed for brittle films on polymer substrates and buckles formed due to tensile straining. For more information on the model and technique see reference [54].

To calculate the interfacial adhesion the dimensions of the buckles are needed, namely, the buckle height, h, and half buckle width, b. When the buckles' dimensions are plotted as $\sqrt{h/\delta}$ as a function of (b/δ), where δ is the film thickness, the data can be described by:

$$\sqrt{\frac{h}{\delta}} = \sqrt[4]{2\alpha}\left(\frac{b}{\delta}\right)\left(1+\sqrt{1+\frac{3\alpha}{4}\left(\frac{b}{\delta}\right)^4}\right)^{-\frac{1}{4}}. \tag{3.4}$$

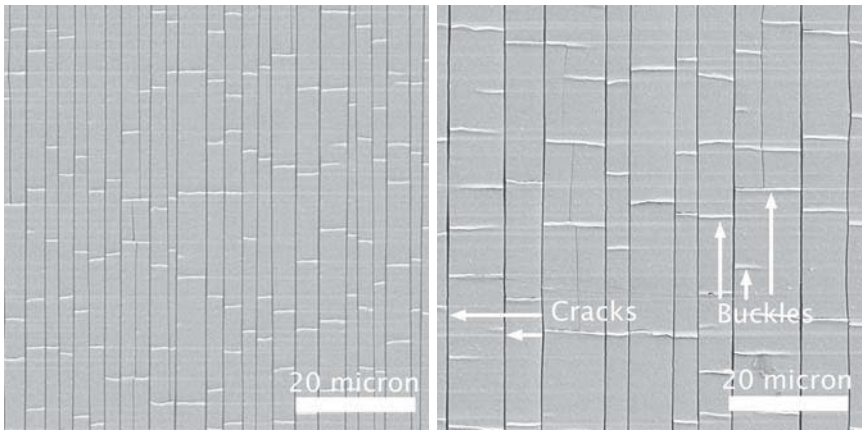

(a) (b)

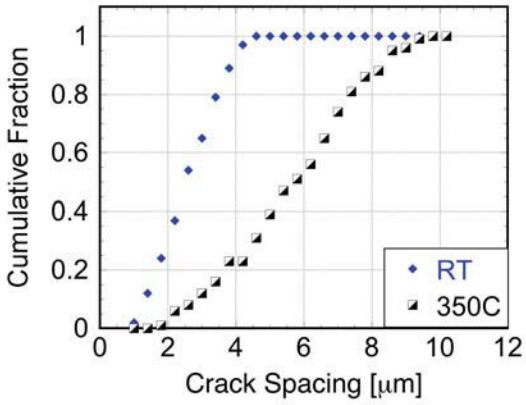

(c)

Figure 3.12 A SEM comparison of Ti/PI samples strained at room temperature, a), and 350°C, b). The crack spacing distributions for the two samples are also presented, c). The crack spacing is observed to increase by more than a factor of two when straining at 350°C.

.

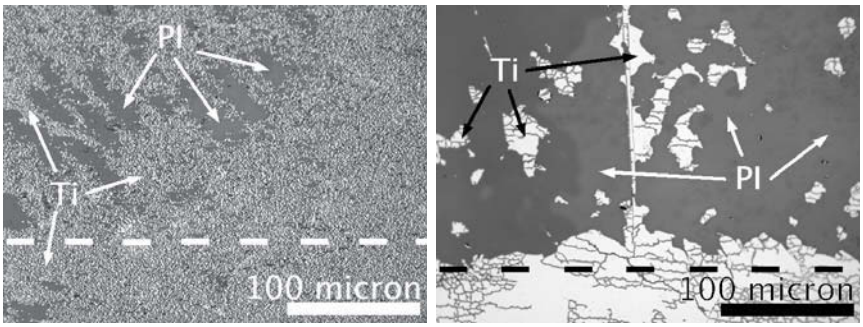

(a) (b)

Figure 3.13 Optical micrographs of the a) as-deposited Ti and b) 350°C tested Ti are presented following the application and removal of adhesive tape to the film surface. Significantly more of the 350°C tested Ti was removed by the tape, indicative of lower adhesion at the Ti/PI interface in this sample. The dashed lines mark the lower edge of the tape.

Where α is a fitting parameter. The α parameter is used to calculated the adhesion energy, Γ, using:

$$\alpha = \frac{4\Gamma}{\delta E'} \left(\frac{2}{\pi}\right)^4. \tag{3.5}$$

In equation 3.5, δ is again the film thickness and E′ is the modified elastic modulus (E′ = 130 GPa). The modified elastic modulus takes into account the elastic modulus, E, and Poissons ratio, ν, of the Ti film as:

$$E' = \frac{E}{1-\nu^2}. \tag{3.6}$$

AFM was used to image and measure the buckle dimensions. It has been previously shown [28, 54, 55] that buckles which do not travel across the whole crack fragment better describe the calculated adhesion energy. In this region of the buckle, there is no cracking of the buckle apex (top) or at the base of buckle. For the Ti buckles here only measurements from the end of partial buckles (figure 3.14) were used to determine adhesion. As shown from the different height scales in figure 3.14, the average buckle size of the film strained at 25°C is larger than at 350°C.

The adhesion energy using equations 3.4 and 3.5 is calculated by fitting α on a diagram like that shown in figure 3.15. For the as-deposited film a minimum α of $\alpha = 4.0{\cdot}10^{-4}$ is fitted, this minimum is $\alpha = 1.2{\cdot}10^{-4}$ for the 350°C tested sample. From the α values the adhesion energy was calculated as (4.7±0.6) J m^{-2} for the as-deposited film and (1.4±0.5) J m^{-2} for the film tested at 350°C. The degree of error was determined by changing the minimum α value by approximately ±0.00005 to better account for the lower data points.

High resolution TEM was used to study the Ti/PI interface. It was found that a Ti/PI interlayer, figure 3.16a, is present in the as-deposited system. This interlayer

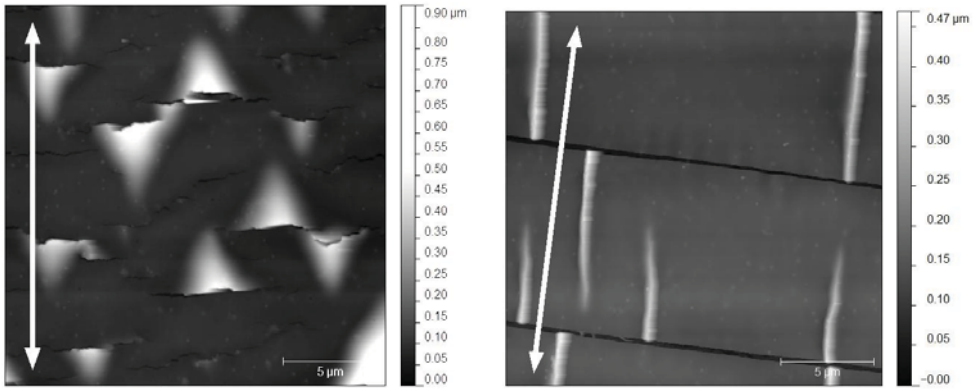

(a) (b)

Figure 3.14 AFM height images of a) the as-deposited Ti film and b) the 350°C Ti film. Note the different shape of the buckles in the samples and larger height range for the as-deposited scan. Arrows indicate the direction of straining.

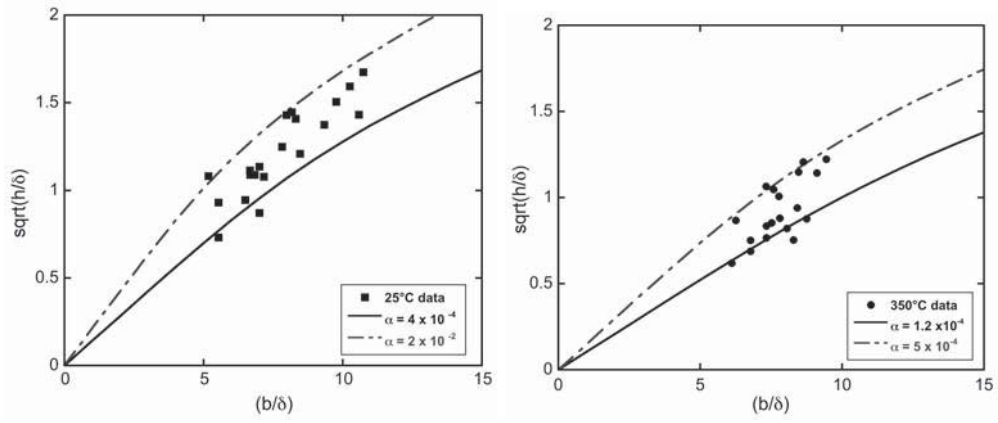

(a) (b)

Figure 3.15 Plots of $\sqrt{h/\delta}$ vs. b/δ for the as-deposited Ti, a), and the 350°C tested Ti, b), as proposed by the Fischer model [54]. The lower limit represents buckles as they first form and hence gives the most reliable measure of interfacial adhesion.

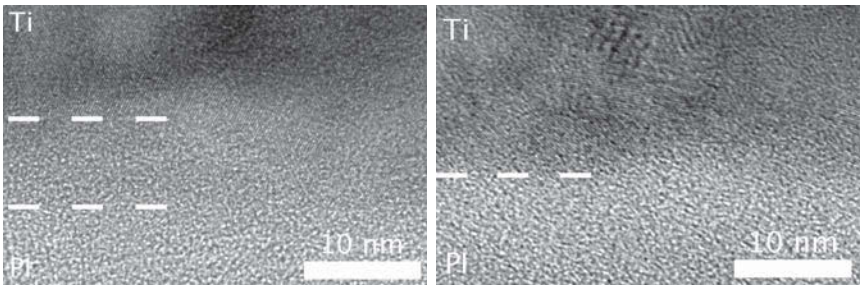

(a) (b)

Figure 3.16 Cross-sectional TEM micrographs of the Ti/PI interface of an as-deposited sample, a), and a 350°C tested sample, b). The two dashed lines in a) mark the interlayer, the dashed line in b) marks the sharper Ti/PI interface.

was not found in cross-sections of the samples tested at 350°C. This result suggests that mixing of material at the Ti/PI interface leads to higher adhesion, this is highly desirable. The Ti adhesion layers used in flexible electronic circuitry are exposed to elevated temperatures during production and use, the data presented here indicates that the adhesion of these layers to the polymer will degrade with time.

4

Guidelines for Fragmentation Testing of Brittle Film/Compliant Substrate Systems

The following is a series of guidelines for performing fragmentation testing experiments. These guidelines specifically concern fragmentation testing in the saturation regime of cracking following the interfacial yield model. Despite this, many of the recommendations made here are also valid for testing in the low strain, i.e. shear lag, regime. Links to the relevant research in this thesis are given where applicable.

- **In situ** techniques are essential for an accurate measurement of the film fracture stress and a better understanding of how cracking, buckling and delamination of the film progresses. For the thicker coatings (>1 μm) usually used in industry an optical system should be sufficient.
- **Characterisation**, particularly of the film thickness, leads to greater understanding of the processes involved and reduces errors when comparing interfacial shear strength. See appendices A.2 and B.4.3.
- Look for signs of **interfacial debonding** in strained samples. If the interface is debonding then the measured crack spacings will not accurately reflect the length of interface over which stress is transferred and calculations of the interfacial shear stress will be inaccurate.
- Uniformity of substrate deformation to high strains is required for crack saturation to be reached and hence usage of the interfacial yield model to be possible. A sufficiently thick substrate is therefore required if **localisation of strain** at film cracks is to be avoided, see appendix D.3.2. This is more likely

to be a problem if the film is significantly stiffer than the substrate, as is often the case for coatings on polymers.

- Care should be taken applying the interfacial shear model to systems with a very large film/substrate **Young's modulus difference**. Experiments infer that a very stiff coating can bend out of the loading plane during testing, greatly complicating the mechanics of the problem. See appendix D.3.4.
- The calculation of **neighbour ratios** (appendix B.4.3) when applying the interfacial yield model to a system can be a useful indicator of whether the model is applicable, see sections 3.2.2 and 3.2.3. If neighbour ratios of greater than three are measured, or if more than 10% of ratios are greater than two then it is likely the model is not applicable and further investigation is required.

5
Conclusions

Methods are presented for better characterisation and comparison of thin brittle films on compliant substrates. Consideration of film thickness variations for Al_xO_y and TiN films on Cu demonstrated that the statistical distribution of strength in the coating is due to long range variations, notably film thickness.

Using the same neighbour ratio approach shown to be effective for Al_xO_y and TiN films on Cu, Cr films on polyethylene teraphthalate and polyimide substrates were shown to not meet the predictions of the interfacial yield model. The formation of small crack spacings in the final stages of straining prior to crack saturation seems to confirm that the interfacial yield model is not appropriate for these materials. AFM measurements show that the brittle films are not coplanar with the strain axis during testing, it it inferred that this behaviour causes the failure of the model. Further work is needed to quantify the effect of film bending on the cracking of the film but the difference in elastic moduli between film and substrate is an important factor.

Through experiments on Al_xO_y/Cu and Ti/polyimide it has been shown that fragmentation testing can be useful in investigating the properties of coatings products at elevated temperatures. The results for the Ti/polyimide system are particularly interesting, suggesting that the adhesion of Ti layers to polyimide substrates can decrease significantly following thermal exposure. A threefold reduction in adhesion was measured using buckle induced film delamination and a total energy approach, as proposed by Fischer [54].

A series of guidelines is presented for the conduction of reliable, reproducible fragmentation testing of brittle films on compliant substrates. By following these guidelines quantitative comparison of different film deposition procedures and dif-

ferent film systems can be made. It is hoped that by producing these guidelines, with experimental data to demonstrate their importance, fragmentation testing can be a useful technique in the development of coated systems both in academia and industry.

Bibliography

[1] DB Marshall, AG Evans, J. Appl. Phys. 56, 2632-2638 (1984)

[2] B Rother, BA Dietrich, Thin Solid Films 250, 181-186 (1994)

[3] A Abdul-Baqi, E Van der Giessen, Thin Solid Films 381, 143-154 (2001)

[4] G Dehm, M Rühle, HD Conway, R Raj, Acta Mater. 45, 489-499 (1997)

[5] SJ Bull, Tribology Int. 30, 491-498 (1997)

[6] RD Arnell, Surf. Coat. Technol. 43-44, 674-687 (1990)

[7] GT Gao, PT Mikulski, JA Harrison, J. Am. Chem. Soc. 124, 7202-7209 (2002)

[8] H Hirakata, T Kitamura, Y Yamamoto, Int. J. of Solids and Structures 41, 3243-3253 (2004)

[9] K Matoy, T Detzel, M Müller, C Motz, G Dehm, Surf. Coat. Technol. 204, 878-881 (2009)

[10] LB Freund, S Suresh, Thin Film Materials, Cambridge University Press, Cambridge (2003)

[11] A Kelly, WR Tyson, J. Mech. Phys. Solids 13, 329-338 (1965)

[12] MS Hu, AG Evans, Acta Metall. 37, 917-925 (1989)

[13] DC Agrawal, R Raj, Acta Metall. 37, 1265-1270 (1989)

[14] F Ahmed, K Bayerlein, SM Rosiwal, M Göken, K Durst, Acta Mater. 59, 5422-5433 (2011)

[15] Y Letterier, L Boogh, J Andersons, J-AE Månson, J. Polym. Sci. B: Polym. Phy. 35, 1449-1461 (1997)

[16] MW Chen, I Dutta, Appl. Phys. Lett. 77, 4298-4300 (2000)

[17] VC Jobin, R Raj, SL Phoenix, Acta Metall. Mater. 40, 2269-2280 (1992)

[18] KA Peterson, I Dutta, MW Chen, Acta Mater. 51, 2831-2846 (2003)

[19] M Yanaka, Y Kato, Y Tsukahara, N Takeda, Thin Solid Films 355-356, 337-342 (1999)

[20] J Rice, Food Process. 78 (1992)

[21] N Bowden, S Brittain, AG Evans, JW Hutchinson, GM Whitesides, Nature 393, 146-149 (1998)

[22] Y Sun, WM Choi, H Jiang, YY Huang, JA Rogers, Nature Nano. 1, 201 (2006)

[23] X Lu, Y Xia, Nature Nano. 1, 163-164 (2006)

[24] Y Leterrier, L Médico, F Demarco, J-AE Månson, U Betz, MF Escolà, M Kharrazzi Olsson, F Atamny, Thin Solid Films 460, 156-166 (2004)

[25] S Frank, UA Handge, S Olliges, R Spolenak, Acta Mater. 57, 1442-1453 (2009)

[26] MJ Cordill, A Taylor, J Schalko, G Dehm, Metall. Mater. Trans. A 41, 870-875 (2010)

[27] J Lohmiller, NC Woo, R Spolenak, Mater. Sci. Eng. A 527, 7731-7740 (2010)

[28] MJ Cordill, AA Taylor, J Schalko, G Dehm, Int. J. Mater. Res. 102, 729-734 (2011)

[29] HL Cox, Br. J. Appl. Phy. 3, 72-79 (1952)

[30] F Bodino, G Baud, M Benmalek, JP Besse, HM Dunlop, M Jacquet, Thin Solid Films 241, 21-24 (1994)

[31] PB Kirk, RM Pilliar, J. Mater. Sci. 34, 3967-3975 (1999)

[32] P Villechaise, X Milhet, B Angleraud, V Fouquet, L Pichon, A Straboni, PY Tessier, Thin Solid Films 482, 324-329 (2005)

[33] MJ Filiaggi, RM Pilliar, D Abdulla, J. Biomed. Mater. Res. 33, 239-256 (1996)

[34] J Plojoux, Y Leterrier, J-AE Månson, F Templier, Thin Solid Films 515 6890-6898 (2007)

[35] XL Peng, TW Clyne, Thin Solid Films 312, 219-227 (1998)

[36] G Singh, Y Yu, F Ernst, R Raj, Acta Mater. 55, 3049-3057 (2007)

[37] WA Curtin, J. Mater. Sci. 26, 5239-5253 (1991)

[38] P Feillard, G Désarmot, JP Favre, Composites Sci. Tech. 50, 265-279 (1994)

[39] J Andersons, Y Leterrier, G Tornare, P Dumont, J-AE Månson, Mech. Mater. 39, 834-844 (2007)

[40] R Gulino, SL Phoenix, J. Mater. Sci. 26, 3107-3118 (1991)

[41] W Weibull, J. Appl. Mech. 18 (1951)

[42] G Saada, Phil. Mag. 85, 3003 (2005)

[43] LA Gianuzzi, F A Stevie, Micron 30, 197 (1999)

[44] JC Bravman, R Sinclair, J. Electron Microscopy Tech. 1, 53 (1984)

[45] AF Jankowski, MA Wall, J. Mater. Res. 9, 31 (1994)

[46] NG Chechenin, J Bøttinger, JP Krog, Thin Solid Films 304, 70-77 (1996)

[47] OS Heavens, J. Phys. Radium 11, 355-360 (1950)

[48] JC Hoogvliet, WP van Bennekom, Electrochemica Acta 47, 599-611 (2001)

[49] Y Letterier, J Andersons, Y Pitton, J-AE Månson, J. Polym. Sci. B: Polym. Phy. 35, 1463-1472 (1997)

[50] M Yanaka, Y Tsukahara, N Nakaso, N Takeda, J. Mater. Sci. 33, 2111-2119 (1998)

[51] E Török, AJ Perry, L Chollet, WD Sproul, Thin Solid Films 153, 37-43 (1987)

[52] NJ Douville, Z Li, S Takayama, MD Thouless, Soft Matter 7, 6493-6500 (2011)

[53] M-H Nadal, P LePoac, J. App. Phy. 93, 2472-2480 (2003)

[54] MJ Cordill, FD Fischer, FG Rammerstorfer, G Dehm, Acta Mater. 58, 5520-5531 (2010)

[55] MJ Cordill, K Schmidegg, G Dehm, Phil. Mag. Lett. 91, 530-536 (2011)

6
List of appended papers

Paper A
A.A. Taylor, M.J. Cordill, G. Moser, G. Dehm
A Mechanical Method for Preparing TEM Samples from Brittle Films on Compliant Substrates
Practical Metallography 48 (2011) 408–413

Paper B
A.A. Taylor, V. Edlmayr, M.J. Cordill, G. Dehm
The Effect of Film Thickness Variations in Periodic Cracking: Analysis and Experiments
Surface Coatings and Technology, doi:10.1016/j.surfcoat.2011.07.047

Paper C
A.A. Taylor, V. Edlmayr, M.J. Cordill, G. Dehm
The Effect of Temperature and Strain Rate on the Periodic Cracking of Amorphous Al_xO_y Films on Cu
Surface Coatings and Technology, doi:10.1016/j.surfcoat.2011.08.011

Paper D
A.A. Taylor, M.J. Cordill, G. Dehm
On the limits of the Interfacial Yield Model for Fragmentation Testing of Brittle Films on Polymer Substrates
Submitted for publication in Philosophical Magazine

Paper E
A.A. Taylor, M.J. Cordill, L. Bowles, J. Schalko, G. Dehm

An Elevated Temperature Study of a Ti Adhesion Layer on Polyimide
Submitted for publication in Materials Science and Engineering A

Remarks

In the appended papers, I, Aidan Taylor, performed all experiments, data analyses and was the primary author with the following exceptions:

- in **paper A** M. J. Cordill and G. Moser assisted in the development of the sample preparation technique.
- In **papers B, C, D and E** M. J. Cordill carried out the AFM measurements.
- In **papers B and C** V. Edlmayr produced the amorphous Al_xO_y coatings.
- In **paper E** L. Bowles performed the *ex situ* experiments and crack spacing analysis as part of a summer project. J Schalko produced the Ti films used in the study.
- My supervisor, G. Dehm, contributed in all the papers by providing expert experimental guidance, helpful discussions and editorial improvement.

A

A Mechanical Method for Preparing TEM samples from Brittle Films on Compliant Substrates

A A Taylor[a], M J Cordill[a,b], G Moser[b], G Dehm[a,b]

[a]Erich Schmid Institute of Materials Science,
Austrian Academy of Sciences, Jahnstraße 12, A–8700 Leoben, Austria
[b]Department Materials Physics, Montanuniversität Leoben, Jahnstraße 12, A–8700 Leoben, Austria

Abstract

Preparing transmission electron microscopy (TEM) samples from thin films is technically challenging and traditional preparation routes can sometimes introduce unacceptable artefacts or even prove impossible. A novel method of preparing plan view TEM samples from thin films by a purely mechanical method is assessed. Two examples of films prepared by this route are briefly presented, a Cr film on PET and an amorphous Al_xO_y film on Cu. The application of this method allows for TEM analysis of the Cr film without the problems associated with a polymer such as PET disintegrating under the electron beam. For the Al_xO_y films it is demonstrated that this purely mechanical preparation prevents crystallisation of the film resulting from conventional ion milling preparation routes. The technique also allows for an upper bound of thickness approximation for these films.

A.1 Introduction

In the present age of microelectronics and high-tech devices, such as sensors and actuators, thin film materials are very important. Flexible electronics and electronics integrated into clothes are presently lauded as exciting prospects for the future [1, 2]. At the same time thin films are being used to enhance the properties of more everyday materials like cutting tools [3, 4] and food packaging [5, 6]. Microstructure is a critical factor in the performance of all materials [7] though arguably more so in the case of thin films. For thin films and lines the geometrical dimensions of the materials are on a similar scale to the microstructure and so relatively small changes in the grain structure and orientation can greatly affect the performance of the system as a whole [8, 9]. Careful assessment of the microstructure of such materials is therefore very important in any investigation concerning other aspects of the film properties such as conductance, adhesion energy and gas permeability.

For some film/substrate systems it is extremely difficult to produce samples for transmission electron microscopy (TEM) by conventional means such as focussed ion beam (FIB) lift-out [10] or dimple grinding and ion milling [11]. For the two cases examined in this article, conventional preparation routes pose difficulties due to instability of the substrate in the electron beam and microstructural modification of the film by ion damage, for Cr films on PET (polyethylene teraphthalate) and amorphous Al_xO_y (a-Al_xO_y) films on Cu, respectively. PET is unstable in the electron beam due to its electrical insulation and relatively low melting point, leading to very rapid heating, distortion and vaporisation of the material. Due to these problems, conventional TEM sample preparation routes, where at least some of the substrate remains with the film, lead to serious difficulties during imaging. Solutions to this problem, including impregnating the polymer with a stain, e.g. RhO_4 [12], and depositing carbon onto the finished TEM sample, can introduce their own artefacts and affect the film material.

In the a-Al_xO_y films it is possible that the input energy of the Ar^+ or Ga^+ ions during sample preparation leads to nucleation of crystallites. A similar effect can be observed *in situ* in the TEM due to energy input from the electron beam [13]. It is therefore very difficult to get an accurate description of the microstructure and crystallinity of such a film. In both of these cases the film is very brittle with little or no plastic deformation expected while the substrate is highly compliant, it was therefore envisioned that a purely mechanical removal of the films might be possible.

A.2 Experimental

The nominally 10 nm thick Cr films were deposited using an industrial web coater on to commercially available 50 μm thick PET substrates by DC magnetron sputtering with an Ar plasma gas. The sputter process was carried out with an Argon pressure of around $8 \cdot 10^{-3}$ mbar. In addition to these films nominally 50 nm and 120 nm thick Cr films were studied to some extent. These thicker films were produced by repeating

the deposition process without breaking vacuum until the desired thickness was reached. The a-Al_xO_y films were deposited in a commercial CemeCon CC800/9MLT plant by reactive magnetron sputtering. An O_2/Ar gas flow was used with a total pressure of 0.87 Pa and the substrate temperature was held at approximately 640°C. Further details on the deposition parameters of the a-Al_xO_y films can be found in reference [14].

The first stage of the preparation of the TEM samples is to uniaxially strain the samples to 15-30% (engineering strain) in order to induce cracking and delamination of the films at the interface (Figure A.1). Film fragments were then carefully transferred from the substrate onto a carbon-coated Cu TEM grid using a ceramic blade. In the case of the Cr film, the grid was then loaded into a plasma cleaner (Fischione Model 1020) using an 80/20 Ar/O2 plasma gas and cleaned for 10 min, this helped to remove any fragments of PET that may have been transferred with the film.

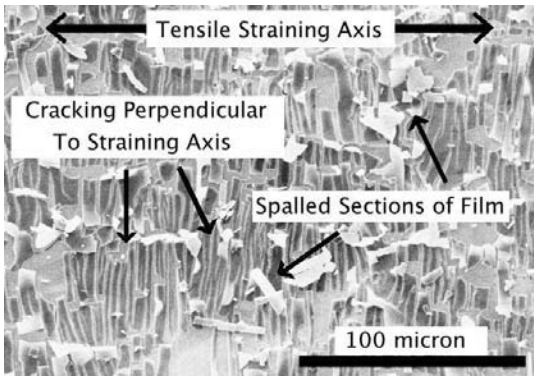

Figure A.1 SEM image of an a-Al_xO_y film following 15% straining, note the large degree of spalling through cracking and buckling.

For comparison, two TEM specimens from the a-Al_xO_y film were also produced by conventional Ar^+ ion milling, one plan view and one cross-sectional. For the plan view sample this involved dimpling of the Cu substrate from the reverse side to approximately 10 μm thickness before Ar-ion milling (Gatan DuoMill, 6 kV) the sample from the Cu side only until a hole was produced. The procedure was the same for the cross-sectional sample with the exception that both film and substrate were, by definition, dimpled and milled simultaneously [11].

The samples were analysed using two microscopes, a Philips CM12 (LaB_6) operating at 120 kV for initial analysis and a JEOL 2100F operating at 200 kV for thicker films and high resolution imaging (HRTEM). The technique produces an agglomeration of film fragments as shown in Figure A.2a. Due to the wide variation in orientation angles of the film fragments it is important to use a double tilt holder in analysing films made by this technique in order to ensure the film plane is perpendicular to the beam. A useful side effect of this technique is that an upper bound estimate of the film thickness can be made. This procedure is carried

out through the following method. A film fragment lying reasonably parallel to the electron beam is identified at zero tilt. The goniometer tilt function is then used to tilt this fragment to an angle where it provides a minimum cross section to the electron beam. The minimum sample cross section should then be found using the secondary tilt of the holder by the same procedure. These two steps are iterated several times to ensure that the minimum cross section of fragment with respect to the beam is achieved. This image can then be used to measure an upper bound to the film thickness. For better accuracy, the use of a TEM calibration standard and the smallest possible film fragments is recommended.

A.3 Results

By tilting the holder such that a film fragment is parallel with the electron beam, Figures A.2b and A.2d, an upper limit to the film thickness can be made. Using this technique the thickness of the Cr film is estimated to be 15 nm while the a-Al_xO_y film is approximately 300 nm thick. In the case of the a-Al_xO_y film this estimate is validated by the conventionally produced sample, Figure A.2c.

Shown in Figure A.3 are selected area diffraction, bright field conventional TEM and HRTEM images of the 15 nm Cr film. It is possible to see from Figure A.3 that the film is crystalline, non-porous and of body centred cubic crystal structure. The last point is of particular interest as the crystal structure of thin metal films can deviate from equilibrium structures [15] and it had not previously been possible to confirm this by laboratory x-ray measurements due to the film being so thin. Due to the presence of moiré fringes, as observed in Figure A.3c, it can be deduced that even at this very low thickness the film is not purely composed of columnar grains. In fact the microstructure of this film seems to be quite complex, some grains appear to be significantly larger than the film thickness, as evident from the dark diffracting regions in Figure A.3b, these grains are surrounded, both to the sides as well as above and/or below, by far smaller grains, as seen in Figure A.3c.

Figure A.4 shows plan view TEM images of the a-Al_xO_y films prepared by the technique presented here and by a conventional ion-thinning method. The principal source of contrast in both of these images is the thickness contrast due to surface roughness of the films, this roughness can be seen in Figure A.2c. An important point to note however is the difference in the diffraction pattern profiles, Figures A.4c and A.4d. In both of the profiles displayed it is possible to make out a broad peak close to the transmitted beam due to scattering from amorphous material as well as sharper peaks due to diffraction from small equiaxed crystallites. These sharp diffraction peaks are consistent with the formation of crystallites with a δ-Al_xO_y [16] structure. Note however the very strong difference in intensity of the crystalline peaks in the two patterns, it is clear that conventional preparation has led to considerable crystallisation of the film. This highlights the care that should be taken in assessing the crystallinity of films such as these.

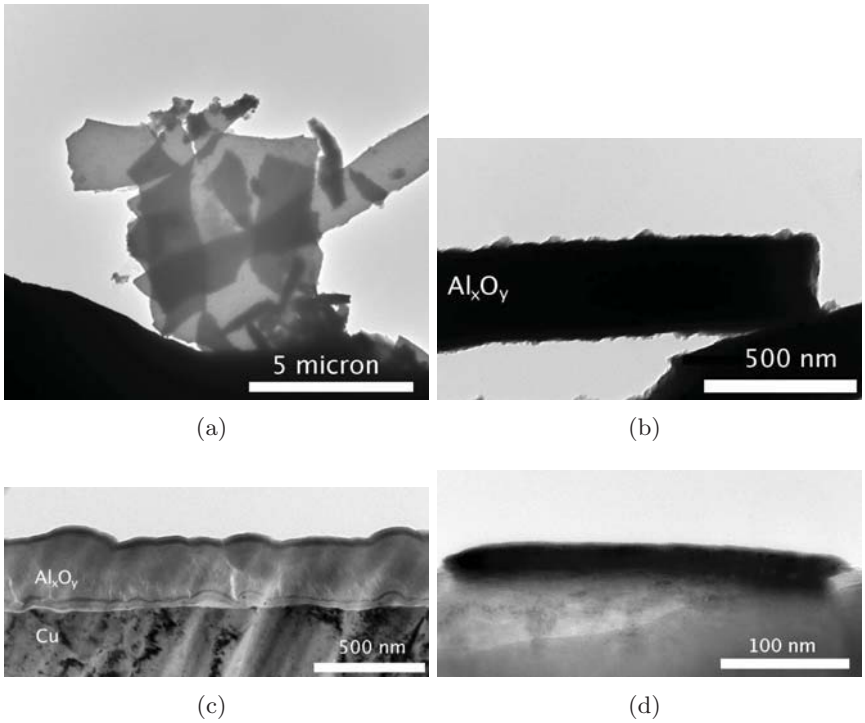

Figure A.2 (a) TEM micrograph recorded at low magnification showing the a-Al_xO_y fragments transferred to the Cu grid. (b) A fragment of the film viewed edge on, giving a thickness estimate of ∼300 nm. (c) TEM sample of the a-Al_xO_y/Cu system prepared by conventional means showing the film roughness and providing a comparison for the thickness measurement allowed by the new technique. (d) A thickness estimate image for the Cr film, here the thickness is approximately 15 nm.

A.4 Discussion

This technique has been used to examine two examples of thin, brittle films on compliant substrates. The brittle nature of these films is deemed critical for the validity of the results obtained. The mechanical means of removing the films could very easily induce plastic deformation in films where this is expected to be possible, such as Cu or Au thin films. Plastic deformation in the film would lead to microstructural artefacts, these artefacts are indistinguishable from original microstructural features and hence the microstructural assessment is flawed. A further disadvantage to this technique is the limited number of systems to which it can be applied. The TEM foils produced by this method are only plan view of the full film thickness and hence only films thin enough to be effectively penetrated by the electron beam can be studied.

The compliance of the substrate is used to aid delamination of the film from the substrate such that it can be more easily removed for study. The important point is that the film delaminates from the substrate. Thus if delamination can be induced

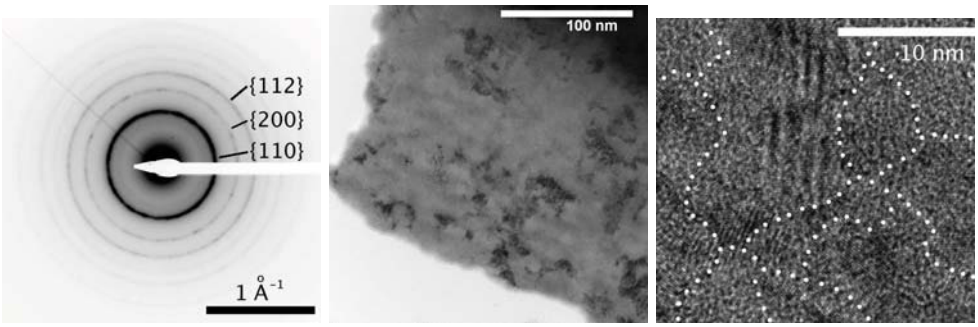

(a) (b) (c)

Figure A.3 (a) Selected area diffraction, (b) conventional TEM and (c) high resolution TEM of the 15 nm Cr film. The ring pattern in (a) is consistent with a bcc structure, indexed, while the fringes in the centre of (c) are moiré fringes, indicative of the electron beam passing through two grains at that point. In (c) some grain boundaries have been highlighted to aid interpretation.

by other means when using stiff, brittle, substrates then this technique may also be applicable for study of such films.

With this technique plan view samples of complete pieces of film are analysed, the thickness of the films to be analysed is therefore an important consideration. The a-Al_xO_y film studied here was approximately 350 nm at its thickest points; this is an upper limit for electron transparency at 120 kV accelerating voltage. As part of this study Cr films on PET up to thicknesses of 150 nm were studied. As these films have a much stronger interaction with the electron beam the upper limit for study at 120 kV was 100 nm. It was possible to study all of these Cr films, including the 150 nm thickness, by operating at 200 kV, though for these particular films the microstructure becomes very difficult to interpret at thicknesses greater than 50 nm due to the large number of overlapping grains. The thickness of film that can be investigated via this preparation route is therefore dependent upon both the electron scattering cross section of the film material and the acceleration voltage of the microscope used, as with standard TEM sample preparation.

A.5 Conclusion and summary

A new TEM specimen preparation technique is presented here for the production of samples from brittle films on compliant substrates. As a purely mechanical technique certain artefacts of conventional TEM preparation routes can be avoided.

It has been demonstrated that this route can produce plan view samples of Cr films on PET for microstructural analysis. Due to ease of preparation, this technique can be more generally applicable to any brittle film on a polymer substrate so long as they are sufficiently thin to be penetrated by the electron beam.

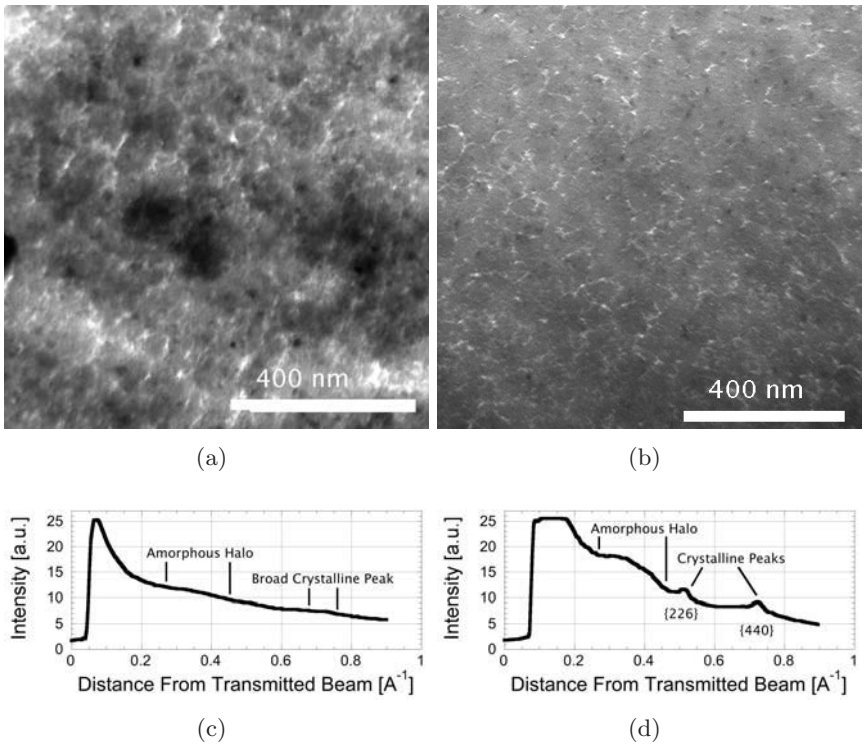

Figure A.4 Plan view TEM images of the a-Al_xO_y film. (a) Bright field TEM image from a sample prepared by the new technique, (b) the sample was dimple-ground and ion-milled from the substrate side. (c) and (d) Line profiles extracted from selected area diffraction patterns of the areas shown in (a) and (b), the drops in intensity close to the origin are due to a beam blanking rod. Note should be taken of the two peaks due to crystalline diffraction found in the ion-milled sample, (d), that are either not present or greatly broadened in the sample prepared by the new technique, (c). The plateau below 0.2 $Å^{-1}$ in (d) is due to saturated pixels from the direct beam and have no significance.

Plan view samples of a-Al_xO_y films can be produced in such a way that the ion damage associated with all other preparation routes is avoided. This method is expected to be applicable to other similar systems like gas barrier and hard coatings.

Acknowledgements

Viktoria Edlmayr and Klaus Schmidegg are gratefully acknowledged for supplying the films used in this study.

Bibliography to paper A

[1] SP Lacour, S Wagner, Appl. Phy. Lett. 82, 2404 (2003)

[2] SP Lacour, C Tsay, S Wagner, IEEE Electron Device Lett. 25, 792 (2004)

[3] O Kyrylov, R Cremer, D Neuschütz, Surf. Coat. Technol. 163-164, 203 (2002)

[4] PH Mayrhofer, C Mitterer, L Hultman, H Clemens, Prog. Mater. Sci. 51, 1032 (2006)

[5] J Rice, Food Process. 78 (1992)

[6] Y Leterrier, Prog. Mater. Sci. 48, 1 (2003)

[7] G Saada, Phil. Mag. 85, 3003 (2005)

[8] G Dehm, TJ Balk, H Edongué, E Arzt, Microelectr. Eng. 70, 412 (2003)

[9] S Zhang, D Sun, Y Fu, H Du, Thin Solid Films 447-448, 462 (2004)

[10] LA Gianuzzi, F A Stevie, Micron 30, 197 (1999)

[11] JC Bravman, R Sinclair, J. Electron Microscopy Tech. 1, 53 (1984)

[12] K Friedrich, Pract. Metallography 16, 321 (1979)

[13] C Pan, P Shen, S-Y Chen, J. Crystal Growth 299, 393-398 (2007)

[14] V Edlmayr, M Moser, C Walter, C Mitterer, Surf. Coat. Technol. 204, 1576-1581 (2010)

[15] AF Jankowski, MA Wall, J. Mater. Res. 9, 31 (1994)

[16] I Levin, D Brandon, J. Am. Cer. Soc. 81, 1995 (1998)

B

The Effect of Film Thickness Variations in Periodic Cracking: Analysis and Experiments

A A Taylor[a], V Edlmayr[b], M J Cordill[a,c], G Dehm[a,c]

[a]Erich Schmid Institute of Materials Science, Austrian Academy of Sciences, A-8700 Leoben, Austria
[b]Department of Metallurgy and Materials Testing, Montanuniversität Leoben, Roseggerstraße 12, A–8700, Leoben, Austria
[c]Department Materials Physics, Montanuniversität Leoben, Jahnstraße 12, A–8700 Leoben, Austria

Abstract

Periodic cracking experiments are frequently used in the assessment of interface quality in brittle film/compliant substrate systems. Through these techniques it is possible to extract a quantitative measure of interface shear strength and therefore assess the mechanical suitability of the films for application. The influence of film thickness inhomogeneities on the crack spacing is assessed in this study. While film thickness inhomogeneities are always present in thin film systems, only nominal thickness values have been considered up to this point. By defining two separate regimes of film thickness variation, roughness and unevenness, in relation to the crack spacing, the influence of such variation on the data is analysed. The results of this analysis are then considered in reference to a model system of an amorphous alumina film on a copper substrate (Al_xO_y/Cu), the limits of this analysis are then discussed.

B.1 Introduction

Brittle films supported by compliant substrates are important in many emerging technological applications including flexible electronic devices [1–4], hard coatings [5–7], joint replacement materials [8, 9] and gas barrier coatings [10–13]. In all these applications the functional properties of the film (eg. electrical conductivity, hardness, gas impermeability) are combined with the compliance of the substrate in order to enhance the properties of the system as a whole. It is desirable in these systems to determine a measure of interface strength as failure of the interface leads to a rapid degradation of properties and component failure. As an example, a replacement joint that has been surface engineered with a hard coating to enhance the wear properties must also be optimised with respect to the film/substrate interface in order to prevent failure by spalling of the film [14].

A number of theoretical approaches have been developed to analyse the data produced by experiments such as uniaxial tension [15–17], instrumented indentation [18–20] and micromechanical testing [21, 22] of these interfacial systems. Uniaxial testing of brittle film/compliant substrate systems, also known as periodic cracking or film fragmentation testing, is relatively simple to perform and as such is frequently applied in the development of coatings for industrial application [8, 23, 24]. The technique is of particular value when considering the effects of substrate preparation [8] and deposition parameters [23, 24]. For this kind of comparison it is critical that differences in film thickness variation between systems can be accounted for.

Periodic cracking analysis is based on the widely-used method to measure the maximum shear stress at the interface that has its roots in the derivation of Kelly and Tyson [25]. Originally derived to determine the interfacial shear forces at play in fibre composite materials, the fragmentation approach has since been modified to apply to a film/substrate interface [11, 15, 17]. In this analysis the saturation of perpendicular cracks in the films observed experimentally is explained by the necessity for stress to be transferred to the film via shear stress at the interface acting over a finite distance. A key prediction of this analysis is that the longest observed spacing between adjacent cracks in the film is twice the length of the shortest crack separation. This prediction arises as follows. For a strained film segment prior to saturation a finite length is required for shear stresses at the interface to transfer tensile stress to the film, figure B.1a. Upon sufficient straining the transfer of shear stress at the interface becomes sufficient to build a tensile stress in the film that exceeds the tensile fracture strength of the film, σ_f. If the fracture strength of the film is taken to be single-valued then the earliest point at which a film can fracture, the minimum fracture length (λ_{min}), is the point at which the fracture stress of the film is first reached, this is indicated in figure B.1a. One can imagine that were the film to fracture at twice this length then transfer of shear stress at the interface would be just sufficient to reach the fracture stress of the film in the centre of the segment, indicated in figure B.1b. As such, any segment longer than this maximum fracture length, $\lambda_{max} = 2\lambda_{min}$, would be expected to fracture until all segments lie between these two values and no further fragmentation can occur, this is the

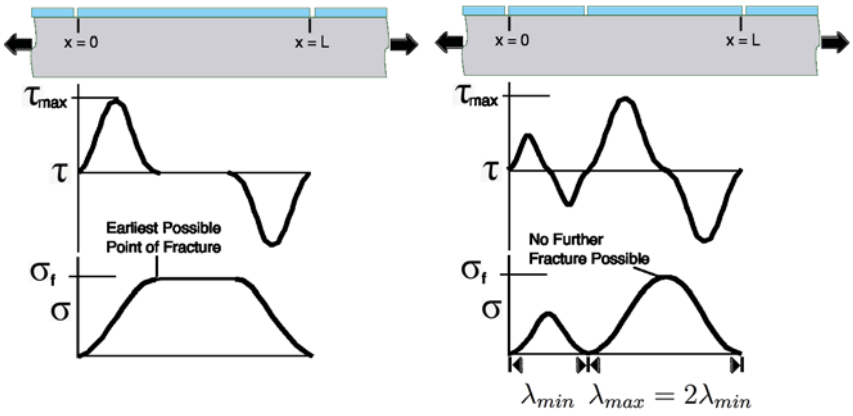

(a) (b)

Figure B.1 Schematic of the theoretical basis of shear lag and the predicted bounding of two between the shortest and longest crack spacings.

saturation condition. This shear transfer analysis leads to the following relation for the maximum shear stress at the interface:

$$\tau_{max} = K\frac{\delta\ \sigma_f}{\lambda_x}. \tag{B.1}$$

In equation B.1, τ_{max} is the maximum shear stress sustained at the interface, δ is the film thickness, σ_f is a failure stress of the film, λ_x is a characteristic film cracking length in the steady state and K is a numerical constant. Depending on the exact model found in the literature, the values of λ_x and K vary according to whether λ_{min}, λ_{mean} or λ_{max} is used, if residual film stress [13] is accounted for and the exact shear stress profile assumed in the model. All the work does follow this general form and hence all the values of τ_{max} determined by this method are directly dependent upon the film thickness. For a more complete understanding of the periodic cracking concept and its application to thin film systems the reader is directed to Agrawal and Raj's paper [17].

It is the aim of this study to shed light on how film thickness inhomogeneities can alter the interfacial shear strength data measured through film cracking experiments. The issue of thickness inhomogeneities has never been addressed in the literature but may have severe implications on the validity of the widely-used approach for determining interfacial shear strength.

In reality, the fracture strength of brittle films are not single-valued and are better described by a Weibull distribution of film strengths. The theoretical treatment by Curtin [26] demonstrated that a broadening of the fragment distribution is expected when fibres or films have a Weibull distribution of strengths. A number of authors have demonstrated this through modelling of fibre composite systems [27–29], a review of this work and fragmentation testing for fibre composites generally has been

written by Feillard et al. [30]. The nature of the flaws leading to the distribution of strengths is not discussed.

Based on analytical work, strategies for how film thickness should be characterised prior to testing in order to minimise data evaluation artefacts are outlined. The results of periodic cracking experiments on amorphous alumina films on copper substrates (Al_xO_y/Cu) are presented along with an analysis of the data according to the principles put forward here. In addition, it is demonstrated that by accounting for film thickness variations it is possible to reduce the bounding of the smallest to largest crack spacings, within the errors of the experiment, to that predicted by periodic cracking of a film with single-valued fracture strength. This suggests the thickness variations are the principal cause of the statistical strength distribution.

B.2 Experimental

The alumina film deposition was carried out in an industrial-scale sputtering plant (CemeCon CC800/9MLT) by DC magnetron sputtering of Al targets in an O_2/Ar atmosphere, total pressure 0.87 Pa, at a temperature of $640 \pm 10°C$. All of the films used in this study were deposited simultaneously, ensuring equivalent properties and thickness. Further details on the deposition set-up are reported in reference [31]. The substrates are commercially electropolished OFHC-grade Cu (min. 99.99% Cu, ASTM designation C10100) dogbone samples.

Atomic force microscopy (AFM, Digital Instruments Dimension 3100) was carried out on both the bare substrate and the deposited film. In order to determine roughness, 5 line scans parallel to the eventual loading direction, approximately the same length as the maximum crack spacing, should be taken for each sample and the maximum peak-to-trough difference determined. These peak-to-trough values are then averaged to give R_z [32, 33], many instruments carry out this evaluation automatically. In the present study 5 μm lines were used.

For analysis of film thickness and a further investigation of the film topography transmission electron microscopy (TEM, Philips CM12 and JEOL 2100F) samples of the films were prepared. These samples were produced by dimple grinding (Gatan Model 656) and Ar^+ ion milling (Gatan DuoMill and Bal-tec RES 101).

The periodic cracking experiments were carried out on a mechanical testing rig (Kammrath & Weiss) capable of highly accurate displacement control. Three experiments were also carried out with this straining rig *in situ* in a SEM (Leo 1525). Using this method, the development of cracks in the film with increasing displacement could be carefully monitored. This led to accurate determination of the film failure strain and the steady state crack spacings. Crack spacing measurements were made using a line intercept method perpendicular to the direction of straining. Only the lengths of the film fragments were measured, i.e. the lengths of the gaps that necessarily open between segments were excluded from the measurements.

The same calibration standard was used for TEM and SEM measurements in order to reduce errors resulting from combining measurements from different instruments.

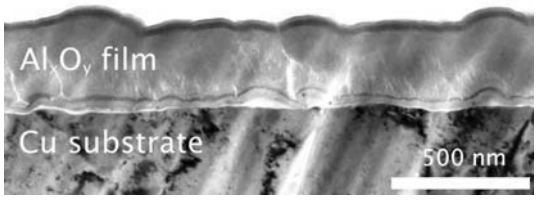

Figure B.2 Cross-sectional transmission electron microscopy reveals the waviness of the film surface in addition to providing a measure of the film thickness.

Table B.1 Comparison of the data obtained for the three samples strained *in situ* in a SEM. In calculating τ_{max} the film thickness is taken to be 350 ± 105 nm for all samples, the quoted error being the standard deviation in the measured film thickness. A value of 160 GPa is used for the Young's modulus, E, of amorphous Al_xO_y [35]. Following Agrawal and Raj [17], equation B.1 was used with the constant $K_{\lambda mean} = 3\pi/4$ for calculation of the interfacial shear, the error in this value is determined using only variation in fracture strain and film thickness.

Sample	σ_f/MPa	$\lambda_{min}/\mu m$	$\lambda_{mean}/\mu m$	τ_{max}/MPa
1	(0.021 ± 0.003)E	2.0	3.3	840±370
2	(0.025 ± 0.001)E	1.7	3.8	870±290
3	(0.022 ± 0.001)E	2.0	4.25	680±230

B.3 Results

The AFM data of the bare Cu substrates indicates a peak-to-trough roughness of 100 nm. The surface of the Al_xO_y film has a peak-to-trough roughness of 160 nm.

Cross-sectional TEM studies (see figure B.2) reveal a waviness on the film surface, this is the cause of the relatively large peak-to-trough roughness found in the AFM measurements. figure B.2 also illustrates the relative flatness of the substrate in comparison to the roughness of the film, this is caused by the physical vapour deposition process [34]. A mean thickness of the Al_xO_y film of 350 nm was measured from two cross-sectional samples using approximately 40 μm of film in total.

Table B.1 presents the data collected from the *in situ* straining experiments. figure B.3 presents the evolution of the crack spacing, B.3a, and the film appearance, B.3b and c, as measured during *in situ* straining of a sample. The crack spacing evolution shows typical initiation to saturation behaviour as first reported by Agrawal and Raj [17]. The film cracking also shows a typical progression from parallel cracking to buckles forming in the cracked segments perpendicular to the cracking direction [3, 11, 17]. From this data a mean failure strain for the films, defined as the point of initial cracking, is determined as $2.3 \pm 0.1\%$. In addition to this, the minimum spacing between cracks was determined to be 1.9 ± 0.1 μm while the mean crack spacing was found to be 3.8 ± 0.4 μm.

Figure B.4 presents the crack distribution profile for sample 1 showing a wide

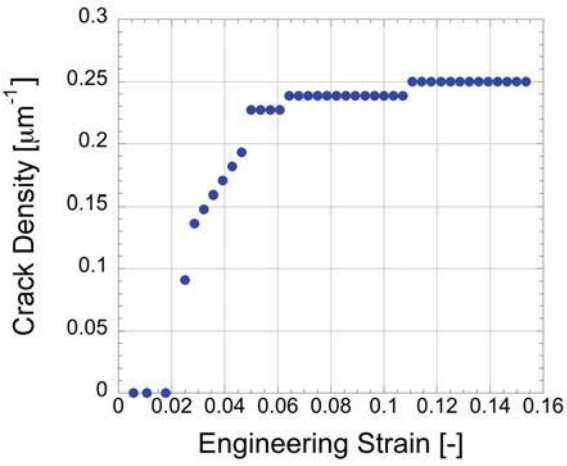

(a)

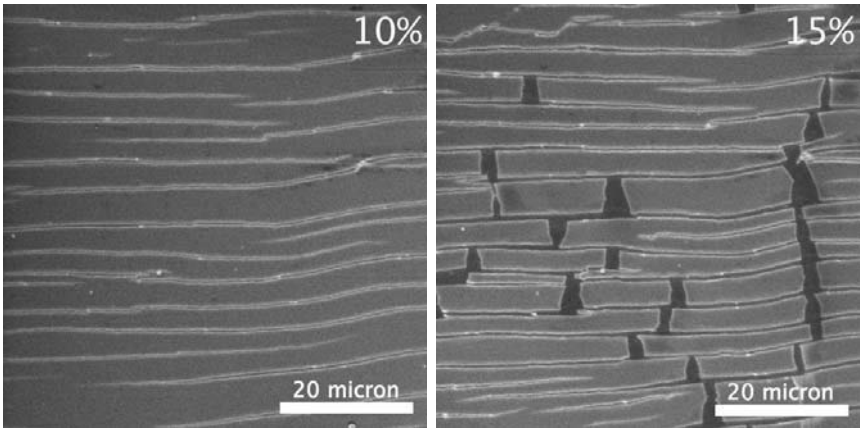

(b) (c)

Figure B.3 The evolution of the film crack density is presented in a) while b) and c) show the crack morphology at 10 and 15% strain respectively.

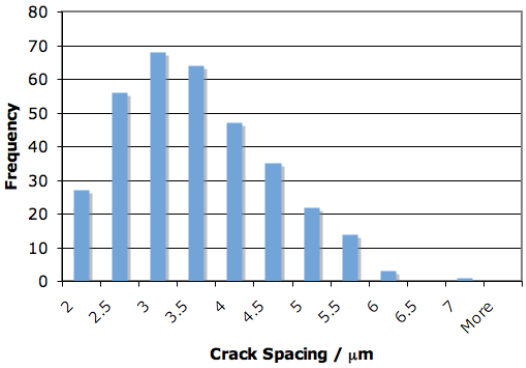

Figure B.4 Crack distribution profile for sample 1. The crack bounding ratio, M, is calculated to be 4.8 for this system.

distribution from under 2 μm to over 6 μm in the crack spacing. Defining the crack bounding ratio, M:

$$M = \frac{\lambda_{max}}{\lambda_{min}}. \tag{B.2}$$

In the case of a film with a single-valued fracture strength in the steady state condition, M should be equal to 2, as discussed earlier. In the present case a crack bounding ratio of M = 4.8 is calculated using the shortest and longest measured spacings between cracks.

B.4 Theoretical Consideration of Film Thickness Variation

When considering variation in the film thickness, the scale over which the variation occurs is critical. This is due to the way that film thickness variations can interact with the periodic cracking in different ways dependent upon how the length scale of the variation compares to the length scale of the cracking. The periodic cracking approach predicts a factor of two difference between the minimum crack spacing and the maximum, these crack spacings define the reference length scale against which thickness variations must be compared. Figure B.5 illustrates the various parameters considered in the following analysis.

For this analysis, μ is defined as the wavelength of the thickness variation while the thickness, δ, is assumed to obey the following relationship:

$$\delta = \delta_{mean} \pm \Delta\delta_{mean} = \delta_{mean}(1 \pm \Delta) \tag{B.3}$$

where Δ is the fractional variation of the film thickness from the mean value. In a real system the variation in film thickness would be expected to be Gaussian or similar but this simplified expression has been chosen to aid an analytical treatment of the variations.

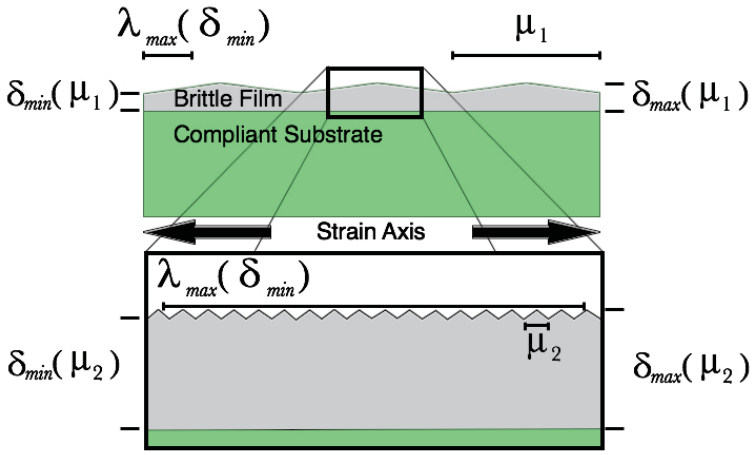

Figure B.5 Diagram outlining the various factors being considered in this analysis. μ_1 and μ_2 are the wavelengths of the thickness variation while δ_{max} and δ_{min} are the maximum and minimum film thicknesses corresponding to these variations. $\lambda_{max}(\delta_{min})$ is the maximum crack length corresponding to the minimum film thickness.

For the purposes of analysis, film thickness variations are separated here into two separate length scales; *roughness* and *unevenness* depending on whether the variation occurs over lengths smaller or larger than the maximum crack spacing. For these two length scales the effect of the variation on crack behaviour and the ratio between minimum and maximum crack spacings, M, will be discussed.

B.4.1 Roughness

The first length scale is *roughness*, defined as variations whose wavelengths are shorter than the maximum crack spacing for the system:

$$\mu_{rough} \leq \lambda_{max} = 2\lambda_{min} \tag{B.4}$$

for reasons which will become clear the maximum and minimum crack spacings used here, λ_{max} and λ_{min}, correspond to the minimum film thickness, $\delta_{min} = \delta_{mean}(1 - \Delta_{rough})$ (Δ_{rough} is the fractional variation of film thickness in the range of roughness). μ_{rough} is the wavelength of variation in the range of roughness, corresponding to μ_2 in figure B.5.

The effect of roughness is illustrated in figure B.6, ie. cracking always occurs at film thickness minima. This effect is important because when the thickness of a film on a substrate is defined it is a *mean* thickness that is measured and used in calculations. If we consider a film possessing only film roughness, like in figure B.6, then we can define, to a first approximation, the following relation:

$$\tau_{max} = K\frac{(\delta_{mean}(1 - \Delta_{rough}))\ \sigma_f}{\lambda_x} \tag{B.5}$$

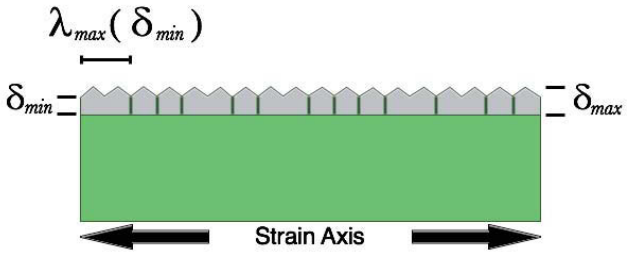

Figure B.6 Schematic illustrating the effect of film roughness on periodic cracking. The λ_{max} indicated is that corresponding to the minimum film thickness, $\delta_{min} = \delta_{mean}(1 - \Delta_{rough})$. Note how cracks will always be expected to travel along film minima.

$$\tau_{meas} = K\frac{\delta_{mean}\ \sigma_f}{\lambda_x} \tag{B.6}$$

$$\frac{\tau_{meas}}{\tau_{max}} = \frac{1}{1 - \Delta_{rough}} \tag{B.7}$$

$$i.e.\ \tau_{meas} > \tau_{max} \tag{B.8}$$

where τ_{max} is the real parameter to be determined through the periodic cracking experiment and τ_{meas} is the value obtained when a mean film thickness is assumed. Only the scale of variation is accounted for here, see section B.9.1 for a discussion of the influence of *shape*. This result indicates that for films exhibiting roughness it is important to use a minimum film thickness in determining the interfacial shear stress, the use of a *mean* film thickness introduces a systematic error into the calculation.

The second effect to consider is the effect on the crack bounding ratio: for the case of film roughness it is expected that no broadening of the crack bounding will occur. While the maximum and minimum crack spacings will correspond to the minimum rather than mean film thickness the largest crack spacing is still expected to be twice the length of the shortest.

B.4.2 Unevenness

The second length scale of film thickness variation, *unevenness*, lies in the range:

$$\mu_{uneven} \geq \lambda_{max} = 2\lambda_{min} \tag{B.9}$$

where μ_{uneven} is the wavelength of variation in the range of unevenness, corresponding to μ_1 in figure B.5.

The effect of *unevenness* is solely on the crack bounding ratio, as illustrated in figure B.7. Here the variation in film thickness over the surface of the substrate leads to a longer maximum crack spacing in somewhat thicker areas of the film and hence

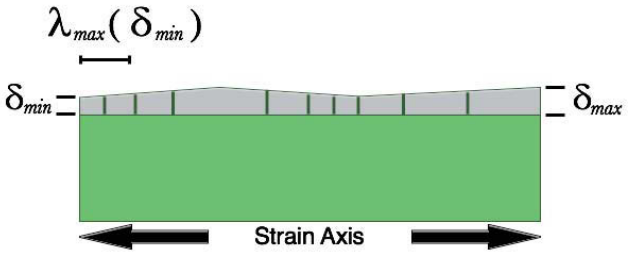

Figure B.7 A schematic of film unevenness and its effect on the crack bounding ratio. The λ_{max} indicated is that corresponding to the minimum film thickness, $\delta_{mean}(1-\Delta_{uneven})$. Note how some crack spacings in the thicker regions of the film exceed the λ_{max} indicated.

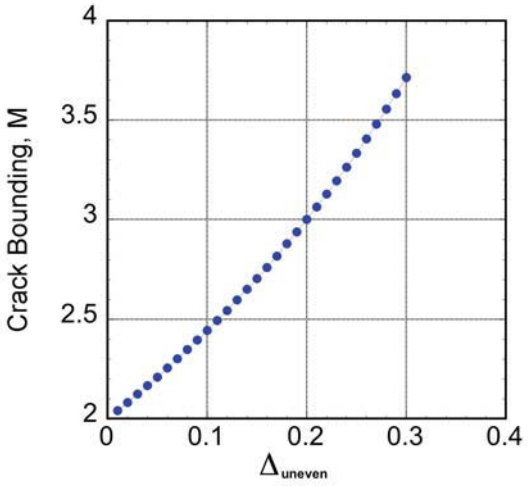

Figure B.8 Chart depicting the dependence of the crack bounding ratio, M, on the unevenness thickness variation, Δ_{uneven}.

the bounding of the crack spacing is broadened with reference to some minimum film thickness. It is possible to analyse the degree of broadening using the definition of M given in equation B.2:

$$M_{uneven} = \frac{\lambda_{max}(\delta_{mean}(1+\Delta_{uneven}))}{\lambda_{min}(\delta_{mean}(1-\Delta_{uneven}))} = \frac{2(1+\Delta_{uneven})}{1-\Delta_{uneven}} \tag{B.10}$$

Δ_{uneven} is the fractional variation in film thickness in the range of unevenness.

It can be seen from this relation that even a relatively low value of thickness variation leads to a large broadening of the crack bounding, figure B.8 plots this relation. For even reasonably low values of thickness variation in thin films, $10-15\%$, an observed crack bounding ratio of $2.4-2.7$ is predicted.

A special case of unevenness is discussed in B.9.2.

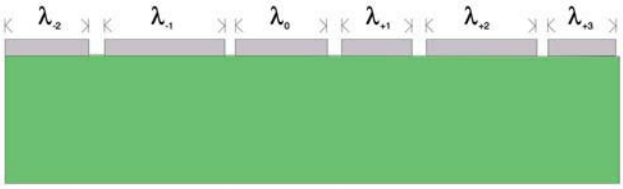

Figure B.9 Schematic illustrating the concept of the neighbour ratio, R. By comparing the length of each crack with only its neighbours the effects of unevenness can be compensated for.

B.4.3 Correcting for Variation

Having outlined a theoretical model for the variation of film thickness over the two length scales, several strategies to account for these variations will now be outlined.

Correcting for film roughness is a relatively straightforward matter. By making assessments of the films and bare substrates with AFM or a similar technique it is possible to make an accurate determination of peak-to-trough height variations occurring on a scale narrower than the maximum crack spacing. If the film and substrate roughnesses are assumed to be independent of each other then a linear superposition can be made to achieve a total thickness variation. In fact, the film and substrate roughnesses are likely to correlate to a greater or lesser extent and so a linear correlation will provide an upper bound to the total variation. Cross-sectional TEM, figure B.2, shows the roughnesses to be independent in the present case but this should be assessed system-by-system for accurate results. If this peak-to-trough variation is taken to be equal to $2\Delta_{rough}$, equation B.11, then this assessment, along with a measure for the mean film thickness, gives a complete experimental description of the film thickness for variations in the range of roughness.

$$\Delta_{rough} = \frac{1}{2}(R_z[substrate] + R_z[film]) \tag{B.11}$$

Due to the necessarily longer length scale of unevenness such experimental assessments become impractical to conduct. However, by introducing the concept of a crack neighbour ratio it is possible to remove the effects of unevenness without knowing its extent. The crack neighbour ratio, R, is defined for a series of cracks of lengths, $\lambda_{-\infty}, ..., \lambda_{-1}, \lambda_0, \lambda_{+1}, ..., \lambda_{+\infty}$, as:

$$R_{-1} = \frac{\lambda_{-1}}{\lambda_0} \quad if \quad \lambda_{-1} > \lambda_0 \tag{B.12}$$

$$otherwise \quad R_{-1} = \frac{\lambda_0}{\lambda_{-1}}. \tag{B.13}$$

This concept is illustrated in figure B.9. By assessing R for each crack neighbour pair, a distribution of R-values analogous to the crack spacing distribution is produced. For a fragmentation test of a film with single-valued fracture strength in the steady state:

$$1 \leq R \leq 2. \tag{B.14}$$

By comparing the distribution in R-values with the crack spacing distribution for a given system the extent of film unevenness can be qualitatively assessed, i.e. if the distribution of R-values is narrower than the crack spacing distribution then at least some effects of long-range film variation have been accounted for. However, this effect is not necessarily specific to film thickness variation. Should other parameters, such as interface quality, vary over a range greater than the maximum crack spacing then this technique will also compensate for the variation. This generality is useful in that it allows for the compensation of variations that would otherwise be very difficult to quantify. However, the disadvantage is that an estimate of Δ_{uneven} cannot be obtained by comparing the highest R-value with M for the system, as would be possible if film thickness unevenness was the only factor being compensated.

B.5 Application of Corrections

The corrections discussed in the previous section will now be applied to the Al_xO_y/Cu system.

Δ_{rough}, as defined in equation B.11, was measured to be 130 nm. Following equation B.3 this leads to the following relation for film thickness on the scale of roughness:

$$\delta = 350\ nm \pm (130\ nm)_{rough} \tag{B.15}$$

The neighbour ratios for sample 1, calculated according to equations B.12 and B.13, are presented in figure B.10. It is immediately clear that the highest R-value for the system, 2.6, is a significant improvement over the value of 4.8 determined for the crack bounding ratio, M. Similar results were found for all other samples investigated.

An additional refinement to the method is the use of λ_{min} in place of λ_{mean}. During testing it is most accurate to use the strain corresponding to the onset of cracking in the film as this value can be accurately measured. In a real system where film fracture strength is not single-valued the shortest film fragments correspond to fractures at the weakest flaws. The minimum fragment length therefore corresponds to the weakest parts of the film whose strength is measured by the onset of cracking in the film. Determining an accurate value for a *mean* fracture strain is much more difficult, the mid-point strain between crack onset and saturation is sometimes used but the stress state in the film is very complex in the range and use of this value could bring significant error into the measurement.

Using the values calculated here it is possible to make a comparison of the interfacial shear stress determined following the guidelines made here and the shear stress made following existing conventions. This data is presented in table B.2. The fracture strain corresponding to λ_{mean} was chosen as the strain where the crack density is half its value at saturation, this can only be estimated to the nearest percent.

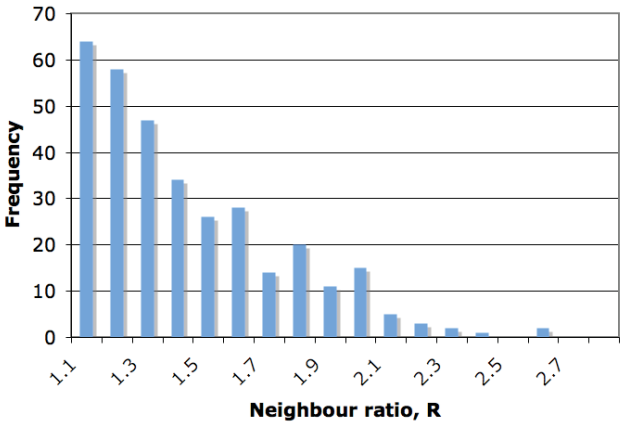

Figure B.10 Crack neighbour ratios, R, for the Al_xO_y/Cu system. Note the significant narrowing of the distribution compared to the crack spacing distribution, figure B.4.

Table B.2 A comparison of mean interfacial shear stress calculations with and without the refinements highlighted here. A value of 160 GPa is used for the Young's modulus, E, of amorphous Al_xO_y [35]. Following Agrawal and Raj [17]; $K_{\lambda mean} = 3\pi/4$ and $K_{\lambda min} = \pi/2$.

	δ/nm	σ_f/MPa	$\lambda/\mu m$	τ_{max}/MPa
Conventional	350	0.03E	$\lambda_{mean} = 3.8$	1040
Corrected	245	0.023E	$\lambda_{min} = 1.9$	600

B.6 Discussion

The films used in this study have a high level of roughness due to the sputtering deposition process. Correcting for this roughness immediately lowers the calculated interfacial shear stress for the system. The combination of these corrections results in a calculated τ_{max} of 600 MPa for this Al_xO_y/Cu system. The large difference between the conventional and corrected values presented in table B.2 is largely due to the higher film fracture strain.

Concerning the accurate determination of the interfacial shear stress, it is important to note that precise measurement of the film fracture strain through *in situ* methods is essential. In the present work a mean value of 0.023±0.01 was obtained, such accurate determination is only possible through *in situ* methods and yet this uncertainty is transferred directly to the measured interfacial shear stress. An uncertainty of ±1% in the fracture strain, not uncommon when using *ex situ* methods, would add a 50% uncertainty to the measured interfacial shear stress in the present case.

The application of the neighbour ratio calculation to this system yields two useful results. The analysis demonstrates that if variation in the film thickness over the surface of the film is accounted for then 96% of the measured crack spacings fall within the limits predicted by simple periodic cracking theory. For the Al_xO_y/Cu

system studied here neighbour ratios in the range $1 \leq R \leq 2.6$ were calculated. This infers that the statistical distribution of strength in this model system is directly correlated with variations in the film thickness. The second result is that the bound of two predicted by the periodic cracking model is met despite the system exhibiting statistical strength variations not included in the theory. This is useful as the periodic cracking technique provides a useful and quick measure of the film and interfacial properties, these results validate the continued application of the method.

Extending the concepts presented here, it follows that in a system for which a large proportion of the measured neighbour ratios do not fall within the $1 \leq R \leq 2$ range classical periodic cracking theory is not applicable. However, defining exact limits within which a system must fall is problematic. No attempt is made in the present work to account for the effects of large film defects or other factors causing strong, highly local, variations in the cracking of the film. Such phenomena, along with unidentifiable failure of the film/substrate interface, most likely account for the small fraction of neighbour ratios falling outside the limits of the predictions in the present study. As a guideline, film/substrate systems exhibiting neighbour ratios greater than 3 and/or more than 10% of the neighbour ratios greater than 2 should be treated with suspicion and possible causes for this behaviour should be investigated.

B.7 Conclusions

Thickness variation in thin film systems used for this type of testing can be separated into two important length scales: variations over a length scale shorter than the maximum crack spacing is termed *roughness* here while variations over a length scale longer than the maximum crack spacing are termed *unevenness*.

By accounting for roughness, the calculated interfacial shear stress for the system is reduced and the validity of comparisons between different film deposition parameters or substrate preparations is greatly enhanced. This analysis also highlights that carrying out periodic cracking and similar experiments without accurately characterising the film thickness could lead to experimental errors of greater significance than that inferred by the data collected.

An analysis of the effects of unevenness leads to a useful approach of refining the crack distribution data produced by periodic cracking experiments. The neighbour ratios utilised by this refinement compensate for long distance variation in the film and interface properties. It is demonstrated that these compensations bring more than 96% of the crack data within the limits predicted by the periodic cracking model. The statistical distribution of strength in this system must then be largely due to said variations in the film thickness.

By being able to account for nearly all the broadening in the crack spacing mea-

surements the understanding of the periodic cracking method is enhanced and its validity as a means of assessing interface quality is validated.

B.8 Acknowledgment

Gabi Moser at the Erich Schmid Institute is acknowledged and thanked for her continued assistance with TEM sample preparation.

Bibliography to paper B

[1] VJ Lumelsky, MS Shur, S Wagner, IEEE Sensors 1, 41-51 (2001)

[2] SP Lacour, S Wagner, Z Huang, Z Suo, Appl. Phy. Lett. 82, 2404-2406 (2003)

[3] S Frank, UA Handge, S Olliges, R Spolenak, Acta Mater. 57, 1442-1453 (2009)

[4] MJ Cordill, A Taylor, J Schalko, G Dehm, Metall. and Mater. Trans. A 41, 870-875 (2009)

[5] JS Wang, Y Sugimura, AG Evans, WK Tredway, Thin Solid Films 325, 163-174 (1998)

[6] BF Chen, J Hwang, GP Yu, JH Huang, Thin Solid Films 352, 173-178 (1999)

[7] T Ohmura, S Matsuoka, Surf. Coat. Technol. 169-170, 728-731 (2003)

[8] MJ Filiaggi, RM Pilliar, D Abdulla, J. Biomed. Mater. Res. 33, 239-256 (1996)

[9] PB Kirk, RM Pilliar, J. Mater. Sci. 34, 3967-3975 (1999)

[10] Y Leterrier, Prog. Mater. Sci 48, 1-55 (2003)

[11] Y Letterier, L Boogh, J Andersons, J-AE Månson, J. Polym. Sci. B: Polym. Phy. 35, 1449-1461 (1997)

[12] Y Letterier, J Andersons, Y Pitton, J-AE Månson, J. Polym. Sci. B: Polym. Phy. 35, 1463-1472 (1997)

[13] M Yanaka, Y Tsukahara, N Nakaso, N Takeda, J. Mater. Sci. 33, 2111-2119 (1998)

[14] JD Witt, M Swann, J. Bone and Joint Surgery. 73-B, 559-563 (1991)

[15] MS Hu, AG Evans, Acta Metall. 37, 917-925 (1989)

[16] BE Alaca, MTA Saif, H Sehitoglu, Acta Mater. 50, 1197-1209 (2002)

[17] DC Agrawal, R Raj, Acta Metall. 37, 1265-1270 (1989)

[18] DB Marshall, AG Evans, J. Appl. Phys. 56, 2632-2638 (1984)

[19] B Rother, BA Dietrich, Thin Solid Films 250, 181-186 (1994)

[20] A Abdul-Baqi, E Van der Giessen, Thin Solid Films 381, 143-154 (2001)

[21] H Hirakata, T Kitamura, Y Yamamoto, Int. J. of Solids and Structures 41, 3243-3253 (2004)

[22] K Matoy, T Detzel, M Müller, C Motz, G Dehm, Surf. Coat. Technol. 204, 878-881 (2009)

[23] H-J Kim, M-W Moon, D-I Kim, K-R Lee, KH Oh, Scripta Mater. 57, 1016-1019 (2007)

[24] W-J Chou, G-P Yu, J-H Huang, Surf. Coat. Technol. 149, 7-13 (2002)

[25] A Kelly, WR Tyson, J. Mech. Phys. Solids 13, 329-350 (1965)

[26] WA Curtin, J. Mater. Sci. 26, 5239-5253 (1991)

[27] R Gulino, SL Phoenix, J. Mater. Sci. 26, 3107-3118 (1991)

[28] J-P Favre, P Sigety, D Jacques, J. Mater. Sci. 26, 189-195 (1991)

[29] J Nairn, Mechanics Mater. 13, 131-157 (1992)

[30] P Feillard, G Désarmot, J-P Favre, Compos. Sci. Technol. 50, 265 (1994)

[31] V Edlmayr, M Moser, C Walter, C Mitterer, Surf. Coat. Technol. 204, 1576-1581 (2010)

[32] ISO 4287:1997 (E/F)

[33] ASME B46.1, 1995, 2002, 2009

[34] M Ohring, Materials Science of Thin Films, 2nd Edition, Academic Press, San Diego, 2002, pg223.

[35] NG Chechenin, J Bøttinger, JP Krog, Thin Solid Films 304, 70-77 (1996)

[36] CE Inglis, Proc. Inst. Nav. Archit. 55, 219-241 (1913)

[37] FI Baratta, DM Neal, J. Strain Analysis Eng. Design 5, 121-127 (1970)

[38] N-A Noda, M Sera, Y Takase, Int. J. Fatigue 17, 163-178 (1995)

[39] WD Pilkey, Peterson's Stress Concentration Factors, 2nd Edition, John Wiley & Sons, Inc, New York, 1997, pg92.

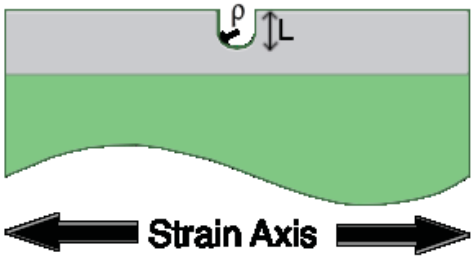

Figure B.11 Film and substrate modelled as a semi-infinite plate. The notch depth, L, and notch tip radius, ρ, define the stress concentration due to film thickness variations.

B.9 Appendix to Paper B

B.9.1 The effect of roughness shape

In discussing the effect of roughness on the fracture of coatings in section B.4.1 the issue of stress concentration was omitted. The periodic cracking approach is based on the principle of film fracture at a critical stress. If this principle is to strictly followed then stress concentrations due to the film surface shape should also be considered.

It was shown by Inglis [36] that notches in a loaded component lead to stresses greater than would be predicted purely by the reduction in component cross section. If this concept is extended to the present case of a film on a substrate, any variation in film thickness should also be expected to cause stress concentrations greater than predictions due to the reduction in film cross section. As the variation in film thickness, or notch depth as it is referred to in the context of stress concentration, is small compared to the combined thickness of film and substrate the problem can be addressed as a notch in a semi-infinite plate. This scenario with the relevant parameters is illustrated in figure B.11.
The notch tip radius, ρ, and the notch depth, L, can then be related to a stress concentration at the notch tip by the relation:

$$k_{tip} = 1 + 2\sqrt{\frac{L}{\rho}} \tag{B.16}$$

where k_{tip} is the stress concentration immediately below the tip of the notch. For more complete discussions of stress concentrations in loaded components the reader is directed to references [37, 38]. In order to apply this to the Al_xO_y/Cu system studied here a notch depth, $L = \Delta_{rough} = 130$ nm, and a tip radius of $\rho = 30$ nm (approximated from AFM data) results in $k_{tip}(Al_xO_y) \cong 5$.

This rough calculation suggests that the presence of any film thickness variation could be expected to reduce the macroscopically observed film failure stress by a factor of 5 or more, dependent on the exact shape of the variation. However, two points should be noted from this analysis; firstly, while stress concentration factors are a useful analytical tool it should be remembered that fracture is controlled by

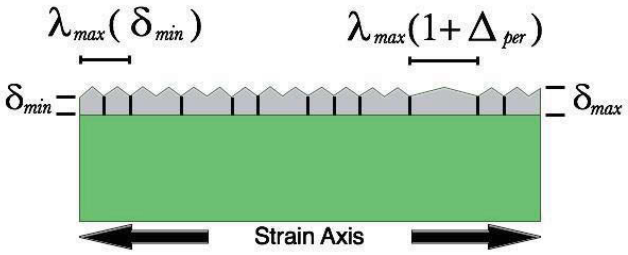

Figure B.12 Schematic illustrating the effect of thickness variation in the range: $\lambda_{max} \leq \mu \leq \lambda_{max}(1+\Delta_{per})$. Δ_{per} is the fractional variation of the film thickness in the perturbation length scale.

thermodynamics and the release of energy rather than simple stress rules. Secondly, an real film has multiple notches across its surface and these will have the effect of reducing the stress concentration observed for any given notch [39].

Further investigation is required if the influence of shape factors on the fracture of a wavy film is to be understood and quantified.

B.9.2 Perturbation

A special case of film unevenness, defined as *perturbation*, occurs over a small regime greater than the maximum crack spacing:

$$\lambda_{max} \leq \mu_{per} \leq \lambda_{max}(1 + \Delta_{per}) \tag{B.17}$$

where μ_{per} and Δ_{per} are the wavelength and fractional thickness variation in the range of perturbation, respectively.

The importance of variation in this range is presently unclear as no strategy has been devised to accurately assess or compensate for this variation. Despite this, a brief analysis of how variations of this type would affect film cracking experiments is worthwhile.

In this range an effect on the crack bounding is expected. The effect of variation in this range is best visualised by a superposition of a variation at the limit of this range with a rough film, figure B.12. This leads to a crack bounding ratio as follows:

$$M = \frac{\lambda_{max}(1 + \Delta_{per})}{\lambda_{min}} = \frac{2\lambda_{min}(1 + \Delta_{per})}{\lambda_{min}} = 2(1 + \Delta_{per}) \tag{B.18}$$

According to this relation a 10% variation in film thickness in the perturbation range would alone cause a broadening of the crack bounding to 2.2. Of more note is that such a variation in the perturbation range would cause an identical broadening of the crack neighbour ratio, R. As such, the limits of R in the steady state condition must be altered to:

$$1 \leq R \leq 2(1 + \Delta_{per}) \tag{B.19}$$

for a system in which perturbation is present.

Equation B.19 and the concept of perturbation are noteworthy for two reasons. Firstly, if it is assumed that variation in the range of perturbation exists in the system then the percentage of crack ratios falling within the bounds defined by periodic cracking increases to over 98%. Secondly, the use of λ_{min} in place of λ_{mean} is further justified as perturbation would also lead to a further artificial increase of the mean crack spacing.

C

The Effect of Temperature and Strain Rate on the Periodic Cracking of Amorphous Al_xO_y Films on Cu

A A Taylor[a], V Edlmayr[b], M J Cordill[a,c], G Dehm[a,c]

[a]Erich Schmid Institute of Materials Science, Austrian Academy of Sciences, A-8700 Leoben, Austria
[b]Department of Metallurgy and Materials Testing, Montanuniversität Leoben, Roseggerstraße 12, A–8700, Leoben, Austria
[c]Department Materials Physics, Montanuniversität Leoben, Jahnstraße 12, A–8700 Leoben, Austria

Abstract

The high temperature properties of metal/ceramic interfaces play an important role in the operation of microprocessors and coated products. Determination of the interface properties over a range of testing conditions is critical in understanding and improving the performance of such systems. Periodic cracking of ceramic films on metal substrates provides a direct measure of the interface strength. A model Al_xO_y/Cu system is investigated over temperatures of $25-650°C$ and at strain rates of $3.5 \cdot 10^{-2}\ s^{-1}$ and $1.7 \cdot 10^{-5}\ s^{-1}$. For this system it is found that temperature does not significantly affect the spacing of film cracks in the steady state, at a given strain rate. However, the high strain rate tests broaden the measured crack spacing distributions compared to the low strain rate tests. This broadening causes an increase in the average crack spacing at high strain rate. The minimum crack spacing was increased $15-20\%$ by both increasing strain rate and increasing temperature.

C.1 Introduction

Although metal-ceramic interfaces have been studied for several decades, these interfaces remain weak links in materials systems such as microelectronic devices [1], thermal barrier coatings [2], metal-matrix composites [3] and even in carbide inclusions in steels [4] . These interfaces often limit the service performance and lifetime of these products. This holds especially true for elevated temperatures where a profound knowledge of the interfacial response to mechanical load is still lacking despite several mechanisms, including interfacial sliding [5] , having been identified.

Interfacial sliding as a result of high temperatures in composite systems has been observed in a number of experimental geometries. These include matrix growth in fibre composites [6, 7], reduced strains in microelectronic devices [8, 9] and films on substrates [10–12]. The constitutive equations and exact phenomena associated with interfacial sliding varies with the geometry, for more comprehensive overviews of the theory underlying interfacial sliding the reader is directed to references [5] and [10].

Cracking of thin films has been successfully used as a technique to understand and quantify the properties of interfaces in many studies [10, 13–16]. The work of Agrawal and Raj [14] and Chen et al. [17] led to the following relation for the interfacial shear stress, accounting for the residual strain of the film:

$$\tau_{max} = K\frac{(\epsilon_f + \epsilon_R)E_f\ \delta}{\lambda_x}. \tag{C.1}$$

This relates the measured properties of film fracture strain, ϵ_f, the Young's modulus of the film, E_f, and the steady state film crack spacing, λ_x, to the maximum shear strength sustained at the film/substrate interface, τ_{max}. ϵ_R is the residual strain in the film due to deposition processes, film/substrate thermal mismatch etc. In equation C.1, K is a numerical constant between π and $\pi/2$ depending on whether the maximum crack spacing, λ_{max}, or the minimum, λ_{min}, is measured, respectively. Like the fragmentation testing theory [18] on which it is based, Agrawal and Raj's model predicts a factor of two difference in crack spacing when brittle films on compliant substrates are strained to the steady state.

Using the periodic cracking model detailed in [14] a Al_xO_y/Cu system was used to investigate a greater range of strain rate and temperature than previous studies have covered. By using an amorphous film any effects of crystallinity on cracking and diffusion of the film are avoided. By increasing the strain rate and temperature range, a more complete understanding of the film cracking and hence interface behaviour of these systems is targeted.

C.2 Experimental

The alumina film deposition was carried out in an industrial-scale sputtering plant (CemeCon CC800/9MLT) by DC magnetron sputtering of Al targets in an O_2/Ar atmosphere, total pressure 0.87 Pa, at a temperature of $640 \pm 10°C$. All of the films used in this study were deposited simultaneously, ensuring equivalent properties and

thickness. Further details on the deposition set-up are reported in reference [19]. The substrates are commercially electropolished OFHC-grade Cu (min 99.99% Cu, ASTM designation C10100) dogbone samples. The samples have a gauge length of 15 mm and a width of 3 mm, the Cu substrate is 1 mm thick.

Concerning the residual strain in the film, attempts were made with both x-ray and curvature measurements to assess the residual strain but both were unsuccessful. The following assumption was therefore made; at room temperature the film possesses a compressive strain equal to the thermal mismatch of the alumina and Cu following cooling from deposition at 640°C. At 650°C the film is assumed to possess zero residual strain, i.e. all residual strain in the film is due to thermal mismatch of substrate and film. As the film is amorphous, strains due to epitaxy and island growth should be minimal [20] and hence the assumption of only thermal mismatch stress is reasonable. Using values of $9 \cdot 10^{-6} K^{-1}$ for the alumina film [21] and $18 \cdot 10^{-6} K^{-1}$ for Cu results in an estimate of $5.6 \cdot 10^{-3}$ for the residual film strain.

For analysis of film thickness, transmission electron microscopy (TEM, Philips CM12 and JEOL 2100F) samples of the films were prepared. These samples were produced by dimple grinding (Gatan) and Ar^+ ion milling (Gatan DuoMill and Baltec RES 101). TEM was also used to ensure that no structural changes in the film or substrate could be observed after annealing the samples in vacuum for 300 minutes at 650°C.

Atomic force microscopy (AFM, Digital Instruments Dimension 3100) was carried out on the bare substrates. Three 25 μm x 25 μm scans were performed and, following Peterson et al. [5], the maximum roughness (R_z [22, 23]) was measured to be 100 nm.

The periodic cracking experiments were carried out on a mechanical testing frame (Zwick) fitted with a non-commercial vacuum oven. Room temperature tests were carried out in air while tests at elevated temperature were conducted at a vacuum of 10^{-4} $mbar$. Tests were conducted at strain rates of $3.5 \cdot 10^{-2}$ s^{-1} and $1.7 \cdot 10^{-5}$ s^{-1} both at room temperature and 650°C.

A second testing rig (Kammrath & Weiss) capable of highly accurate displacement control was used to carry out three tests *in situ* in a scanning electron microscope (SEM, Leo 1525) at $6.7 \cdot 10^{-4}$ s^{-1}. Using this *in situ* method, the development of cracks in the film with increasing displacement could be carefully monitored. This led to accurate determination of the film failure strain and indicated the strain value to which films must be strained for the steady-state crack condition to be reached. The same SEM was used to carry out post-mortem imaging of the samples strained *ex situ*. Crack spacing measurements were all made using a line intercept method perpendicular to the direction of straining. Only the length of the film fragments were measured, this prevents crack opening and film spallation affecting the measurements.

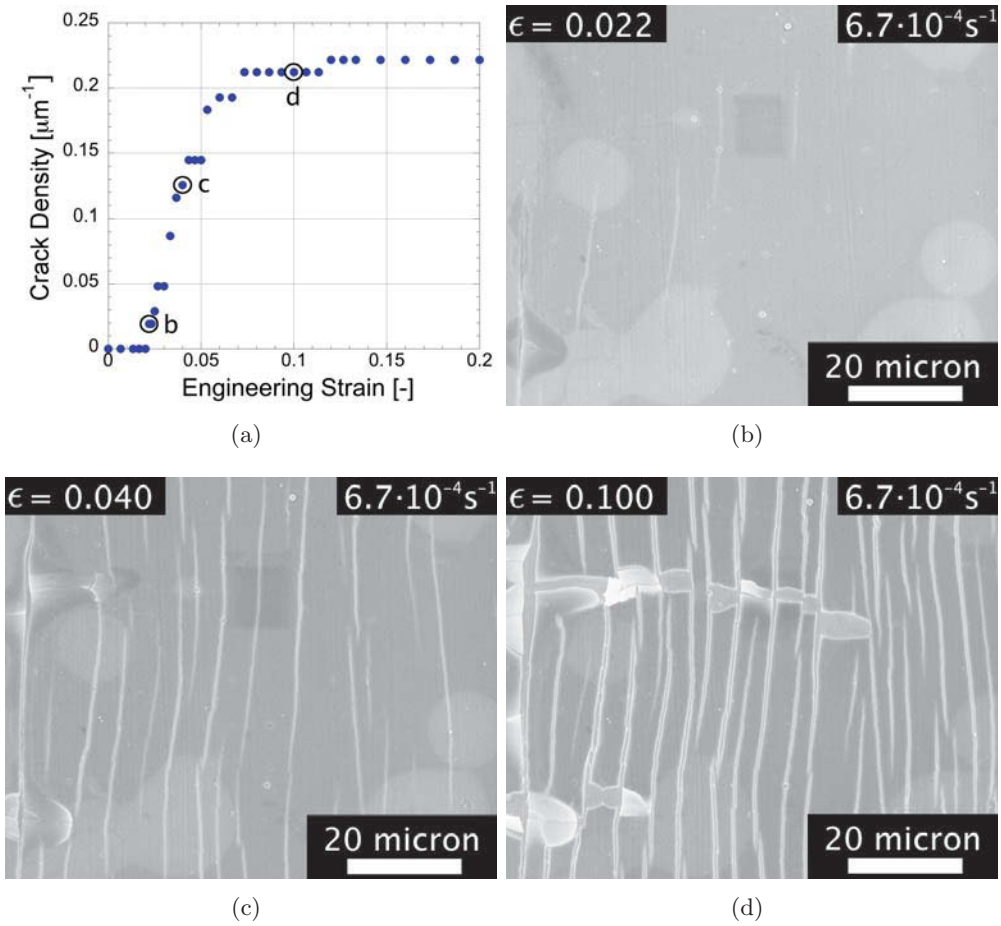

Figure C.1 The evolution of the crack density in a sample strained *in situ* in a SEM. a) plots the crack density while b), c) and d) show the surface of the film at 2.2, 4.0 and 10%, respectively. Film failure starts at a strain of 0.022 and reaches saturation at a strain of 0.12. In all micrographs the strain direction lies parallel to the image horizontal.

C.3 Results

The crack development profile produced by the *in situ* testing is presented in figure C.1a, figures C.1b-d show the surface of the film at 0.022, 0.040 and 0.10 substrate strain, respectively. The average film cracking onset strain for this system, determined from three such *in situ* tests, is $2.3 \pm 0.1 \cdot 10^{-2}$. All strains quoted in this study are engineering strains. Figure C.1 also indicates that cracking of the film reaches the steady state where no more cracking occurs after $0.10 - 0.12$ strain. The *ex situ* samples were strained to 0.20 to ensure that they also reach the steady state.

Using the data from the *in situ* experiments along with a film thickness of 350 nm determined by TEM and a Young's modulus of 160 GPa for Al_xO_y from the literature [24], an interfacial shear strength of 740 MPa was determined for the *in situ*

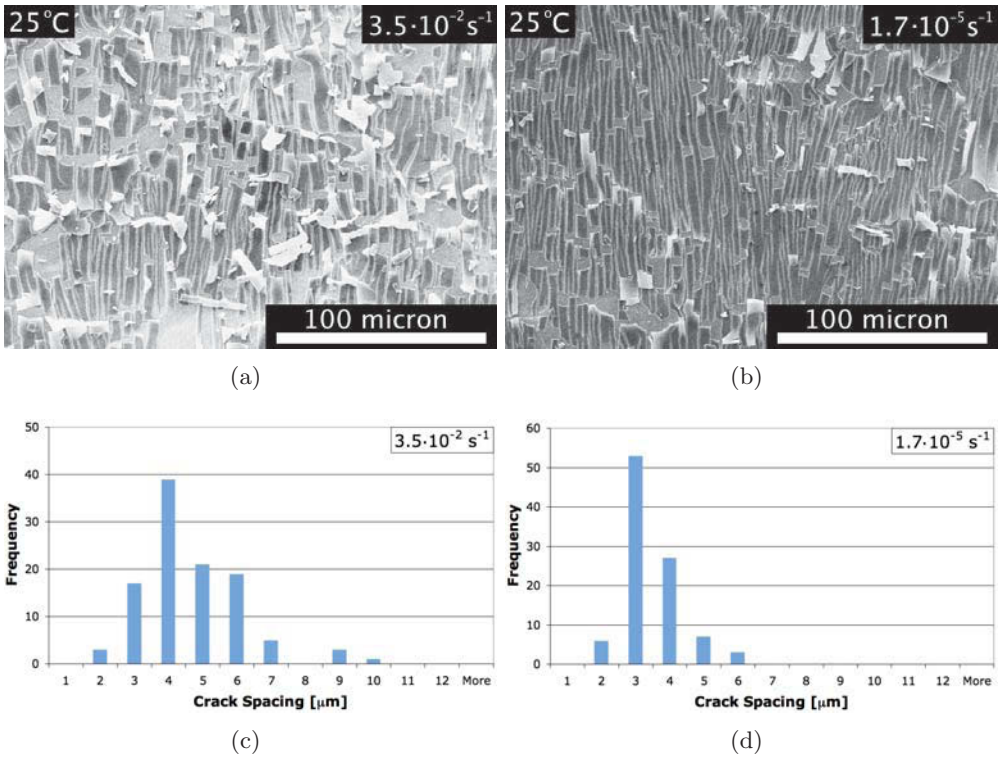

Figure C.2 Micrographs and crack spacing distributions of samples strained to 0.20 at room temperature; a) and c) correspond to a sample strained at $3.5 \cdot 10^{-2}\ s^{-1}$, b) and d) at $1.7 \cdot 10^{-5}\ s^{-1}$.

samples according to equation C.1. The TEM of cross-sectional samples before and after annealing in vacuum showed no differences in film or substrate microstructure; microstructural changes during testing at $650°C$ are therefore not expected.

Figure C.2 presents representative SEM micrographs of samples strained at room temperature along with the measured crack spacing distributions (CSDs). For ease of comparison all CSDs presented use the same size and number of histogram bins, approximately 100 crack spacing measurements were made for each sample. From a comparison of the micrographs a greater degree of film spalling is evident in the sample strained at $3.5{\cdot}10^{-2}\ s^{-1}$. Two points should be noted from the CSDs. Firstly, the minimum and maximum crack spacing values, λ_{min} and λ_{max}, are higher for the higher strain rate, see table C.1. Secondly, the change to the maximum crack spacing is much larger and this leads to a broadening of the CSD, figure C.2c. The mean crack spacing increases from 2.9 μm to 4.2 μm for the low and high strain rate samples respectively (table C.1).

Representative micrographs and CSDs for the samples strained at $650°C$ are presented in figure C.3. Immediately clear from the micrographs is that film spalling is reduced when straining at elevated temperature. These high temperature samples

Table C.1 Test parameters and resultant crack spacings of samples investigated. Minimum and maximum values are mean values from the five smallest and five largest measured spacings, respectively. The errors are the standard deviations of these values.

Sample	Test Temp./$^\circ C$	Strain Rate/x 10^{-5}	$\lambda_{min}/\mu m$	$\lambda_{max}/\mu m$	$\lambda_{mean}/\mu m$
1	25	3500	1.9 ± 0.2	8.6 ± 1.0	4.2
2	25	1.7	1.7 ± 0.2	4.9 ± 0.2	2.9
3	650	3500	2.4 ± 0.1	9.3 ± 0.6	4.9
4	650	1.7	2.0 ± 0.1	5.2 ± 0.2	3.1

also exhibit a broader CSD for the high strain rate sample, figure C.3c. The minimum and maximum crack spacings are again larger for the high strain rate sample, 2.4 versus 1.9 μm for the minimum spacing. The minimum crack spacings at $650^\circ C$ are raised $15 - 25\%$ compared to those measured at room temperature. The mean crack spacings are 3.1 μm and 4.9 μm for the low and high strain rate samples respectively.

C.4 Discussion

The crack spacing data collected indicates that strain rate has a greater effect on film cracking than temperature for the Al_xO_y/Cu system investigated. The effect of strain rate and temperature on the minimum crack spacing, λ_{min}, is comparable while the effect of strain rate on the maximum crack spacing, λ_{max}, is much stronger. Increasing the strain rate leads to a 12% and 20% increase in λ_{min} at $25^\circ C$ and $650^\circ C$, respectively, while increasing temperature leads to 18% and 26% increases at $1.7 \cdot 10^{-5}\ s^{-1}$ and $3.5 \cdot 10^{-2}\ s^{-1}$. For the maximum crack spacings 76% and 79% increases are observed when increasing the strain rate at $25^\circ C$ and $650^\circ C$ respectively. In contrast to this 6% and 8% increases are measured at $1.7 \cdot 10^{-5}\ s^{-1}$ and $3.5 \cdot 10^{-2}\ s^{-1}$ when the temperature is increased. This strong effect on the maximum crack spacing is also observed in the broader CSDs of those samples strained at $3.5 \cdot 10^{-2}\ s^{-1}$.

All this analysis indicates that interfacial sliding was not observable in the experiments presented here. In addition to this, the crack spacing is found to *increase* for the higher strain rate studied here. Jobin et al. [10] had previously found that the crack spacing remains stable for strain rates higher than $1.5 \cdot 10^{-4}\ s^{-1}$ at all investigated temperatures.

Contrary to these observations, both Jobin et al. and Singh et al. [12] reported interfacial sliding in periodic cracking experiments for ceramic films on Cu and Al and, in the case of Jobin et al. [10], at lower homologous temperatures than those investigated here. A possible reason for this discrepancy is discussed in the following.

Diffusion is expected to occur in all materials systems so long as the atomic mobility, controlled predominantly by temperature, is high enough and the time of the experiment is sufficiently long. For diffusion to be observable both of these

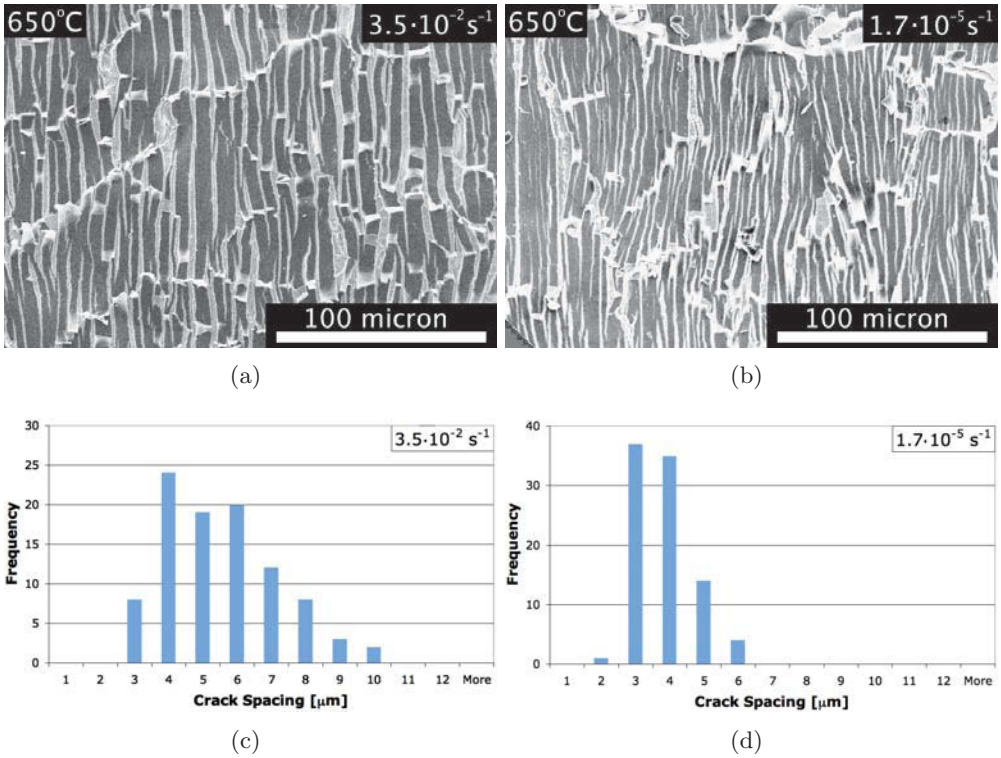

Figure C.3 Micrographs and crack spacing distributions of samples strained to 0.20 at $650°C$; a) and c) correspond to a sample strained at $3.5 \cdot 10^{-2}\ s^{-1}$, b) and d) at $1.7 \cdot 10^{-5}\ s^{-1}$.

requirements must be met. Another system parameter, related to the length of diffusion paths and hence the time dependency of diffusion, is the roughness of the interface. In references [10] and [12] the substrate roughness and, by extension, the interface roughness was not characterised and hence a direct comparison cannot be made. Peterson et al. [5] characterise the interfacial roughness and investigate its effect on interfacial sliding using a different experimental geometry. They observed an order of magnitude decrease in the rate of interfacial sliding as the measured sample R_z values increased from 18 to 174 nm. It therefore seems likely that the lack of measurable interfacial sliding in this study can be attributed to the relatively high measured sample roughness ($R_z = 100\ nm$).

Both the room temperature and $650°C$ tests exhibit a broadening of the CSDs to higher crack spacings for high strain rates. This is an effect that has not previously been observed. Broadening of the crack spacing distribution was previously observed in references [10] and [12] but this was as a result of interfacial sliding and was only observed at elevated temperatures and low strain rates. However, the high strain rate used in this study was more than 5 times higher than that used in previous studies of strain rate in periodic cracking.

According to periodic cracking theory, the minimum crack spacing corresponds to the minimum fragment length required for the tensile fracture stress to be loaded into the fragment via shear stresses at the interface. Periodic cracking theory assumes that this length is dependent only on the properties of the interface. Both the Young's modulus of the film and any residual strain are expected to be temperature dependent. The Young's modulus should not affect any temperature dependence of the crack spacing as if the fracture *stress* of the film is assumed to remain constant then the fracture *strain* of the film will increase correspondingly and the crack spacing will be unaffected. Assuming a residual strain of $5.6 \cdot 10^{-3}$ at room temperature, a *reduction* in crack spacing of $20-25\%$ is predicted for the $650°C$ test. Both Leterrier et al. [26] and Yanaka et al. [27] found that crack spacings of coatings on PET (polyethylene teraphthalate) increased at elevated temperature, this was attributed to a reduction in stiffness of the substrate. A modulus drop of 25% is expected [28] for Cu between room temperature and $650°C$, correlating well with the $15-25\%$ increase in minimum crack spacing observed. Periodic cracking theory cannot account for the $20-30\%$ increases in λ_{min} observed when the strain rate is increased. It is speculated that the CSD broadening and the increase of λ_{min} at high strain rate are due to the cracking of the coating being non-equilibrium in this range.

When performing the *in situ* tests a degree of time-dependency to the film cracking is observed, i.e. further cracking is observed in the film after sample extension is halted, a load drop is also observed during this time. Good data on this effect is difficult to obtain due to the short time period of this relaxation, approximately the first 60 s after extension is halted, and the SEM scan time necessary to resolve such fine cracks, more than 30 s. The high strain rate tests were performed without pause and had a duration of only 6 seconds. This extremely short test duration alters the nature of the cracking in the film from a near-equilibrium condition to a dynamic condition. At room temperature, this difference also leads to the greater degree of

spallation observed in the high strain rate test, i.e. the dynamic cracking leads to the film channelling cracks being diverted along the film/substrate interface and causing film spallation. Aliyu and Daniel [29] demonstrated that the strain energy release rate for cracking along a graphite/epoxy interface *increased* with crack velocity. It has not been explicitly demonstrated that the crack velocity changes in the present tests, but it is not unreasonable given the 1000-fold increase in sample strain rate. An increase in strain energy release rate could well alter the cracking behaviour, causing more delamination and altering the crack spacings as observed.

Finally, a key prediction of periodic cracking theory is the limit of two between the shortest and broadest crack spacing. Using the values in table C.1 limits of $2.6 - 4.5$ can be calculated for the samples studied here. The low strain rate tests yield limits closer to two, 2.6 and 2.9, than the high strain rate tests, 3.9 and 4.5, but the limit of two was not observed. The larger limit of the high strain rate tests is another indicator of non-equilibrium behaviour. For a more detailed analysis of this limit of two in the cracking of thin films please see reference [30] in this issue.

C.5 Conclusions

A model Al_xO_y/Cu system was investigated at room temperature and $650°C$ at strain rates of both $3.5 \cdot 10^{-2}\ s^{-1}$ and $1.7 \cdot 10^{-5}\ s^{-1}$. No interfacial sliding could be observed in these experiments, this is attributed to a relatively high interfacial roughness preventing sliding.

It is reported for the first time that periodic cracking behaviour can be influenced by very high as well as very low strain rates. The broadening of the crack spacing distribution at a high strain rates is attributed to a change from near-equilibrium film cracking to dynamic film cracking. This change also leads to a greater degree of film spallation at room temperature.

C.6 Acknowledgment

The help of B. Gludovatz is acknowledged in performing the elevated temperature tests.

Bibliography to paper C

[1] F Fantini, C Morandi, IEEE Proc. G 132, 74-81 (1985)

[2] RA Miller, CE Lowell, Thin Solid Films 95, 265-273 (1982)

[3] TW Clyne, PJ Withers, An Introduction To Metal Matrix Composites, Cambridge University Press, Cambridge, 1993, pg166

[4] JT Barnby, Acta Metall. 15, 903-909 (1967)

[5] KA Peterson, I Dutta, MW Chen, Acta Mater. 51, 2831-2846 (2003)

[6] S Yoda, N Kurihara, K Wakashima, S Umekawa, Metall. Trans. 9A, 1229-1236 (1978)

[7] I Dutta, Acta Mater. 48, 1055-1074 (2000)

[8] DV Zhmurkin, TS Gross, LP Buchwalter, J. Electronic Mater. 26, 791-797 (1997)

[9] M Gosz, AF Okyar, Mech. Mater. 31, 317-329 (1999)

[10] VC Jobin, R Raj, SL Phoenix, Acta Metall. Mater. 40, 2269-2280 (1992)

[11] MW Chen, I Dutta, Appl. Phys. Lett. 77, 4298-4300 (2000)

[12] G Singh, Y Yu, F Ernst, R Raj, Acta Mater. 55, 3049 (2007)

[13] MS Hu, AG Evans, Acta Metall. 37, 917-925 (1989)

[14] DC Agrawal, R Raj, Acta Metall. 37, 1265-1270 (1989)

[15] S Frank, UA Handge, S Olliges, R Spolenak, Acta Mater. 57, 1442-1453 (2009)

[16] MJ Cordill, FD Fischer, FG Rammerstorfer, G Dehm, Acta Mater. 58, 5520-5531 (2010)

[17] BF Chen, J Hwang, IF Chen, GP Yu, J-H Huang, Surf. Coat. Technol. 126, 91-95 (2000)

[18] A Kelly, WR Tyson, J. Mech. Phys. Solids 13, 329-350 (1965)

[19] V Edlmayr, M Moser, C Walter, C Mitterer, Surf. Coat. Technol. 204, 1576-1581 (2010)

[20] M Ohring, Materials Science of Thin Films, 2nd Edition, Academic Press, San Diego, 2002, pg742.

[21] AM Huntz, L Maré chal, B Lesage, R Molins, App. Surf. Sci. 252, 7781-7787 (2006)

[22] ISO 4287:1997 (E/F)

[23] ASME B46.1, 1995, 2002, 2009

[24] NG Chechenin, J Bøttinger, JP Krog, Thin Solid Films 304, 70-77 (1996)

[25] JP Poirier, Acta Metall. 25, 913-917 (1977)

[26] Y Letterier, L Boogh, J Andersons, J-AE Månson, J. Polym. Sci. B: Polym. Phy. 35,1449-1461 (1997)

[27] M Yanaka, Y Kato, Y Tsukahara, N Takeda, Thin Solid Films 355-356, 337-342 (1999)

[28] M-H Nadal, P LePoac, J. App. Phy. 93, 2472-2480 (2003)

[29] AA Aliyu, I. Daniel, Delamination and Debonding of Materials, ASTM STP 876, W.S. Johnson, Ed., American Society for Testing and Materials, Philadelphia, 1985, pg346.

[30] AA Taylor, V Edlmayr, MJ Cordill, G Dehm, Surf. Coat. Technol. doi:10.1016/j.surfcoat.2011.07.047

D

On the limits of the Interfacial Yield Model for Fragmentation Testing of Brittle Films on Polymer Substrates

A A Taylor[a], M J Cordill[a,b], G Dehm[a,b]

[a]Erich Schmid Institute of Materials Science,
Austrian Academy of Sciences, Jahnstraße 12, A–8700 Leoben, Austria
[b]Department Materials Physics, Montanuniversität Leoben, Jahnstraße 12, A–8700 Leoben, Austria

Abstract

Fragmentation testing is frequently used to probe film fracture strain and the interfacial properties of thin brittle films on compliant substrates. A model based upon complete yield of the film/substrate interface is frequently used to analyse data after cracking has saturated. Additionally, the film is either assumed to have a single-valued failure stress or a distribution of strengths described by Weibull statistics. Recent work by the authors (Taylor et al., Surf. Coat. Technol., 2011) showed that consideration of film thickness variations and the application of neighbour ratio analysis brought 96% of the data for an Al_xO_y/Cu film/substrate system into compliance with the predictions for a film with a single-valued failure stress. In the present work Cr/PI (polyimide) and Cr/PET (polyethylene teraphthalate) systems are analysed according to the same methodology. The Cr films on polymer substrates crack such that the neighbour ratios considerably exceed the predicted limit of 2. The influence of the relative thickness of the film and substrate and the strain rate of the test is investigated. A deviation from the idealised mechanical model

due to the large difference in elastic moduli of film and substrate is put forward as a possible cause of the observed behaviour. The importance of these results to the application of the interfacial yield model is discussed.

D.1 Introduction

Thin films have become a mainstay of technological innovation. They are used in microelectronic devices, thermal/gas barrier, hard, and aesthetic coatings applications. The importance of thin films and their ever-increasing use has led to the mechanics of thin film systems being intensively studied [1–5]. Originally, metal and ceramic films on ceramics substrates for microelectronic devices [1, 2, 4] and hard films on metal substrates for abrasion and environmental resistance [6, 7] were of particular interest. More recently, metal and ceramic films on polymer substrates for use as gas barriers [8, 9] and flexible/stretchable electronics [10–12] have become a focus. Characterising film failure modes [13, 14], adhesion strengths [4, 15, 16] and stress distributions [5, 17] is essential for materials selection and component design in these applications.

It has been observed [3, 13] that cracking of the film in brittle film/compliant substrate systems saturates after a certain level of uniaxial straining, i.e. further straining does not lead to the formation of further film cracks. This phenomenon was first addressed for fibre composite systems under uniaxial load [18]; in both systems the brittle component becomes disconnected from direct loading once fracture starts, all further load must then be transferred to the film/fibre across the interface. It is reasonable to assume that the interface can only sustain a finite level of shear stress, once this stress is reached either the interface or the neighbouring substrate/matrix can be expected to yield. As straining continues, this yielded zone will travel further along the interface, this limits the rate at which load can be transferred from the substrate/matrix to the film/fibre. Saturation of cracking is expected once the interface has yielded along its complete length as at this point further straining can transfer no more load. Application of this analysis to brittle film/compliant substrate systems was first carried out by Agrawal and Raj [3] and has the advantage that the interfacial shear stress (τ_{IFSS}) for systems can be determined experimentally through a simple uniaxial tensile test. Equation D.1 gives the dependence of τ_{IFSS} on the film thickness, δ, the fracture stress of the film, σ_f, and the crack spacing, λ, in the steady state:

$$\tau_{IFSS} \propto \frac{\delta\ \sigma_f}{\lambda}. \tag{D.1}$$

A key prediction of this theory, applicable to both fibres and films, is that in the crack saturation regime the longest spacing between cracks is twice as large as the smallest. This can be understood as follows; the transfer of tensile stress to the film via shear at the interface requires a finite interfacial length, the length of interface required to load a film to its fracture stress is often referred to as the shear transfer length, λ_s, figure D.1. A film fragment exactly twice the shear transfer length can only fracture further at its exact midpoint, producing two fragments of length λ_s, these fragments are unable to fracture further. Conversely, in a film fragment whose length is infinitesimally smaller than twice the shear transfer length, i.e. it has a length of approximately $2\lambda_s$, the fracture stress for the film is not reached and

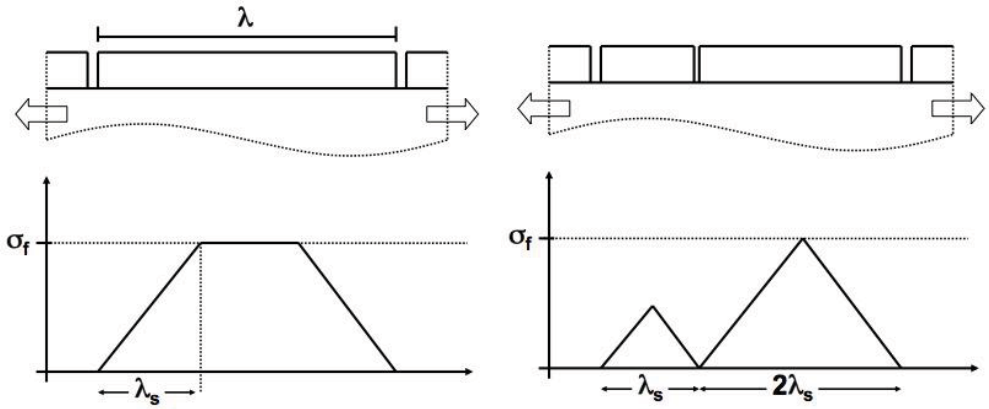

Figure D.1 Schematic of the theoretical basis of the interfacial yield model and the predicted bounding of two between the shortest and longest crack spacings. In a) the stress in the coating reaches the failure stress and can crack further, in b) the film can not crack further and saturation has been reached. λ is the general term for the spacing between film cracks while λ_s is the shear transfer length for the system.

further fracture is not possible, figure D.1b. These limits provide the factor of two difference.

The bound of two in the crack spacings is never observed experimentally, neither for fibre/matrix or film/substrate systems. One reason for this is that the fracture stress of the film is not really single-valued. Several authors [19–22] have demonstrated that the distribution of fibre/film fragment lengths can be well described by a Weibull distribution [23], indicative of a statistical distribution of film strength. Analysis of such distributions delivers the parameters α and β, the Weibull shape and scale parameters, respectively [13, 21]. The Weibull shape parameter is also known as the Weibull modulus. Figure D.2 illustrates the concept of a statistical distribution of strength in the coating. Initial coating cracks appear where the failure stress of the film is lowest, figure D.2a. Further coating cracks appear as the far-field loading of the substrate is increased and the local failure stresses of further areas of the coating are reached, figures D.2b and D.2c. Cracking finally ceases when the shear transfer lengths of the breaks interact along the length of the coating, preventing further transfer of tensile load, figure D.2d.

These simple diagrams also illustrate why a crack bounding ratio greater than two can be expected if the film does not possess a single-valued fracture stress. Three film fragments are shown in figure D.2d, the shortest, left-most, fragment is clearly more than three times shorter than the longest, right-most, fragment. This is possible when a coating does not have a single-valued fracture stress as the shortest fragment was defined by a lower fracture stress, at location *1*, and hence lower shear transfer length than the longest, defined by fracture at location *3*. Two predictions follow on from this work; firstly, it is expected that the shortest measured crack

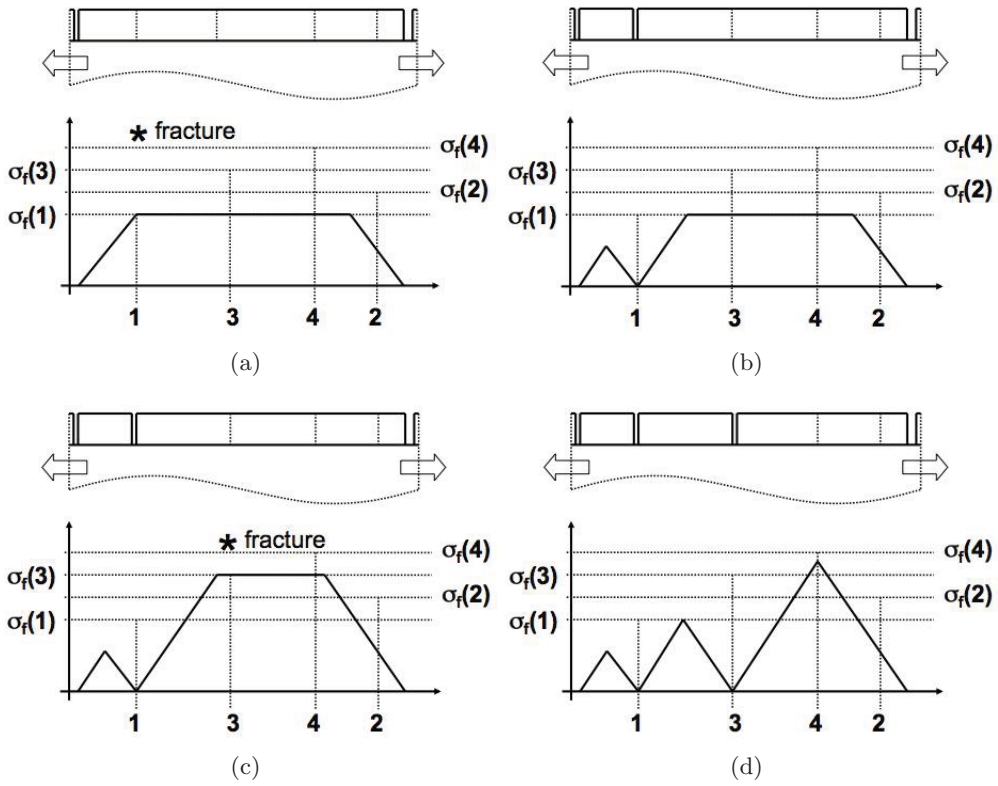

Figure D.2 The effect of a statistical distribution of strength in the film, failure occurs at locations i when the film failure stress at that location, $\sigma(i)$, is reached. In a) cracks begin to appear at the weakest points in the film. Cracking continues, figures D.2b and D.2c, until the stress drops associated with cracking all overlap and further cracking becomes impossible, d).

spacings will be formed in the earliest stages of straining when the effective shear transfer length is at its lowest. Secondly, the film fragments defined by cracks formed in the final strain increment prior to saturation should follow the predictions of a coating possessing a single-valued fracture stress. The concept of considering the film fragments produced during successive strain increments is dealt with mathematically by Curtin [19].

Following on from this, the work of the authors [24] demonstrated that the bound of two could be reached for a model Al_xO_y/Cu system by considering the effects of film thickness variations. The variation in film thickness and the horizontal distance over which the variation occurred was considered in reference to an expected maximum crack spacing, designated in this work as $2\lambda_s$. Thickness variations taking place over a horizontal distance greater than $2\lambda_s$ are termed *unevenness*, this is illustrated schematically in figure D.3. The local film thickness of the film determines the crack spacing when unevenness exists, rather than the globally measured mean film thickness, δ_{mean}.

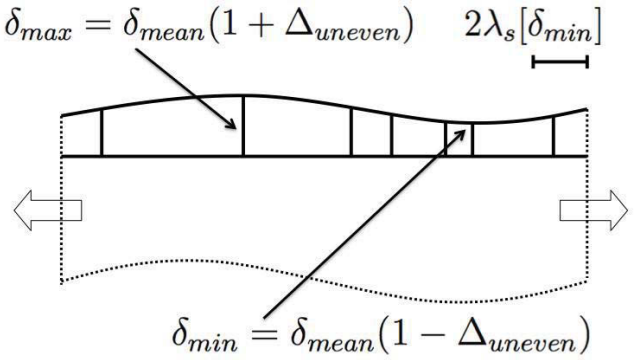

Figure D.3 A schematic of film unevenness and its effect on the crack bounding ratio. Note how crack spacings in the thicker regions of the film are greater than those in the thinner region. The locations of the maximum, δ_{max}, and minimum, δ_{min}, film thicknesses are indicated.

For a model film obeying the relation:

$$\delta = \delta_{mean} \pm \Delta\delta_{mean} = \delta_{mean}(1 \pm \Delta) \tag{D.2}$$

where δ is the film thickness and Δ is the fractional variation in thickness, it can be demonstrated that a systematic broadening of the crack spacing distribution is expected. Firstly, a crack bounding ratio, M, is defined:

$$M = \frac{\lambda_{max}}{\lambda_{min}}. \tag{D.3}$$

This ratio is calculated from the experimentally observed largest, λ_{max}, and smallest, λ_{min}, crack spacings. If the film thickness varies by an amount Δ_{uneven} over a horizontal length greater than $2\lambda_s$ then the crack bounding ratio is expected to increase with Δ_{uneven} as follows:

$$M_{uneven} = \frac{\lambda_{max}(\delta_{mean}(1 + \Delta_{uneven}))}{\lambda_{min}(\delta_{mean}(1 - \Delta_{uneven}))} = \frac{2(1 + \Delta_{uneven})}{1 - \Delta_{uneven}} \tag{D.4}$$

Equation D.4 infers that a film thickness variation of 20% in the unevenness range would lead to an observed crack bounding ratio of three rather than two.

In order to investigate whether unevenness was the cause of the observed broadening in the crack spacing distribution to values of M >2, Taylor et al. [24] compensated for unevenness by introducing the concept of a *neighbour ratio*. Neighbour ratios are determined by comparing the length of each crack spacing with only the two adjacent spacings, the larger spacing always being divided by the smaller. This analysis removes the effects of longer length-scale variations in the film thickness. Neighbour ratio values ranging from one to two are predicted for the case of a single-valued film fracture strength. The previous work demonstrated that this approach worked to good effect in bringing 96% of the data for the model Al_xO_y/Cu system

into this range. This infers that the observed statistical distribution of strength can be attributed to film variations on a length-scale greater than the maximum crack spacing, notably film thickness variation. For a more thorough analysis of the effects of film thickness variations see reference [24].

Polymers deform very differently to metals, both elastically and plastically. Initial experiments have shown that the crack spacing distributions for brittle films on polymer substrate systems are significantly broader than those observed for coatings on metal substrates, values of M greater than 10 observed for polymer substrates versus values under 5 for metal substrates. Although the same mechanical models are applied to both systems it has never been shown that this is a valid approach for coated polymer systems. If the neighbour ratio approach cannot account for crack spacing distribution broadening for polymer substrate systems as it has for films on metal substrates then the mechanical models used to analyse these systems must be scrutinised. Of particular interest is the interfacial yield model used to quantitatively relate film cracking at saturation to the interfacial shear stress, equation D.1. This model is frequently used to understand the interfacial properties of metal/polymer systems and to predict the size of film fragments following large substrate strains [9, 29].

The present work applies the neighbour ratio analysis to two metal/polymer systems, Cr/PET (polyethylene teraphthalate) and Cr/PI (polyimide). Cr films on PET and PI are scientifically interesting due to their use as adhesion-promoting layers [25–27] for conducting lines on polymer substrates for flexible electronics. They are treated as representatives for brittle films on polymer substrates. Existing work on the systems studied here [14, 28] has shown that the Cr films crack in quite different ways, parallel versus network cracking. Studying the two systems therefore keeps this investigation more general as regarding brittle films on polymer substrates.

D.2 Experimental

Cr films of nominal 10, 20, 50 and 120 nm thickness were deposition by industrial-scale web coating onto 50 μm PET (Mitsubishi Hostaphan RN) substrates by DC magnetron sputtering with an Ar plasma gas. Sputtering was carried out at an approximate Ar pressure of $8 \cdot 10^{-3}$ mbar. In this set-up, a fixed thickness of film is deposited per substrate pass, i.e. film thickness is increased through multiple substrate passes without vacuum being broken. In addition to these systems, nominal 10 nm Cr films were deposited onto PET substrates of 12, 25, 75 and 100 μm thickness by the same process.

Nominally 10, 50, 200 and 500 nm thickness Cr films were deposited onto 50 μm PI substrates (UBE Industries UPILEX-R). The films were E-beam evaporated (Balzers BAK 550) at a vacuum pressure of $2.10 \cdot 10^{-7}$ mbar with a depostion rate of 0.5 nm/s. Further details of the deposition process are found in reference [14].

Cross-sectional and plan-view transmission electron microscopy (TEM, Phillips CM12 and JEOL 2100F with a CEOS C_s image corrector) was used to characterise

the microstructure of these films. Cross-sectional samples were produced of the Cr/PI films by dimple-grinding (Gatan) followed by ion milling (Gatan DuoMill, Bal-Tec, Gatan PIPS). Plan view samples of the Cr/PI and Cr/PET were produced by a film removal technique described in [30].

Testing of the samples was performed both *in situ* in a scanning electron microscope (SEM, Leo 1525) with a highly accurate, $\pm$ 1 μm, displacement controlled straining stage (Kammrath and Weiss) and *ex situ* with a versatile testing rig capable of higher displacement rates (MTS Tytron). The *in situ* tests were all performed at a strain rate of 4 $\cdot 10^{-4}$ s^{-1} and straining was carried out in a stepwise manner so that images could be recorded at the different levels of strain. The *ex situ* tests were performed at strain rates of 4 $\cdot 10^{-5}$, 4 $\cdot 10^{-4}$ and 4 $\cdot 10^{-3}$ s^{-1}. In addition to these techniques, a compact in-house developed screw-driven tensile frame was used to record atomic force microscopy (AFM, Digital Instruments Dimension 3100) images of several of the films while under load.

Measurement of the crack spacings, and hence the neighbour ratios, was performed by drawing lines perpendicular to the cracks on SEM micrographs. Gaps open up between crack flanks in the saturation regime as the substrate continues to strain while further film cracking is inhibited, these gaps are excluded from measurements of the crack spacing, i.e. crack spacing is here defined as the film fragment widths. In order to ensure good statistics, over 250 crack spacings were measured for each sample investigated.

D.3 Results and Discussion

D.3.1 Microstructure and Crack Morphology

The Cr films deposited onto PET have a nano-crystalline equiaxed structure that remains approximately constant with varying film thickness, this is presumably a consequence of the multi-pass deposition procedure by which they are produced. Further discussion of the microstructure of these films can be found in a previous study by the authors [30]. TEM examination of film fragments [30] was used to determine values for the actual film thicknesses of all the films studied. The Cr/PET films were found to have actual thicknesses of 15, 25, 70 and 150 nm, somewhat thicker than the nominal values, while no significant deviation from the nominal values was observed for the Cr/PI films. There is a 10% uncertainty in these thickness measurements. The Cr coatings on PET exhibit very straight cracks perpendicular to the straining axis, figure D.4a.

The Cr films on PI have a columnar structure where the grain size varies linearly with the film thickness, i.e. the 50 nm thick films have a lateral grain size of 15 nm while for the 500 nm thick films a grain size of 70 nm was observed. Further discussion of these films, their microstructure and periodic cracking behaviour, can be found in [14]. On PI, the Cr coatings exhibit a more network-type cracking with cracks regularly deviating from the direction perpendicular to straining, figure D.4b. In addition to the stark difference in crack morphology between the Cr films on

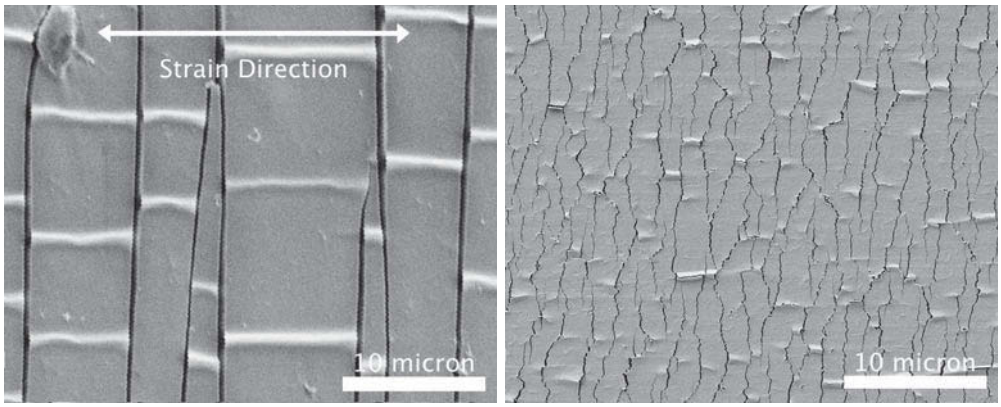

(a) (b)

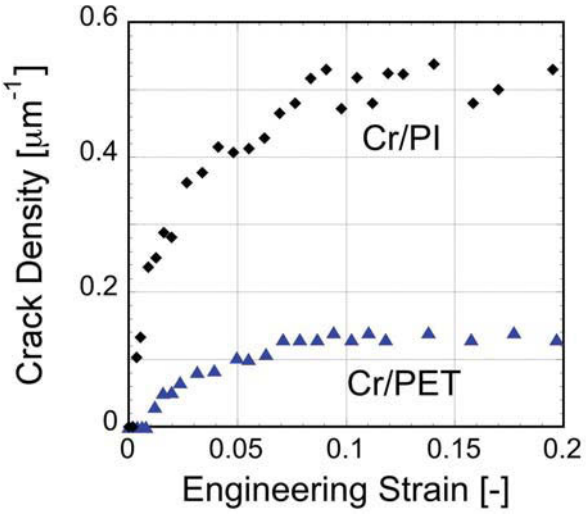

(c)

Figure D.4 SEM micrographs of a) the 70 nm Cr coating on PET and b) the 50 nm Cr coating on PI, both strained to 19%. The differences in both crack morphology and spacing should be noted. c) presents the evolution of cracking in the films with applied strain, both systems reach saturation at around 10% applied strain. The buckles formed between crack due to lateral substrate contraction are treated elsewhere [5, 16].

Table D.1 Comparison of experimentally determined parameters for the various Cr thicknesses on PI and PET investigated in this study. λ_{min} is the minimum measured crack spacing, M is the crack bounding ratio (as defined in equation D.3), R_{max} is the maximum measured neighbour ratio and R >2/% represents the percentage of measured neighbour ratios found to exceed two.

Film Thickness, δ/nm	Substrate	$\lambda_{min}/\mu m$	M	R_{max}	R >2/%
15	50PET	0.63	6.8	4.1	22
25	50PET	1.0	6.8	4.6	19
70	50PET	1.5	10.7	4.9	34
150	50PET	1.5	11.4	8.3	33
10	50PI	0.31	5.7	3.8	12
50	50PI	0.35	11.8	11.7	29
200	50PI	0.78	11.2	5.4	25
500	50PI	1.9	16.6	11.5	45

the two substrates, a large difference in the saturation crack spacing is clear. The images in figure D.4 were taken at the same magnification and the systems were both strained to 19% yet the Cr/PET sample has a crack spacing approximately four times that of the Cr/PI, 1.5 versus 0.35 μm minimum measured crack spacing, table D.1. The lower fracture strain of the Cr films on PI (0.37% for the 50 nm film on PI compared to 0.80% for PET, figure D.4c) accounts for about half of this difference and the slightly greater thickness of the Cr film on PI accounts for a further 25% but this leaves a 25% increase in crack spacing. This increase indicates that the PI substrate is more able to transfer shear stress across the film/substrate interface ("strong" interface), causing smaller crack spacings than in the Cr/PET system ("weak" interface).

The network cracking of the Cr films on PI is proposed to be a consequence of the columnar nature of the grains in these films compared to the equiaxed grains of the Cr on PET. Cracks in the film are expected to follow these columnar grain boundaries as they provide a reduced-energy fracture surface through the film [31, 32]. In following the grain boundaries the cracks are repeatedly deflected, leading to the observed crack morphology.

D.3.2 Neighbour Ratios

The crack spacings and neighbour ratios assessed for the different thickness Cr films on PI and PET are presented in figure D.5. The crack spacing distributions, figures D.5a and D.5c, show the films all possess an even distribution of spacings with thicker films having broader spacings, as predicted by equation D.1. The neighbour ratios, figures D.5b and D.5d, can be seen to significantly exceed two for all the samples investigated. It can additionally be seen that the thicker films have broader distributions of neighbour ratios with greater proportions of the measured ratios exceeding two.

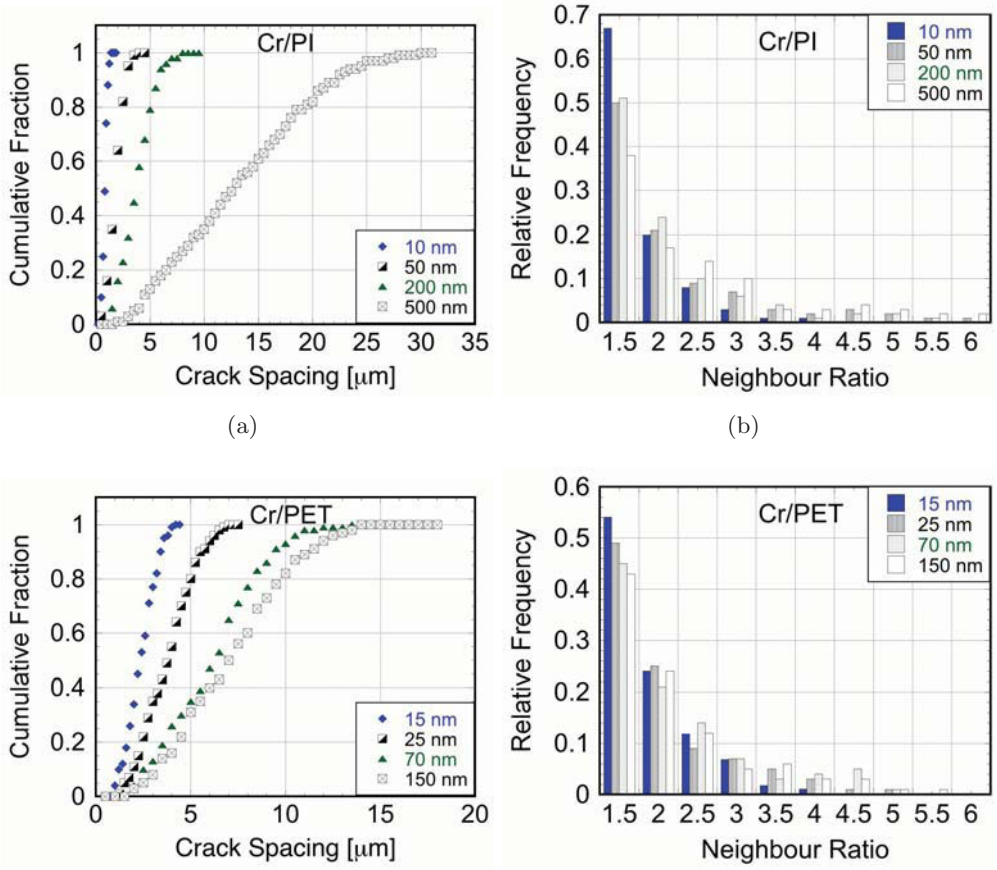

Figure D.5 Crack spacing distributions, a) & c), and neighbour ratios, b) & d), for the Cr/PI, a) & b), and Cr/PET, c) & d), systems. Note that the neighbour ratio distributions for all systems considerably exceeds the predicted bound of two.

A summary of the mechanical properties of these systems is presented in table D.1, the minimum measured crack spacing, λ_{min}, crack bounding ratio, M, maximum measured neighbour ratio, R_{max}, and percentage of neighbour ratios greater than two, R >2, are presented. One trend is observable from this data; all these metrics tend to increase with increasing film thickness. In addition to the crack spacings, the crack bounding ratios also increase with the film thickness, going from 6.8 and 5.7 for the thinnest films to 11.4 and 16.6 for the thickest. The neighbour ratios for the two substrates also show this trend, both the maximum measured ratios and the percentage of ratios exceeding two tend to increase as the films get thicker. Due to the very similar behaviour of these two substrate systems all further analysis will focus on the Cr/PET system as this similarity continues through all the analysis.

The most important point to note from the analysis of the Cr/PET and Cr/PI is that none of the tested samples, with the possible exception of the 15 nm film on 23 μm PET discussed shortly, meet the prediction of a bound of two in the neighbour ratios, unlike the observation of the authors [24] for Al_xO_y films on Cu. Neighbour ratios higher than 11 were observed on several occasions in the Cr/PI and Cr/Pet systems with up to 45% of the ratios being greater than the predicted value of two. These systems are fairly typical of those investigated elsewhere in regard to both the substrate material and thickness and the coating thickness. Closer investigation of what might be causing this deviation is therefore of some importance.

The results for Cr/PET and Cr/PI systems suggest that film thickness plays a significant role in the cracking. In both systems the highest recorded R_{max} was for the thickest film and the lowest for the thinnest film, table D.1. In addition, the lowest percentage of neighbour ratios greater than two was also found for the thinnest films. A possible cause for this behaviour is strain localisation in the polymer substrate between the film cracks. Uniform deformation of the substrate is a key assumption of the interfacial yield approach and if strain localisation is occurring then it could prevent the film cracking from reaching a true saturation state.

The combination of the very large difference in Young's modulus for the materials, 3-4 GPa for PET and PI versus 290 GPa for Cr, with the relatively low thickness of the substrate leads to the film carrying a significant fraction of the total stress in the un-cracked state. Using a simple equal strain approach, rule of mixtures, for the systems prior to cracking and moduli of 290 GPa for Cr and 3 GPa for the polymer substrate it is estimated that the 500 nm Cr/50μm thick system has an effective modulus of 5.8 GPa, this effective modulus decreases to 3.3 GPa for a 50 nm film. While this effective modulus of the composite will reduce following first cracking of the film, it does provide an indicator of the reduction in stiffness expected for the substrate where the coating has cracked and could explain the observed thickness effect. The interfacial yield approach requires that transfer of stress at the film/substrate interface prevents further cracking in the saturation state. If localisation of strain to the reduced stiffness regions under coating cracks instead causes the saturation in cracking then the predictions of the interfacial yield model are unlikely to apply.

In order to further investigate the possibility that strain localisation is preventing

Table D.2 Comparison of experimentally determined parameters for 15 nm Cr films on PET substrates of varying thickness. δ is the film thickness, M is the crack bounding ratio (as defined in equation D.3), R_{max} is the maximum measured neighbour ratio and R >2/% represents the percentage of measured neighbour ratios found to exceed two.

PET Thickness/μm	δ/nm	$\lambda_{min}/\mu m$	M	R_{max}	R >2/%
12	15	0.68	6.0	4.3	13
23	15	1.0	4.8	3.5	6
50	15	0.63	6.8	4.1	22
75	15	0.73	5.5	3.9	24
100	15	0.78	6.1	4.5	18

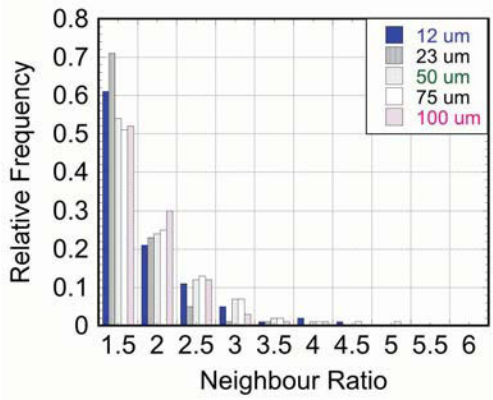

Figure D.6 Neighbour ratios for 15 nm Cr coatings on PET substrates ranging from 12 to 100 μm in thickness. No significant affect of the substrate thickness on the film neighbour ratios is observable.

saturation, and hence invalidating an interfacial yield analysis, the 15 nm coating on PET was deposited on different thickness substrates, ranging from 12 – 100 μm. This was chosen over further decrease of the film thickness to ensure that the films remained continuous. A comparison of the mechanical properties is presented in table D.2. With the exception of the 23 μm substrate the mechanical properties of the the Cr/PET samples do not depend on substrate thickness in this range, all metrics show similar values.

The 23 μm substrate sample shows a much tighter distribution of neighbour ratios with only 6% being greater than two, this sample is taken to be anomalous as coatings on both the thinner and thicker substrates due not show this behaviour. Figure D.6 presents the full neighbour ratio data for these samples.

The effective composite stiffness for these samples ranges from 3 to 3.4 GPa, i.e. the reduction in stiffness expected under the cracks in the 100 μm substrate is negligible. The neighbour ratios for the samples with the thickest substrates remain in contravention of the predictions. The lack of improvement in the neighbour ratios for the substrates thicker than 50μm strongly suggests that while strain localisation

Table D.3 Comparison of experimentally determined parameters for the 15 nm Cr on 50 μm PET samples investigated at different strain rates. λ_{min} is the minimum measured crack spacing, M is the crack bounding ratio (as defined in equation D.3), R_{max} is the maximum measured neighbour ratio and R >2/% represents the percentage of measured neighbour ratios found to exceed two.

Strain Rate/s^{-1}	Substrate	$\lambda_{min}/\mu m$	M	R_{max}	R >2/%
$4 \cdot 10^{-5}$	50PET	0.56	8.0	6.7	27
$4 \cdot 10^{-4}$	50PET	0.63	6.8	4.1	22
$4 \cdot 10^{-3}$	50PET	0.57	8.4	5.7	28

is causing some of the deviation from the bound of two, it cannot completely account for the behaviour.

In the work of Jobin et al. [33] it was found that the cracking behaviour of a SiO_x film on Cu becomes strain rate dependent at temperatures as low as 300°C. Critically, it was observed that the distribution of cracks in the film became significantly broader in this regime. This effect was attributed to diffusional sliding at the interface and its activation depends on the homologous temperature of the lower melting point component. For the SiO_x/Cu system diffusional sliding was first observed at a homologous temperature of 0.44 for Cu. If a melting point for PET of 250°C is taken [34] then room temperature (25°C) corresponds to a homologous temperature of 0.57, this is higher than for Cu and so it is possible that rate dependent processes are active even at room temperature. If rate dependent processes are active then the normal interfacial yield model is not valid and the spacings between cracks would not be expected to follow the predictions of the model.

To investigate the possibility of time dependent effects on the film cracking several 15 nm coatings on 50 μm PET were strained at different strain rates. Straining at 4 $\cdot 10^{-5}$, 4 $\cdot 10^{-4}$ and 4 $\cdot 10^{-3}$ s^{-1}, two orders of magnitude variation, did not affect the neighbour ratios or crack spacings. The mechanical metrics for these samples are presented in table D.3, the neighbour ratios in figure D.7. The unchanged nature of the crack spacings and neighbour ratios over this range of strain rates strongly indicates a lack of time-dependent effects on the cracking of the films.

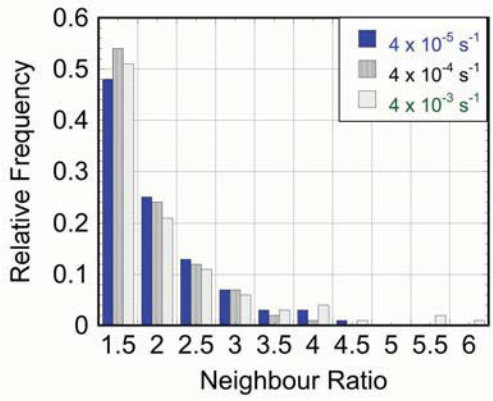

Figure D.7 Neighbour ratios for 15 nm Cr coatings on PET substrates ranging from 12 to 100 μm in thickness. No significant affect of the substrate thickness on the film neighbour ratios is observable.

D.3.3 Small Crack Spacings Prior to Saturation

In the introduction it was highlighted in figure D.2 that the statistical theory of film strength indicates that the smallest spacings between cracks are expected to form in the earliest stages of cracking where the weakest film areas are failing and the effective shear transfer length is at its shortest. As a further measure of whether the Cr coatings are behaving as the models predict, analysis has been carried out on several series' of images of Cr coatings on PET recorded during *in situ* straining. One series for a 150 nm Cr/PET sample is shown in figure D.8. In these images it can be seen that the smallest spacings between cracks are often formed during cracking at high strains, figures D.8c and D.8d. According to the statistical distribution of fracture stress theory [19], the final cracks to form before cracking saturates cannot form crack spacings smaller than half the length of the longest spacings remaining at saturation. This is because the behaviour of the system just prior to saturation is identical to the behaviour of a system with a single-valued fracture stress. Figure D.8d shows a 150 nm Cr/PET film in the saturation condition, an arrow indicates one of the final cracks to form in this sample, this crack clearly defines a new crack spacing that is more than a factor of three shorter than the longest remaining spacings. This behaviour is a strong indicator that the films investigated in this study do not follow the predictions of existing models for cracking of brittle coatings in the saturation regime.

D.3.4 Out of Plane Film Deflection

The theory and analysis relating to interfacial yield and saturation of cracking in brittle films on compliant substrates makes several assumptions, the violation of which could lead to deviations from the mechanical predictions. One of these, uniformity of deformation in the substrate, has already been discussed. Other assumptions

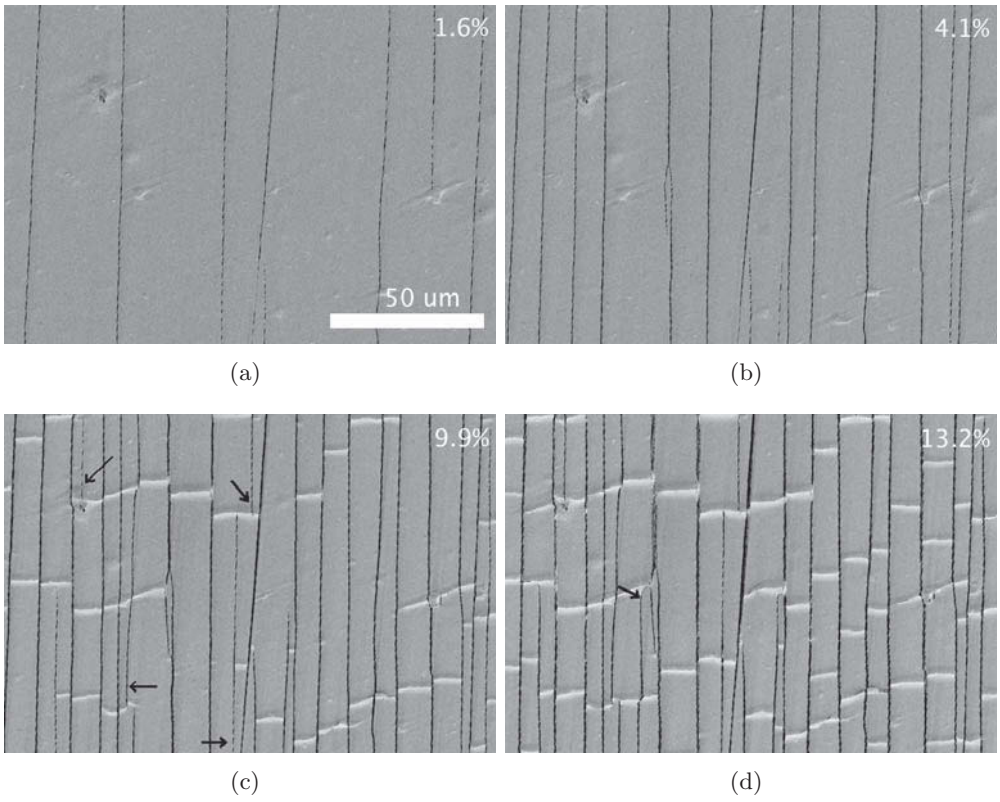

Figure D.8 A series of SEM images recorded during the *in situ* straining of a 150 nm Cr film on PET, the same area is shown throughout. The arrows on c) & d) indicate the continued formation of closely spaced cracks at high strains. The sample engineering strain is marked for each image.

inherent in the models are that both the film fracture stress and interfacial strength are single-valued and that the interface remains parallel with the loading direction. In any real system some variation is to be expected in both the interfacial strength and the film fracture stress. However, an advantage of the neighbour ratio analysis is that it accounts for all long-range variations, not just variations in film thickness. It is therefore very unlikely that variation in these properties could lead to the large deviations observed. The effect of how parallel to the load direction the interface remains during testing has never been assessed. In the following the parallel interface problem will be discussed as a possible cause of the anomalous behaviour of these brittle films on polymer substrates.

In order to understand why the film/substrate interface may not remain coplanar with the straining axis during testing it is useful to consider a simplified picture of the film and substrate during loading. In addition to this, only elastic strains are analysed in the following. In figure D.9a the classical model of a brittle film/compliant substrate system is shown. In the model the interface is coplanar with the load axis and load can only be transferred to the film via shear at the interface. In figure D.9b the film is shown alone with the shear along the interface simplified to a force, T, acting at the lower edges of the film. From this diagram it is easy to understand that the film would bend, as illustrated, in response to being loaded along one edge. In figure D.9c the film is shown, once again attached to the substrate, but now with a curled interface. Some curling at the film/substrate interface is in fact an inevitability of the tensile stress in the film loaded via the interface, the extent of this curling will depend on the difference in stiffness between the film and substrate. Lower stiffness substrates are expected to allow the interface to curl more as the force exerted by the film will be the same but the substrate deflection due to this force will be greater. This could explain why the model Al_xO_y/Cu system previously studied (E_{AlxOy} = 160 GPa, E_{Cu} = 115 GPa) [24] complied well with the predictions while the polymer substrate systems (E_{Cr} = 290 GPa, $E_{PET} \approx E_{PI}$ = 3-4 GPa) do not. Figure D.9c also illustrates schematically how significant curling of the film/substrate interface can complicate the mechanics of the system, leading to bending stresses in the coating and direct transferral of tensile stress from the substrate into the film.

To learn if the films investigated were curling in the manner described in figure D.9 a small screw-driven tensile frame was designed such that the samples could be strained and held at load under an AFM. Figure D.10 shows an AFM height image of a film fragment from a 150 nm Cr/PET sample strained to ∼10%, figure D.10a, while figures D.10b and D.10c present a 3D view and a line scan across the same fragment. Figure D.10d presents a film fragment line scan from a 50 nm Cr/PI sample, the scatter in the scan is due to the roughness of the film. This AFM data clearly shows the vertical deflection of the films at the edges, the deflection is not as simple as that shown schematically in figure D.9 because the substrates are in the plastic behaviour regime, complicating the forces involved. The magnitude of the deflections, around one third of the film thickness for both samples, is likely to be sufficient to cause major complications in the loading of the coating. Vertical

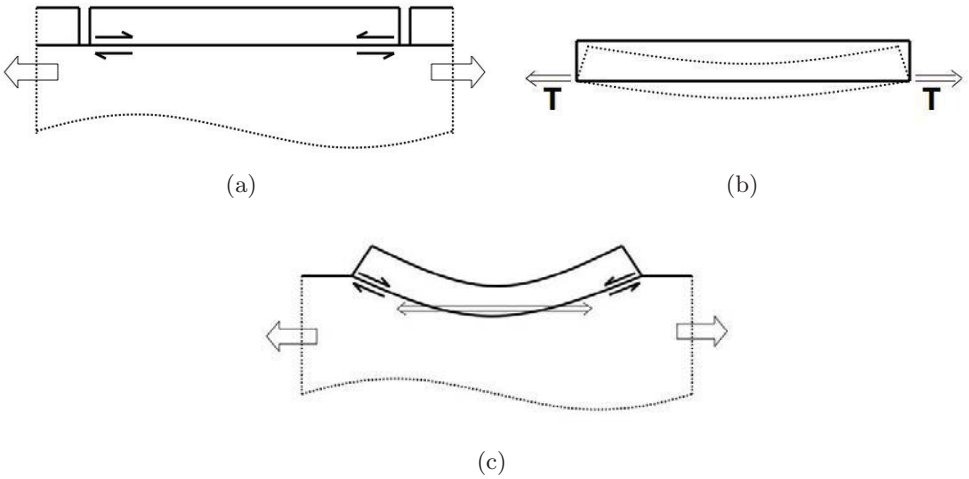

Figure D.9 Schematic of a), the classical brittle film/compliant substrate model, b), a free body diagram of the film being loaded along one edge and c), a system with a curled film/substrate interface. Note in c) how the transfer of tensile load into the film is no longer purely through shear at the interface.

deflections like those shown in figure D.10 were observed for every sample imaged under load, these deflections are not observed for unloaded samples. A recent paper by Douville et al. [35] found similar curling of the film/substrate interface both experimentally and through finite element analysis. This behaviour could be the cause of the anomalous cracking behaviour outlined in this paper.

D.4 Conclusions

The evidence presented in this work strongly suggests that the existing models for describing the cracking of brittle films on polymers in the saturation regime are inadequate. The high neighbour ratios, small crack spacings forming at high strains and the presence of a film/substrate interface that is not coplanar with the load axis all support this. By investigating different film and substrate thicknesses and different testing strain rates it has been shown that neither localisation of strain under coating cracks or rate dependent effects are responsible for this behaviour.

The observed curling of film fragments complicates the stress states in the film and across the film/substrate interface. The assumptions made by the interfacial yield model do not hold in these circumstances and hence it is not valid to use the model to quantitatively describe film cracking in the steady state or calculate interfacial shear stresses. Qualitative comparison of film crack spacings in relation to the film thickness remains valid. To understand these findings new mechanical models must be developed, models which account for a non-coplanar interface. Due to the complexity of this geometry it is also anticipated that computer simulation

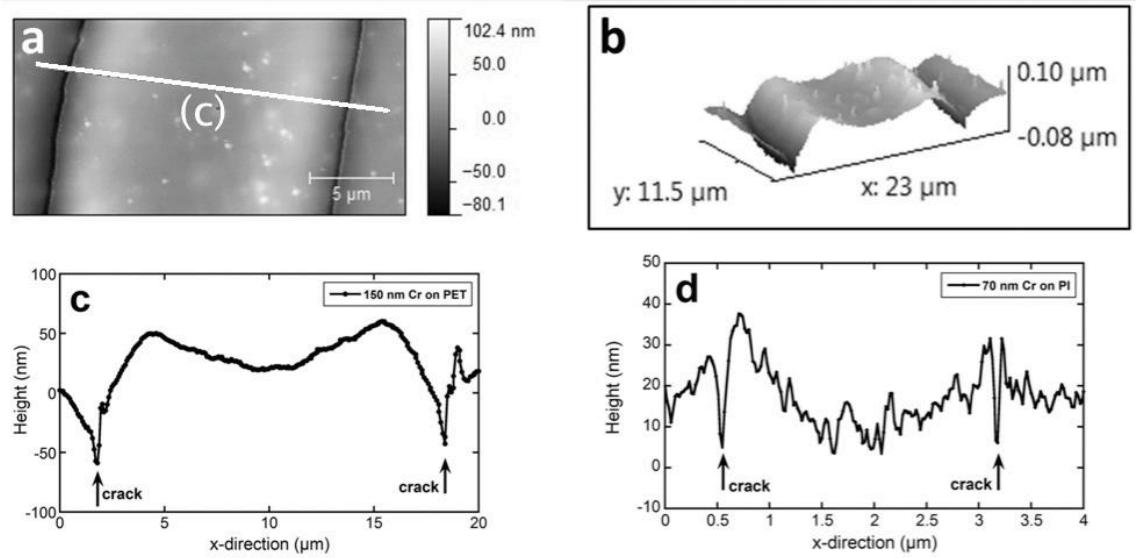

Figure D.10 An AFM height image of the 150 nm Cr/PET system at ∼10% strain, a), shows the extent of the out-of-plane deflection in the film. This is made clearer with a 3D image, b), of the same area and c) presents a line scan across the film fragment marked in a). A similar line scan from a 50 nm Cr/PI sample is shown in d) to illustrate that this effect is general.

will be a useful tool in understanding the observations and providing practical limits for the use of the existing interfacial yield approach to understand coating fracture and interfacial strength.

Acknowledgements

K Schmidegg (Hueck Folien GmbH) and J Schalko (Institute for Integrated Sensor Systems of the Austrian Academy of Sciences and Institute of Sensor and Actuator Systems, TU Vienna) are acknowledged and thanked for providing the chromium films used in this study. In addition, A. Hohenwarter and F. Hubner of the Erich Schmid Institute are thanked for developing the screw-driven tensile frame used in this study. Lastly, MJC gratefully acknowledges funding from the Austrian Science Fund (FWF) under project P22684-N20.

Bibliography to paper D

[1] MS Hu, AG Evans, Acta Metall. 37, 917-925 (1989)

[2] WD Nix, Met Trans A 20A, 2217-2245 (1989)

[3] DC Agrawal, R Raj, Acta Metall. 37, 1265-1270 (1989)

[4] JW Hutchinson, Z Suo, Adv. Appl. Mech. 29, 63-191 (1992)

[5] S Frank, UA Handge, S Olliges, R Spolenak, Acta Mater. 57, 1442-1453 (2009)

[6] PC Jindal, DT Quinto, GJ Wolfe, Thin Solid Films 154, 361-375 (1987)

[7] PH Mayrhofer, C Mitterer, L Hultman, H Clemens, Prog. Mater. Sci. 51, 1032-1114 (2006)

[8] J Rice, Food Process. 78 (1992)

[9] Y Leterrier, Prog. Mater. Sci. 48, 1 (2003)

[10] K Nomura, H Ohta, A Takagi, T Kamiya, M Hirano, H Hosono, Nature 432, 488 (2004)

[11] Y Sun, WM Choi, H Jiang, YY Huang, JA Rogers, Nature Nano. 1, 201 (2006)

[12] JA Rogers, T Someya, Y Huang, Science 327, 1603 (2010)

[13] Y Letterier, L Boogh, J Andersons, J-AE Månson, J. Polym. Sci. B: Polym. Phy. 35, 1449-1461 (1997)

[14] MJ Cordill, A Taylor, J Schalko, G Dehm, Metall. Mater. Trans. A 41, 870-875 (2010)

[15] PS Ho, F Faupel, Appl. Phys. Lett. 53, 1602-1604 (1988)

[16] MJ Cordill, FD Fischer, FG Rammerstorfer, G Dehm, Acta Mater. 58, 5520-5531 (2010)

[17] F Ahmed, K Bayerlein, SM Rosiwal, M Göken, K Durst, Acta Mater. 59, 5422-5433 (2011)

[18] A Kelly, WR Tyson, J. Mech. Phys. Solids 13, 329-338 (1965)

[19] WA Curtin, J. Mater. Sci. 26, 5239-5253 (1991)

[20] P Feillard, G Désarmot, JP Favre, Composites Sci. Tech. 50, 265-279 (1994)

[21] J Andersons, Y Leterrier, G Tornare, P Dumont, J-AE Månson, Mech. Mater. 39, 834-844 (2007)

[22] R Gulino, SL Phoenix, J. Mater. Sci. 26, 3107-3118 (1991)

[23] W Weibull, J. Appl. Mech. 18 (1951)

[24] AA Taylor, V Edlmayr, MJ Cordill, G Dehm, Surf. Coat. Technol. *accepted* doi:10.1016/j.surfcoat.2011.07.047

[25] OS Heavens, J. Phys. Radium 11, 355-360 (1950)

[26] JC Hoogvliet, WP van Bennekom, Electrochemica Acta 47, 599-611 (2001)

[27] KE Paul, WS Wong, SE Ready, RA Street, Appl. Phys. Lett. 83, 2070-2072 (2003)

[28] MJ Cordill, K Schmidegg, G Dehm, Phil. Mag. Lett. 91, 530-536 (2011)

[29] M Heinrich, P Gruber, S Orso, UA Handge, R Spolenak, Nano Lett. 6, 2026-2030 (2006)

[30] AA Taylor, MJ Cordill, G Moser, G Dehm, Prakt. Metallogr. 48, 408-413 (2011)

[31] PG Shewman, Metall. Mater. Trans. A 29, 1535-1544 (1998)

[32] A Gilbert, GT Hahn, CN Reid, BA Wilcox, Acta Metall. 12, 754 (1964)

[33] VC Jobin, R Raj, SL Phoenix, Acta Metall. Mater. 40, 2269-2280 (1992)

[34] http://www.m-petfilm.com/Europe/Hostaphan technical data.htm

[35] NJ Douville, Z Li, S Takayama, MD Thouless, Soft Matter 7, 6493-6500 (2011)

E

An Elevated Temperature Study of a Ti Adhesion Layer on Polyimide

A A Taylor[a], M J Cordill[a,b], L Bowles[a], J Schalko[c,d], G Dehm[a,b]

[a]Erich Schmid Institute of Materials Science,
Austrian Academy of Sciences, Jahnstraße 12, A–8700 Leoben, Austria
[b]Department Materials Physics, Montanuniversität Leoben, Jahnstraße 12, A–8700 Leoben, Austria
[c]Institute for Integrated Sensor Systems,
Austrian Academy of Sciences, Viktor Kaplan Straße 2, A–2700 Wiener Neustadt, Austria
[d]Institute of Sensor and Actuator Systems,
Vienna University of Technology, Gusshausstraße 27–29, A–1040 Vienna, Austria

Abstract

Titanium layers are used to promote adhesion between polymer substrates for flexible electronics and the Cu or Au conducting lines. Good adhesion of conducting lines in flexible circuits is critical in improving circuit performance and increasing circuit lifetime. Nominally 50 nm Ti films on polyimide (PI) are investigated by fragmentation testing under uniaxial load in the as-deposited state, at 350°C, and after annealing. The cracking and buckling of the films show clear differences between the as-deposited and the thermally treated samples, cracks are much straighter and buckles are smaller following heat treatment. These changes are correlated to a drop in adhesion of the samples following heat treatment. Adhesion values are determined from the buckle dimensions using a total energy approach as described in the work of Cordill et al. (Acta Mater. 2010). Cross-sectional TEM of the Ti/PI interface

found evidence of a ∼10 nm thick Ti-PI interlayer in the as-deposited sample not observed in heat treated samples. Ti-PI phase separation at the interface is therefore put forward as the cause of adhesion reduction in Ti/PI samples following a heat treatment.

E.1 Introduction

The realisation of electronic circuitry on flexible and stretchable substrates [1–3] requires the patterning of conducting lines onto flexible substrates like polyimide (PI) and polydimethylsiloxane (PDMA). Cr and Ti adhesion layers are used to improve the adherence of the conducting line material [4–6], usually Cu or Au. The exact mechanisms by which materials such as Ti and Cr function as effective adhesion layers are not yet fully understood [7, 8].

The mechanical properties of adhesion layers are critical for device performance and lifetime. The failure of the adhesion layer or any of the interfaces leads at least to reduced performance, if not total failure, of the flexible circuit. Much work is ongoing in the characterisation of adhesion layer materials and substrate/adhesion layer/conducting material systems [9–12]. A common means of investigating the mechanical properties of the film and interface of film on compliant (polymer) substrates is the uniaxial fragmentation test [12–15]. In this experiment, samples of coated substrate are strained uniaxially and the evolution of damage in the coating (cracks, buckles and coating delamination) are tracked with increasing applied strain. With this method the film failure stress and statistical distribution of strength can be assessed [15, 17], the shear stress at the film/substrate interface can be characterised [14, 18] and the film substrate adhesion can be measured [19, 20].

In addition to the characterisation of these systems in their as-deposited state, it is important to consider the effects of external stimuli such as temperature due to further processing steps and use of the circuit. In a previous study [16] it was found that annealing a Cu/Ti/PI system led to the formation of intermetallic phases and the adhesion of the polymer interface was reduced compared to as-deposited samples. Further investigation of the Ti/PI interface was required to understand the effect of temperature on adhesion. In this study the Ti/PI interface was exposed to 350°C, a rather high temperature for a metal/polymer system, which should accelerate interfacial ageing conditions The temperatures involved are not typical of those experienced by flexible electronics either during processing or in service but this approach provides a means of investigating the long-term effects of thermal loading on these materials. In order to resolve the microstructural processes taking place at the interface, transmission electron microscopy (TEM) investigation of these Ti/PI samples is employed.

E.2 Experimental

A Ti film of nominal 50 nm thickness was deposited onto a cleaned PI substrate (50 μm thick UBE Industries UPILEX-R) by e-beam evaporation (Balzers BAK 500) at a pressure of $3{\cdot}10^{-7}$ mbar. A deposition rate of approximately 0.5 nm s^{-1} was maintained during the process. TEM investigation revealed the film to be (60±3) nm in thickness where the error corresponds to the standard deviation of the measurements.

The samples were tested with a mechanical testing frame (Zwick) fitted with a non-commercial vacuum oven. Room temperature tests were carried out in air while tests at elevated temperature were conducted at a vacuum of 10^{-4} mbar and a temperature of 350°C. This set-up typically required 90 minutes to reach 350°C and took 60 minutes to cool down to a temperature at which the sample could be exchanged. All tests were performed at a strain rate of $4{\cdot}10^{-4}$ s^{-1} on samples with 7 mm width and 24 mm gauge length. Sample load data could not be recorded during testing as the low loads developed in these samples at elevated temperature could not be reliably resolved above the noise of the system. As no means of assessing the film crack spacing *in situ* was available in the current set-up, crack development profiles were produced by straining multiple samples to different levels of strain. 8-10 samples are required to be tested to different levels of strain to create a profile of the crack density versus strain equivalent to that produced by an *in situ* test. In addition to the samples strained at room temperature and 350°C, several samples were heated to 350°C in the vacuum oven and held at this temperature for 90 minutes, these samples were then tested at room temperature.

The microstructure and thickness of the films and the structure of the film/substrate interface were examined with transmission electron microscopy (TEM, Philips CM 12 and JEOL 2100F with a CEOS image aberration corrector). Cross-sectional TEM samples were produced by dimple-grinding (Gatan) and ion-milling (Gatan PIPS). In addition to the cross sections, plan view TEM samples were produced by the technique outlined in reference [21]. TEM samples of the films were produced from the as-deposited, annealed and 350°C tested material.

Examination of the samples after mechanical testing was carried out by optical microscopy (Olympus BX51), by scanning electron microscopy (SEM, Leo 1525) and by atomic force microscopy (AFM, Digital Instruments Dimension 3100) in tapping mode. Several *in situ* tests of samples in the as-deposited and annealed states were performed inside the SEM using a miniaturised testing frame (Kammrath and Weiss). These tests were carried out at the same nominal strain rate as the *ex situ* experiments but were strained step-wise such that secondary electron images of the film cracking were recorded at progressively higher levels of strain. AFM measurements were used to determine the dimensions of buckles formed by the Ti film after straining, the measured dimensions were then used to calculate film adhesion energies for the as-deposited and 350°C tested samples.

E.3 Results

E.3.1 Microstructure and Cracking

The plane view TEM of the as-deposited, 350°C tested, and annealed samples revealed the grain size of the samples to be unaffected by the heat treatments, figure E.1. The grain sizes of these samples were measured to be (32±8), (28±8) and (24±9) nm for the as-deposited, 350°C tested and annealed samples, respectively. The error presented in these measurements is the standard deviation of the data,

there is no statistically significant difference between these grain size estimates. The moiré fringes [22] in all the plan view TEM micrographs, figure E.1, indicate that overlapping grains are present through the film thickness, i.e. the films do not have a purely columnar structure. This was confirmed from the TEM cross-sections. Finally, selected area diffraction (SAD) of the samples, not presented, confirmed the Ti films to be hexagonal close packed α-Ti.

The fragmentation testing of the samples revealed a stark difference in fracture and buckling behaviour, figure E.2. The as-deposited sample has cracks with rough edges and uncracked broad buckles with a triangular footprint, figure E.2a. The 350°C tested and annealed samples have cracks with very straight edges and cracked narrow buckles with an approximately rectangular footprint, figures E.2b and E.2c. Figure E.2d presents the evolution of crack density in the coatings with applied strain, there is a strong difference in density between the three types of sample. The crack density of the annealed sample at crack saturation is highest at 0.40 μm^{-1} while the as-deposited sample has a density of 0.24 μm^{-1} and the 350°C tested sample 0.14 μm^{-1}. The crack density data for the sample tested at 350°C was obtained from *ex situ* experiments, this causes the greater scatter between data points compared to the crack density data of the as-deposited and annealed samples. A difference in the strain at which cracking is first observed is also found. The annealed sample has the lowest crack onset strain with 1.6% compared to 5% for the as-deposited sample. An accurate crack onset strain could not be determined for the 350°C tested sample, due to the larger strain intervals between *ex situ* tests.

E.3.2 Film Adhesion

The interfacial adhesion energy is quantitatively measured with the buckles that form between the cracks. The model developed by Fischer et al [20] takes into account the strain energy between buckles, the debonding energy and the strain energy of the buckled material. This model was developed for brittle films on polymer substrates and buckle formation therein caused by the compressive stress evolved in the film perpendicular to the tensile straining axis [20].

To calculate the interfacial adhesion the dimensions of the buckles are needed, namely, the buckle height, δ, and half buckle width, b. When the buckles dimensions are plotted as $\sqrt{\delta/h}$ as a function of (b/h), where h is the film thickness, the data can be described by:

$$\sqrt{\frac{\delta}{h}} = \sqrt[4]{2\alpha}\left(\frac{b}{h}\right)\left(1+\sqrt{1+\frac{3\alpha}{4}\left(\frac{b}{h}\right)^4}\right)^{-\frac{1}{4}}. \tag{E.1}$$

Where α is a fitting parameter. The α parameter is used to calculated the adhesion energy, Γ, using:

$$\alpha = \frac{4\Gamma}{hE'}\left(\frac{2}{\pi}\right)^4. \tag{E.2}$$

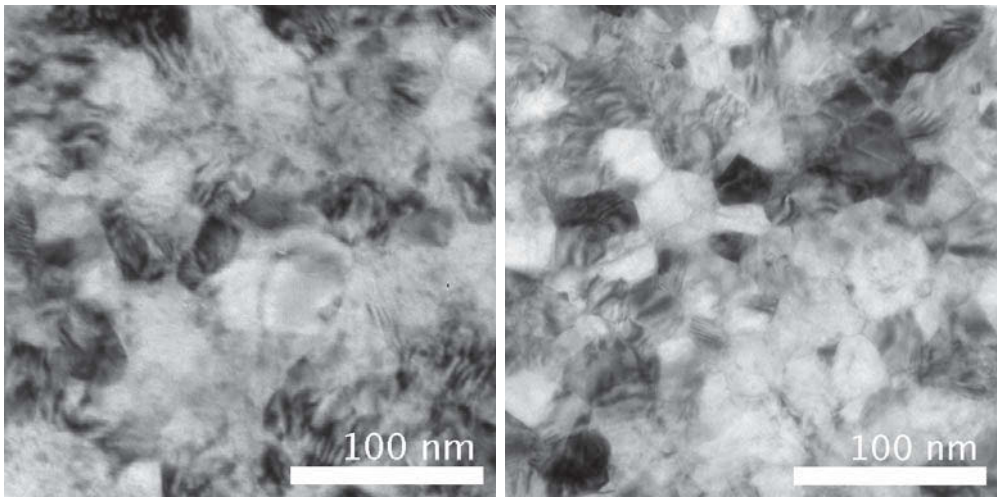

(a) (b)

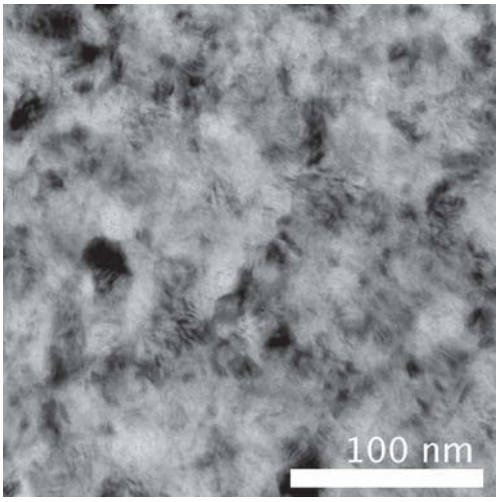

(c)

Figure E.1 Plane view TEM micrographs of the a) as-deposited, b) 350°C tested and c) annealed Ti films. No significant difference in the film microstructure or grain size was observed.

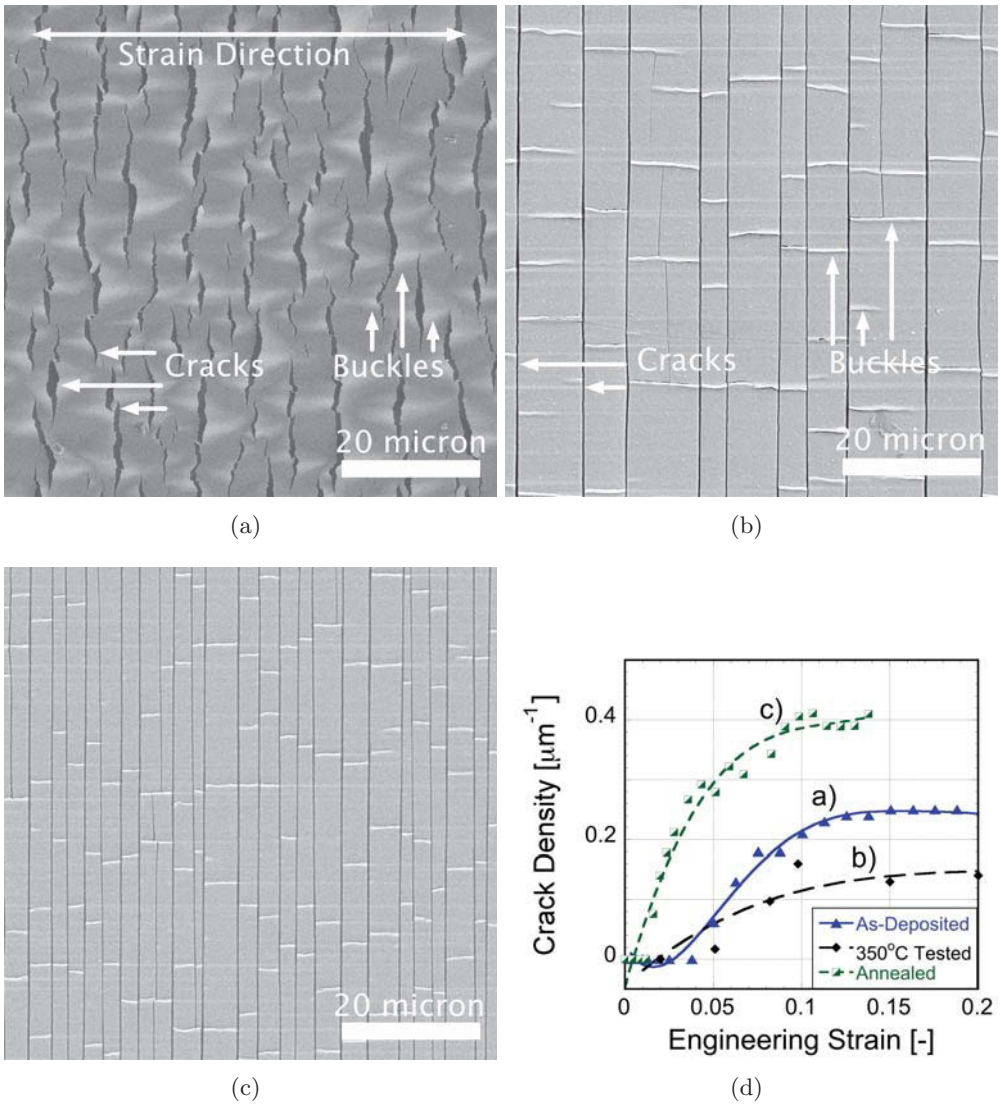

Figure E.2 SEM micrographs of the samples after cracking has saturated. a) is as-deposited, b) 350°C tested and c) is the annealed film. Shown in d) are the crack development profiles for the three samples, the lines are purely to guide the eye. Note the different crack and buckle morphology of the as-deposited sample compared to the heated samples.

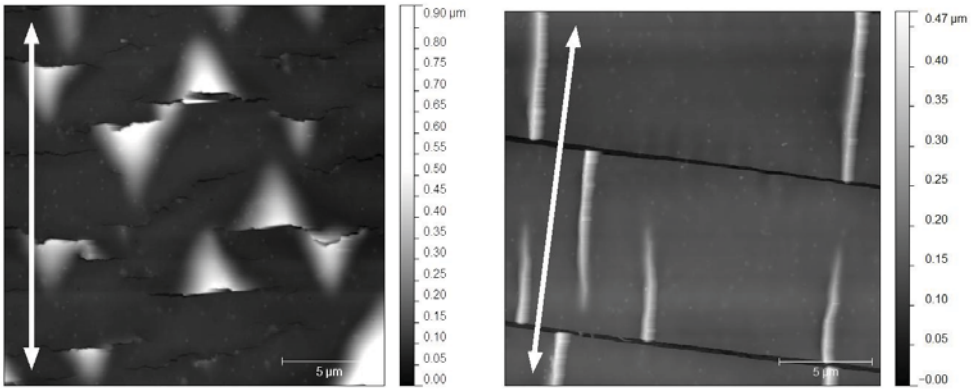

(a) (b)

Figure E.3 AFM height images of a) the as-deposited Ti film and b) the 350°C Ti film. Note the different shape of the buckles in the samples and larger height range for the as-deposited scan. Arrows indicate the direction of straining.

In equation E.2, h is again the film thickness and E′ is the modified elastic modulus (E'_{Ti} = 130 GPa). With:

$$E' = \frac{E}{1-\nu^2}. \tag{E.3}$$

where E and ν are the Young's modulus and Poisson's ratio of the Ti film, respectively.

AFM was used to image and measure the buckle dimensions. As has been previously discussed [16, 20, 23], buckles which do not travel across the whole crack fragment better describe the calculated adhesion energy. In this region of the buckle, there is no cracking of the buckle apex (top) or at the base of buckle. For the Ti buckles here only measurements from the end of partial buckles (figure E.3) were used to determine adhesion. As shown from the different height scales in figure E.3, the average buckle size of the film strained at 25°C is larger than at 350°C.

The adhesion energy using equations E.1 and E.2 is calculated by fitting α on a diagram like that shown in figure E.4. For the as-deposited film a minimum α of $\alpha = 4.0{\cdot}10^{-4}$ is fitted, this minimum is $\alpha = 1.2{\cdot}10^{-4}$ for the 350°C tested sample . From the α values the adhesion energy was calculated as (4.7±0.6) J m^{-2} for the as-deposited film and (1.4±0.5) J m^{-2} for the film tested at 350°C. The degree of error was determined by changing the minimum α value by approximately ±0.00005 to better account for the lower data points. A summary of the data for the three types of sample is given in table E.1.

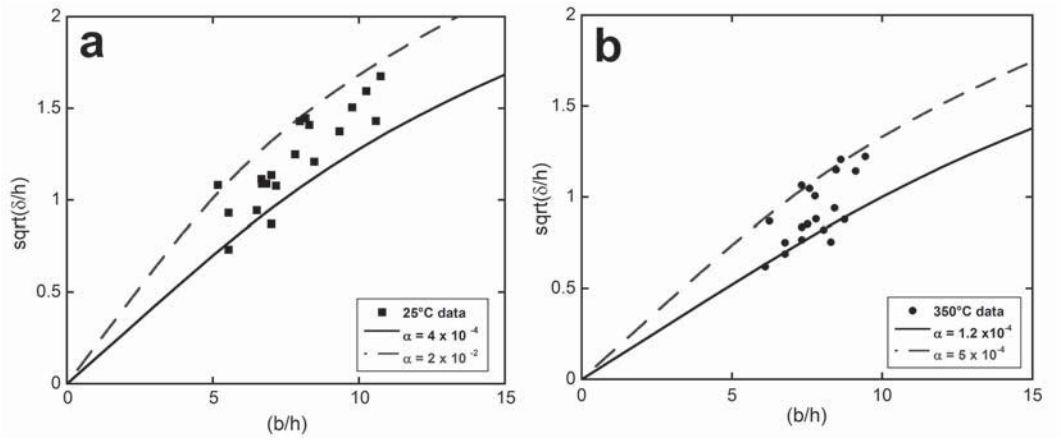

Figure E.4 Plots of $\sqrt{\delta/h}$ vs. b/h for the as-deposited Ti, a), and the 350°C tested Ti, b), as proposed by the Fischer model [20]. The lower limit represents buckles as they first form and hence gives the most reliable measure of interfacial adhesion.

Table E.1 Summary of the film properties determined. ϵ_f is the observed fracture strain, this could not be accurately determined for the samples tested at 350°C. The value of adhesion is calculated according to the Fischer model [20]. It was not possible to find partial buckles in the annealed samples so a reliable adhesion measurement could not be made.

Condition	Grain Size/nm	ϵ_f/%	Crack Density/μm^{-1}	Adhesion/J m^{-2}
As-Deposited	32±8	5	0.24	4.7±0.6
350°C tested	28±8	2–5	0.14	1.4±0.5
Annealed	24±9	1.6	0.40	–

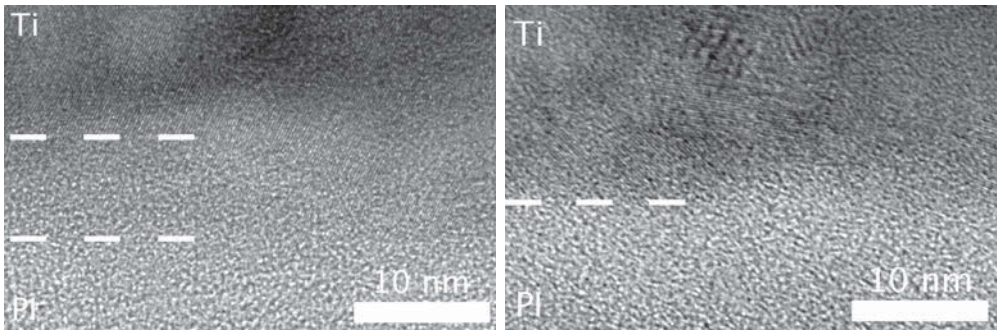

(a) (b)

Figure E.5 Cross-sectional TEM micrographs of the Ti/PI interface of an as-deposited sample, a), and a 350°C tested sample, b). The two dashed lines in a) mark the interlayer, the dashed line in b) marks the sharper Ti/PI interface.

E.3.3 Cross-sectional TEM

To further investigate the Ti/PI interface, cross-sections of all three sample types were investigated with TEM. Images from an as-deposited sample and a 350°C tested sample are presented in figure E.5, of particular note is the different interfacial structure. An interlayer between the Ti and PI is seen in the cross section from the as-deposited material, this interlayer is not seen for the 350°C tested material. All the TEM samples made from as-deposited material possessed this 5 to 10 nm thick interlayer while it was never observed in samples from 350°C tested or annealed material.

E.4 Discussion

The observed change in cracking and buckling behaviour of the annealed and 350°C tested Ti compared to the as-deposited films is a strong indicator of a change in interfacial adhesion. The change in buckle morphology between the 350°C tested and annealed Ti compared to the as-deposited material is due to the reduced adhesion in the heated samples. The drop in adhesion, more than a factor of three from 4.7 to 1.4 J m^{-2}, causes the observed switch from triangular footprint buckles in the as-deposited samples to rectangular footprints in the 350°C tested and annealed Ti. This occurs as the lower tensile stress at the fragment edges causes a greater mismatch between film and substrate in the lateral direction and hence larger compressive stresses [12], this is illustrated in figure E.6. The result of this gradient in compressive stress from fragment edge to fragment centre is that the strain energy release driving cracking also decreases towards the fragment centre. For a system with low film/substrate adhesion, rectangular footprint buckles will form as a rectangle gives the greatest release of strain energy for a given area of film delamination. If adhesion is sufficiently high then triangular buckles will form.

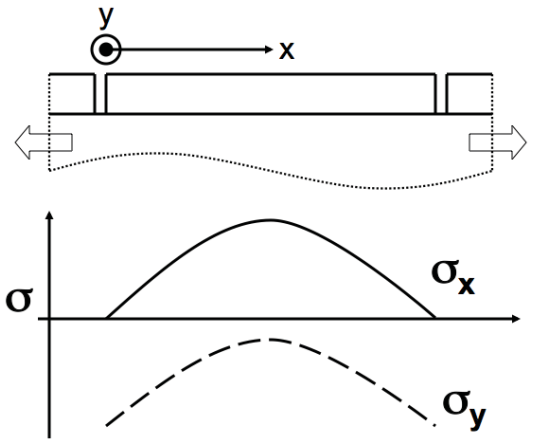

Figure E.6 Illustration of the stresses in a film fragment both parallel, x-direction, and lateral, y-direction, to the applied load. The parallel tensile stress reaches a maximum at the fragment centre while the lateral compressive stress is highest at the fragment edges. After Frank et al. [12].

Rectangular footprints would still lead to a greater reduction in system energy but the lower buckling driving force towards the fragment centre kinetically favours the triangular footprint.

The reasons for the change in cracking behaviour are less clear. TEM observations, figure E.1, indicate that no change in film microstructure takes place during elevated temperature testing or annealing. In addition, the similar crack morphology of the 350°C tested and annealed samples demonstrates that the effect is permanent following heating at 350°C rather than being due to the elevated temperature properties of Ti. As all heating was performed in moderate vacuum and titanium's native oxide is highly protective [24, 25] it can also be assumed that the change in crack morphology is not due to the infiltration of environmental impurities into the film, causing embrittlement. A final possibility is hydrogen embrittlement of the Ti film. It has been shown that hydrogen environments can cause embrittlement of Ti and its alloys [26–28], it is possible that reactions within the PI at 350°C lead to the release of hydrogen into the Ti film. No evidence of titanium hydride (TiH_2) formation [27] was found in selected area diffraction of any of the coatings but interaction of hydrogen with grain boundaries and dislocation cores can also lead to embrittlement [26].

A final observation relating to the cracking of the Ti films is the variation in crack density between the samples. The samples tested at 350°C have the lowest crack density. This is consistent with the findings of Leterrier et al. [18] and Yanaka et al. [29] that saturation crack densities of brittle coatings correlate with substrate mechanical properties, i.e. that the reduced substrate stress at 350°C leads to a reduced crack density. This difference is most clearly seen by comparing figures E.2b and E.2c, the crack density of the annealed sample tested at room temperature is more than a factor of two greater than that of the sample tested at 350°C. It is

less clear why the crack density of the annealed sample is higher than that of the as-deposited Ti. Several groups [13, 30, 31] have related the average film crack spacing at saturation to the adhesion of the film/substrate interface, the assumption being that if an interface can maintain a higher shear stress, leading to more closely spaced cracks, then the adhesion of the film/substrate interface is likely to be higher. In the present case, the annealed Ti/PI has been shown to have a significantly reduced interfacial adhesion compared to as-deposited Ti/PI by the tape test and yet the annealed sample has a greater crack density. It is put forward here that this effect is also a result of the Ti becoming embrittled by heat treatment. The annealed sample has a significantly lower fracture strain, 1.6 versus 5%, than that seen for the as-deposited Ti, table E.1, this is indicative of a lower film fracture stress. A reduction in film fracture stress is also expected to increase the crack density at saturation [14, 15, 18]. These results show that relating crack spacing and interfacial shear stress to film/substrate adhesion should be done with caution, ensuring all other experimental factors remain constant.

The quantitative adhesion energy results derived from buckle measurements found a factor three reduction for the samples tested at 350°C. In addition to the quantitative measure of adhesion supplied by buckle dimension measurement, a qualitative tape test was also carried out on the samples. In this test an adhesive tape was applied to the samples following testing, the removal of the tape also leads to some of the film being removed. By examining the degree of film removal a simple indicator of film/substrate adhesion is achieved. This test was not carried out according to any defined standards and hence should be treated as a purely qualitative test. The results from this test, figure E.7, support the adhesion measurements made from tensile test-induced buckles, i.e. that the 350°C tested sample has significantly lower adhesion. Tape-testing of the 350°C tested and annealed samples all removed the majority of the Ti coating, limited film removal was only achieved for highly strained, >10% strain, as-deposited samples.

A similar study of the adhesion energy of Cu/Ti films on PI also found a decrease in adhesion energy after annealing for 1 hr at 350°C [16]. For the Ti/PI system investigated in this study, the interfacial TEM observations suggest that this change in adhesion is related to the presence of a Ti/PI interlayer at the interface. A ∼10 nm thick interlayer was always observed between the Ti and PI in the as-deposited state, this interlayer was never observed in 350°C tested and annealed samples. The interlayer is formed during the deposition of the films, thermal treatment of the system then leads to phase separation and reduced film/substrate adhesion. This is most clearly seen in the optical micrographs of the tape tested samples, figure E.7. Although only a qualitative test, the tape test shows the stark difference in adhesion; almost all the film is removed by the tape for the heat treated samples while 20% or less film is removed from the as-deposited Ti.

The observation of reduced film adhesion following heat treatment is important for the emerging field of flexible electronics, regardless of the cause of this reduction. Elevated temperatures, >100°, are routinely experienced by electronic circuitry during deposition, processing and use, if this can lead to reductions in interfacial adhesion

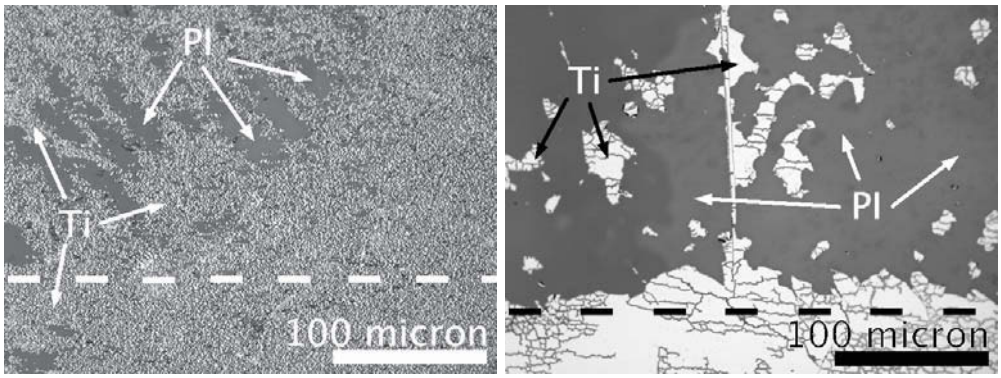

(a) (b)

Figure E.7 Optical micrographs of the a) as-deposited Ti and b) 350°C tested Ti are presented following the application and removal of adhesive tape to the film surface. Significantly more of the 350°C tested Ti was removed by the tape, indicative of lower adhesion at the Ti/PI interface in this sample. The dashed lines mark the lower edge of the tape.

of components then circuit lifetime will drop. The 350°C testing and annealing carried out is not representative of the temperatures experienced by flexible circuitry but as an accelerated test it does illustrate that circuit thermal history is an important factor in circuit lifetime. If the adhesion drop observed is due to demixing of a Ti-PI layer then this process will also occur at lower temperatures but more slowly, understanding and learning to counteract this effect should then lead to improved circuit lifetimes and performance.

E.5 Conclusions

Ti adhesion layers on polyimide (PI) flexible substrates exhibit very different cracking and buckling when uniaxially strained in the as-deposited state and at 350°C. The shape of the cracks and buckles changes and analysis of the buckles shows a significant drop in interfacial adhesion when tested at 350°C. TEM of the films in the two states and room temperature testing of samples annealed at 350°C shows that these changes are not due to changes in the Ti microstructure.

A cross-sectional TEM study infers that the difference in adhesion caused by heat treatment of these Ti films is linked to the disappearance of an interfacial interlayer between the Ti and PI. The implications of this for the processing, use and lifetimes of flexible electronic circuits are extensive. Additionally, this greater understanding of how Ti acts as an effective adhesion layer between polymers and metallisation materials such as Au and Cu could lead to more adherent, and hence failure-resistant, flexible circuitry.

E.6 Acknowledgment

Gabi Moser at the Erich Schmid Institute is acknowledged and thanked for her continued assistance with TEM sample preparation. In addition, MJC gratefully acknowledges funding from the Austrian Science Fund (FWF) under project P22684-N20.

Bibliography to paper E

[1] N Bowden, S Brittain, AG Evans, JW Hutchinson, GM Whitesides, Nature 393, 146-149 (1998)

[2] Y Sun, WM Choi, H Jiang, YY Huang, JA Rogers, Nature Nano. 1, 201 (2006)

[3] X Lu, Y Xia, Nature Nano. 1, 163-164 (2006)

[4] OS Heavens, J. Phys. Radium 11, 355-360 (1950)

[5] JC Hoogvliet, WP van Bennekom, Electrochemica Acta 47, 599-611 (2001)

[6] KE Paul, WS Wong, SE Ready, RA Street, Appl. Phys. Lett. 83, 2070-2072 (2003)

[7] C-A Chang, Y-K Kim, AG Schrott, J. Vac. Sci. Technol. A 12, 3304-3309 (1990)

[8] SH Kim, SW Na, N-E Lee, YW Nam, Y-H Kim, Surf. Coat. Technol. 200, 2072-2079 (2005)

[9] J Lohmiller, NC Woo, R Spolenak, Mater. Sci. Eng. A 527, 7731-7740 (2010)

[10] MJ Cordill, A Taylor, J Schalko, G Dehm, Metall. Mater. Trans. A 41, 870-875 (2010)

[11] T Li, Z Huang, Z Suo, SP Lacour S Wagner, Appl. Phys. Lett. 85, 3435-3437 (2004)

[12] S Frank, UA Handge, S Olliges, R Spolenak, Acta Mater. 57, 1442-1453 (2009)

[13] MS Hu, AG Evans, Acta Metall. 37, 917-925 (1989)

[14] DC Agrawal, R Raj, Acta Metall. 37, 1265-1270 (1989)

[15] WA Curtin, J. Mater. Sci. 26, 5239-5253 (1991)

[16] MJ Cordill, AA Taylor, J Schalko, G Dehm, Int. J. Mater. Res. 102, 729-734 (2011)

[17] J Andersons, Y Leterrier, G Tornare, P Dumont, J-AE Månson, Mech. Mater. 39, 834-844 (2007)

[18] Y Letterier, L Boogh, J Andersons, J-AE Månson, J. Polym. Sci. B: Polym. Phy. 35, 1449-1461 (1997)

[19] J Andersons, S Tarasovs, Y Leterrier, thin Solid Films 517, 2007-2011 (2009)

[20] MJ Cordill, FD Fischer, FG Rammerstorfer, G Dehm, Acta Mater. 58, 5520-5531 (2010)

[21] AA Taylor, MJ Cordill, G Moser, G Dehm, Prakt. Metallogr. 48, 408-413 (2011)

[22] Transmission Electron Microscopy, DB Williams and CB Carter, p444, Springer, New York (1996)

[23] MJ Cordill, K Schmidegg, G Dehm, Phil. Mag. Lett. 91, 530-536 (2011)

[24] RW Schutz, DE Thomas, ASM Handbook, Vol. 13: Corrosion, 669-706 (1987)

[25] KL Luthra, Oxidation of Metals 36, 475-490 (1991)

[26] MR Louthan, GR Caskey, JA Donovan, DE Rawl, Mater. Sci. Eng. 10, 357-368 (1972)

[27] DS Shih, IM Robertson, HK Birnbaum, Acta Metall. 36, 111-124 (1988)

[28] CL Briant, ZF Wang, N Chollocoop, Corr. Sci. 44, 1875-1888 (2002)

[29] M Yanaka, Y Kato, Y Tsukahara, N Takeda, Thin Solid Films 355-356, 337-342 (1999)

[30] DR Wheeler, H Osaki, Am. Chem. Soc. Symp. Ser. 440, 500-512 (1990)

[31] F Bodino, G Baud, M Benmalek, JP Besse, HM Dunlop, M Jacquet, Thin Solid Films 241, 21-24 (1994)